POLITECNICO
DI TORINO

UNIVERSITÀ
DEGLI STUDI
DI TORINO

Doctoral Dissertation

Doctoral Program in Pure and Applied Mathematics (30^{th} cycle)

THE SLICER MAP: MOMENTS, CORRELATIONS AND UNIVERSALITY

By

Muhammad Tayyab

* * * * *

Supervisor:

Prof. Lamberto Rondoni

Co-Supervisors:

Prof. Claudio Giberti

Prof. Jürgen Vollmer

Università degli studi di Torino - Politecnico di Torino

2018

Doctoral Examination Committee:

Prof. Paolo Cermelli[1]

Prof. Matteo Colangeli[2]

Prof. Cecilia Vernia[3]

Examination date:

July 25, 2018

[1]Dipartimento di Matematica "G. Peano" - Università degli Studi di Torino, Italy

[2]Dipartimento di Ingegneria e Scienze dell'Informazione e Matematica - Università degli Studi dell'Aquila, Italy

[3]Dipartimento di Scienze Fisiche, Informatiche e Matematiche - Università di Modena e Reggio Emilia, Italy

Declaration

I hereby declare that, the contents and organization of this dissertation constitute my own original work and does not compromise in any way the rights of third parties, including those relating to the security of personal data.

Muhammad Tayyab

Torino, 2018

∗ This dissertation is presented in partial fulfillment of the requirements for **Ph.D. degree.**

Dedication...

To my beloving parents

Muhammad Ilyas

&

Fatima Ilyas

Preface

This thesis is submitted to the Università degli studi di Torino (UniTO) and Politecnico di Torino (PoliTO) for partial fulfillment of the requirements for the degree of Philosophiae Doctor. This doctoral work was performed in the Department of Mathematical Sciences "Giuseppe Luigi Lagrange", PoliTO, with Professor Lamberto Rondoni as the main supervisor, while co-supervised by Prof. Claudio Giberti from Università di Modena e Reggio Emilia, Italy and Distinguished visiting Prof. Jürgen Vollmer from Georg-August-Universität Göttingen, Germany.

Acknowledgements

Summarizing few things in acknowledgement is seemingly a difficult task. Nevertheless, this is probably the place to thank most of them who continuous by motivated me during the last years.

First and foremost, I express my gratitude to Lamberto Rondoni for his kind supervision during my doctoral time. His intuitions on physical phenomenon and its rigorously related mathematical models, substantially influenced me in scientific field as well as my way of physical thinking and adequate mathematical interpretation. Moreover he introduced me with the working scientists of various fields and opened a window into the world of leading scientific research. I shall also remain grateful of providing freedom for attending summer schools, workshops, conferences and seminars, as well as for visiting scientific collaborators in different parts of Europe. Moreover in the middle of my Ph.D time L. R. expanded his research group with visiting professors and researchers. Many thanks goes to the group members for the motivations and fruitful discussions.

Moreover I cannot forget to mention two scientific collaborators as well as co-tutors, because without them this list is admittedly incomplete. The first one is Prof. Claudio Giberti. I really thank him for fruitful discussions and his very warm hospitality in Modena, Italy. He incredibly paved a path for me to FORTRAN programming, that has eventually become the numerical part of my thesis. Secondly, I am obliged to Prof. Jürgen Vollmer for his one year stay in Turin, Italy as a distinguished visiting professor. At this point again I am indebted to L. R. for inviting him in the department. My gratitude to J. V. extends to his warm welcome during a research visit to Leipzig, Germany, in his new affiliation at the Institut für

Theoretische Physik: ITP - Universität Leipzig, Germany. Indeed we had numbers of meetings and meaningful discussions. His knowledge on many physical problems indulge me to the data analysis, which has now become one of my favourite part of research both quantitatively and qualitatively.

There are some of my doctoral colleagues, without them it was inevitable to pursue the journey of last few years. My gratitude for Antonella Verderosa and Lorenzo Zino who helped me a lot in bureaucratic stuff when I came to Turin, Italy first time and was not able to speak Italian.

I am grateful to the computational resources provided by HPC@POLITO, a project of Academic Computing within the Department of Control and Computer Engineering at the Politecnico di Torino (`http://hpc.polito.it`). Without these computational resources I had been unable to obtain the results from extensive numerical simulations, which are a major contribution to this dissertation and my scientific publications.

Finally, without tremendous support of my family it was inevitable to complete my doctoral studies. Countless regard to my parents to whom I dedicate my thesis, and my sisters Sara Tehreem and Mamoona Umair and brother Uzair Ilyas who continuous by supported me throughout this journey, plus their unconditional love and encouraging words that gave me inspirational motivation to accomplished this work and make my dream in reality.

Muhammad Tayyab

Torino, 2018

Abstract

This thesis concerns the relation of different models of anomalous transport, and the possibility of identifying a corresponding universality class. Investigation of transport of matter in highly confining media is a very active field of research with numerous applications to bio- and nano-technology. We proceed from a model, called Slicer Map (SM), developed by Salari *et al.* CHAOS 25, 073113 (2015), that captures some features of anomalous transport, while being analytically tractable.

The SM is a one-parameter family of non-chaotic, one-dimensional dynamical systems. Different trajectories neither converge nor separate in time, except at discrete instants, when the distance between trajectories jumps discontinuously, because they are separated by a *slicer*. This is reminiscent to the role of corners in polygonal billiards. The SM shows sub-, super-, and normal diffusion as a function of its control parameter α, that characterises the power-law distribution of the length of ballistic flights. Salari and co-authors analytically expressed the time dependence of the moments of positions as a function of α, and compared it with the mean-square displacement of the Lévy-Lorentz gas (LLg), that also depends on a single parameter β. The LLg is a stochastic process, that is much more complex than the SM. Surprisingly it was found that the moments of the positions distributions of the SM and the LLg have the same asymptotic behaviour when the parameters α and β are chosen in order to match the exponent of the second moment. However, moments only partially characterise transport processes. Hence in this thesis we derive analytic expressions for the position auto-correlations of the SM, and we compare them with the numerically estimated position auto-correlations of the LLg. Remarkably, the same relation that produces the agreement of the moments

leads to the agreement of the position auto-correlation functions, at least for the low scatterers density of LLg. In the search of a universality class for these phenomena, we introduce an exactly solvable model called Fly-and-Die (FnD) dynamics that generates anomalous diffusion, and we derive analytical expressions for all moments of the displacements, for the position auto-correlation function, and for the velocity auto-correlation functions. The parameters of the model can be mapped to other anomalous transport processes by matching the exponents for the mean-square displacement and the prefactor of the corresponding power law. Indeed, this simplification of the SM, generates the same transport regimes as the SM.

It is conjectured that the FnD provides the asymptotic behaviour of all the position moments and the auto-correlation functions, for the universality class of systems whose positions statistics are dominated by the ballistic events. The conjecture is motivated by the fact that the sub-dominant terms in the SM and of the FnD contribute like the ballistic fights to the asymptotic behaviour, *i.e.*, they contribute the maximum allowed for a system to belong to such a universality class. Different models in the class may be distinguished considering other variables. This is demonstrated here for the velocity auto-correlation function. Numerical results on the Lévy-Lorentz gas support our conjecture.

List of Acronyms

SM	Slicer Map
LLg	Lévy-Lorentz gas
LLg^+	Lévy-Lorentz gas (positive strip)
FnD	Fly and Die
VACF	Velocity auto-correlation function

Contents

Chapter 1

Introduction

"We are what we repeatedly do. Excellence,
then, is not an act, but a habit."
— Aristotle

In this chapter, we start with the motivation of current developments in nonlinear diffusion processes. Explicit studies on anomalous transport are rare in literature, but in last few decades analyzing transport properties of energy and mass are emerging and they settle many questions, like for example, a recent applications to an osmotic-like phenomenon [28] with anomalous transport of molecules. Models of transport in pores of size comparable to the transported molecules, exhibit wide range of transport properties reminiscent to polygonal billiards with zero Lyapunov exponent, a hallmark of non-chaotic dynamics [32, 31, 26]. Still, the billiards are difficult to understand in as much detail as wanted (see [23, 60] and Refs. therein).

The original, point of interest was to construct an exactly solvable model that would reproduce the transport regimes found numerically in polygonal billiards. We wanted to capture the following main ingredients of their behavior:

- zero Lyapunov exponent with no expanding or contracting region ,
- occasional (discrete set of) sudden jumps ,
- volume preservation ,

- deterministic dynamics ,
- at least a weak notion of time reversibility .

To this end Salari *et al.* [53] construct a non-chaotic map, that mimics the possible features of polygonal billiards and reproduces all possible transport regimes. Moreover these non-chaotic deterministic systems are not highly appreciable unless the knowledge of time auto-correlation functions is fully characterised, since moments carry only the partial information of systems. In this dissertation, we compute the moments of displacement in alternative fashion from Salari *et al.* [53]. These computation set a stage for sophisticated derivation of time auto-correlation functions. Hence we compute time auto-correlation functions and focus on the super-diffusive transport of many systems and we propose an universal class in which the moments of displacement and the position auto-correlation functions of systems exhibiting super-diffusive transport are dominated by ballistic trajectories.

1.1 Outline and emerging research questions

The main object of interest in studies of anomalous transport is the *transport exponent*. This is the exponential rate γ at which the mean-square displacement of the positions, $\langle \Delta \mathbf{x}_n^2 \rangle$, diverges as the time n grows

$$\gamma := \lim_{n \to \infty} \frac{\log \langle \Delta \mathbf{x}_n^2 \rangle}{\log n} \,. \tag{1.1}$$

Provided the above limit exists, processes with finite maximum speed yield $\gamma \in [0, 2]$. Regimes with $\gamma < 1$ are called sub-diffusion; they are called diffusion if $\gamma = 1$, and super-diffusion if $\gamma > 1$. The generalised diffusion coefficient D_γ, defined by:

$$D_\gamma := \lim_{n \to \infty} \frac{\langle \Delta \mathbf{x}_n^2 \rangle}{n^\gamma} \,, \tag{1.2}$$

is then a non-negative number.

Transport properties afford only a rather coarse representation of the typically very rich underlying microscopic dynamics. Understanding them from a microscopic perspective is an open problem, that motivates a wide and very active research

community [30, 58]. In the realm of deterministic dynamics, it is understood that uniformly hyperbolic dynamical systems produce rapid correlations decay. In turn, rapid decay of correlations is commonly associated with standard diffusion [23, 37]. Because randomly placed non-overlapping wind-trees and related maps [12, 17] enjoy a sort of stochasticity analogous to that generated by chaotic dynamics, they may also show standard diffusion.

On the contrary, for fully deterministic systems with vanishing Lyapunov exponents, like periodic polygonal billiards [32], the nature of transport is still a matter of investigation [2, 37, 53, 63]. A major challenge of the latter systems is that correlations persist or decay rather slowly as compared to what happens in chaotic systems [32]. This makes their asymptotic statistics much harder to understand than in presence of chaos. Indeed, the unpredictability of single trajectories in chaotic systems, that is one aspect of the fast decay of correlations, is associated with regular behaviour on the level of ensembles, as proven, for instance, by the differentiability of SRB states [51] that implies linear response [52]. In contrast, for non-chaotic systems the parameter dependence of the transport exponent can be quite irregular [32].

In the field of fully fledged stochastic processes, numerous questions remain open as well [3, 4, 15, 37, 40, 58, 63]. Among such systems, the Lévy-Lorentz gas, a random walk in random environments, in which the scatterers are randomly distributed on a line according to a Lévy-stable probability distribution, has been thoroughly investigated by various authors. Different types of anomalous and standard diffusion were observed, upon tuning the parameter β characterising the Lévy-stable probability distribution [3, 4]. These authors noted that ballistic contributions to the mean-square displacement, which are considered irrelevant when diffusion is normal, are in fact important for the transport. Under certain simplifying assumptions, Burioni *et al.* [10] analytically calculated the mean-square displacement of the travelled distance for this model, and numerically verified the validity of their reasoning. More recently, Bianchi *et al.* [7] rigorously established the validity of the Central Limit Theorem.

The Slicer Map (SM) introduced in [53] was motivated by observations of the mass transport of periodic polygonal billiards [32]. Like in polygonal billiards, the dynamics of the SM are free of randomness. Their trajectories do not separate exponentially in time, and they experience sudden deviations from their motion, at isolated points that are regularly placed in space. Despite these facts, the dynamics of the SM differs substantially from all other models mentioned so far. For instance, after an initial transient all trajectories of the SM turn periodic. However, anomalous transport may be dominated by ballistic flights [1]. Rather than commonalities in the microscopic dynamics, the equivalence of the transport exponents requires in that case that the length of ballistic flights in the initial ensemble follows a corresponding power-law distribution. The transport of the SM is of this kind, and the power-law distribution of its ballistic flights can be tuned by adjusting its parameter α.

In [53] it was shown that once α is adjusted so that the transport exponent of the SM coincides with that of the LLg at a given β, all higher order moments of the position distribution of the SM scale in time like those of the LLg [10]. Of course such an agreement does not imply a full equivalence of the dynamics, as mentioned above and further stressed in Chp. 3 and Chp. 6. For instance, from the particle-transport viewpoint, the LLg can only be super-diffusive ($1 < \gamma_\beta < 2$), while the SM can exhibit all possible diffusion regimes, $0 \leq \gamma_\alpha \leq 2$. Moreover, the β-dependence of the transport exponent of the LLg is not simple: it splits in three different functional forms. In contrast, $\gamma = 2 - \alpha$ for all SM regimes.

The agreement of the moments constitutes a striking example of the fact that the characteristics of a transport process, like the moments of the displacement, do not fully characterise its nature in general. The common wisdom is that also correlations should be considered [2, 58], and the two-point correlation functions should suffice for the rather reduced, but physically relevant, description afforded by transport properties.

In Sec. 3.4 we derive explicit analytic expressions for the position auto-correlations of the SM, to check whether they suffice to distinguish its transport properties from those of the LLg. Information on the correlations of the LLg is minimal in the

literature, hence we resort to numerical simulations of the LLg, to compare the two models in Sec. 4.3. Remarkably, we find that the equivalence of the positions moments obtained in [53] extends to the case of the position-position auto-correlation functions; for $1.5 \lesssim \gamma < 2$ their functional forms have been numerically found to match without adjustable parameters.

The reason of this equivalence lies in the fact that the transport processes of the SM and of the LLg get an asymptotically relevant contribution from the ballistic flights, the flights that in a finite time n travel a distance $v\,n$ with constant velocity v [21]. Such flights constitute rare events in both systems, because the probability of bouncing back tends to 1 as n grows. However, because the associated travelled distance is the largest possible, the contribution of ballistic fights to transport is sizable. In particular, the ballistic flights of the SM give the smallest possible contribution to asymptotic transport regimes dominated by ballistic flights, since they contribute like the non-ballistic flights. From this point of view, the SM can be taken as a representative of the *universality class* of transport phenomena asymptotically dominated by ballistic motions.

The essence of the SM transport properties is that any "particle" travels ballistically, till it reaches a period 2 periodic orbit, which consists of one step forward followed by one step backward. This suggests an even simpler representative for the universality class, *i.e.*, a map whose particles travel ballistically up to a given (random) time and then they stop. We call this map Fly-and-Die (FnD), and introduce it in Sec. 5.1. The simplicity of the FnD easily leads to a scaling form for the position auto-correlation function, that depends on a single parameter, *cf.* Section 5.1.2.

We compare the transport properties of various systems, finding out that the class in which the asymptotic transport regimes are dominated by ballistic flights includes stochastic as well as deterministic particle systems, with quite different microscopic dynamics. In particular, the billiard systems[1] include the Lorentz gas with infinite

[1]This thesis does not cover results on billiard systems, that are still under discussion with an other collaborator. This work will be furnished in a forthcoming research article.

horizon, which is chaotic, and non-chaotic polygonal channels with finite horizon. The main point related to the above is that the asymptotic transport properties of any element in the class can be predicted using the FnD map, something useful when direct evaluation is not possible or problematic. For instance, the FnD map allows a simple calculation even of the n-point position auto-correlation functions, that can be associated with any other element in the class, from mere knowledge of the scaling of the second moment. Having strongly different dynamics, the equivalence of FnD, SM, LLg and other transport models cannot be complete, as discussed *e.g.,* in Refs. [25, 53]. For instance, they have quite different velocity auto-correlation functions, as shown in sections 3.7 and 5.1.5.

1.2 Structure of the thesis

This thesis is organised as follows: In chapter 2 we review different notions of the general models for standard and anomalous diffusion. Some deterministic and stochastic dynamics are focused in the eye of anomalous transport.

Chapter 3 formally introduces the SM and summarises its main properties. They are derived here in an alternative fashion, compared to that of [53]. Some examples of the SM position auto-correlation functions are explicitly computed in Sec. 3.4. In Sec. 3.5 results are furnished for moments of the velocity. The 1-, and 2-time(s) velocity auto-correlation function are present in Sec. 3.6 and 3.7 respectively.

Chapter 4 summarises the LLg and its analytical derivation of the moments for the displacement. The correspondence between the LLg and the SM is discussed in Sec. 4.2. The correlations of the SM and the LLg are compare in Sec. 4.3. In Sec. 4.4 a quantitative comparison of the SM and the LLg position auto-correlation is presented.

In Chapter 5, the FnD dynamics is introduced, which simplifyies the recently developed SM [53]. Section 5.1 introduces the FnD map, it illustrates its main properties and provides a universal formula for the 2-, 3-, and n-point position auto-correlation function. The velocity auto-correlation function is computed in

Sec. 5.1.5, to accomplish the difference between different dynamics in the universality class. Sections 5.2 and 5.3 briefly summarises the 2-, and 3-point position auto-correlation of the SM in connection with the universal formula for the position auto-correlation function and test the universal scaling for LLg position correlation with analysis of data.

Lastly but not least, in Chp. 6 we conclude the thesis with a discussion of our main result: In the strongly super-diffusive regime, $1.5 \lesssim \gamma < 2$, the position auto-correlations of the SM and of the LLg scale in the same fashion with time. We defined a universality class for many systems that show super-diffusive transport dominated by ballistic trajectories. It comprises many systems with totally different microscopic dynamics, that share the same asymptotic transport properties (*i.e.*, moments of displacement and position auto-correlation function). They are hardly distinguishable as far as statistics or positions are concerned. Hence other observables *e.g.,* the velocity auto-correlation function, are needed to separate the different system in the class.

In an appendix A some technical points of the proof concerning the time asymptotics of the SM moments and the position auto-correlation function are provided. The proof of proposition 3.5.1 and lemma 3.5.3 are also shown to ease down the computation of velocity auto-correlation function of the SM. Later on App. A.4 devote to the 3-point position correlation of the SM.

In an appendix B, the construction of the position auto-correlation function and the derivation for the scaling of the correlation function of the FnD dynamics are provided. Moreover proof of lemma 5.1.2 for scaling of the n-point position correlation of the FnD dynamics is presented.

Chapter 2

Models of anomalous transport

"Bring forth what is true; Write it so it it's clear
Defend it to your last breath"
— Ludwig Boltzmann

In this chapter, we discuss the basic framework of dynamical systems from both physical and mathematical point of view, and we define their dynamics in terms of *continuous* and *discrete*-time. Moreover some general and classical framework of standard and anomalous diffusion is reviewed in the eye of deterministic maps. Finally we provides a brief discussion on Lévy walk approach to anomalous diffusion.

2.1 Dynamical system

As a scientific trend, the investigation of dynamical frameworks most likely originates at the end of nineteenth century through the work crafted by *Henri Poincaré* in his investigation of celestial mechanics [46]. Once the system of equations describing the motion of the planets around the sun were figured *i.e.*, the mathematical model was built, he searched for mathematical solutions as a way to depict the planets movements and make predictions of positions in time finding solution for the sets of equation was impossible he concentrated on the mathematical structure of the system to narrow down the possible solution functions [47]. This perspective, to concentrate on the nature and structure of the equations in a mathematical model

in order to obtain (pieces of) information with regards to the nature and structure of its possible solutions is the general thought behind the procedures and hypothesis (or somehow possible techniques) of what we now call dynamical frameworks. Being just hundred years of age, the mathematical idea of a dynamical framework is a moderately new thought. Moreover, since it truly is an focused investigation of the concept of functions of a usually single and real independent variable, it is a sub-branch of real analysis on the other hand the theory of dynamical system draws its techniques and theory from numerous branches of mathematics, from real analysis to algebra and topology and into geometry. One might call mathematical areas like geometry, topology and dynamics second generation mathematics, since they tend to bridge other more pure areas in their theories. But as the study of what is actually means to model phenomena via functions and equations, dynamical systems is sometimes called the mathematical study of any mathematical concept that evolves over time. So as a way to characterize this idea more definitely, we start with the broad [8]:

Definition 2.1.1 (**Dynamical system**)**.** A dynamical system consist of phase space $\mathcal{P}$ and collection of transformations $\psi^t : \mathcal{P} \to \mathcal{P}$, where t is the time parameter. The time parameter t is from $\mathbb{R}$ (*time-continuous system*) or from $\mathbb{Z}$ or from $\mathbb{Z}^+$ (*time-discrete system*). Furthermore for $x \in \mathcal{P}$ the transformation obeys $\psi^0(x) = x$, and $\psi^t(\psi^s(x)) = \psi^{t+s}(x)$ for all t, s.

In the following some characteristics of dynamical system will come under discussion. The time set is denoted by Υ. If $\Upsilon = \mathbb{R}$ then the dynamical system is called *flow*, if $\Upsilon = \mathbb{Z}$ or $\Upsilon = \mathbb{Z}^+$ then the dynamical system is *discrete*. When $\Upsilon = \mathbb{R}$ or $\Upsilon = \mathbb{Z}$ then the inverse mapping $(\psi^t)^{-1} = \psi^{-t}$ may exist. Such systems are known as *invertible dynamical systems*. If the dynamical system is not invertible then $\psi^{-t}(A)$ means the pre-image of A with respect to ψ^t, for any arbitrary set $A \subset \mathcal{P}$ and arbitrary $t > 0$, *i.e.*, $\psi^{-t}(A) = \{x \in \mathcal{P} : \psi^t(x) \in A\}$.

If the mapping $\psi^t : \mathcal{P} \to \mathcal{P}$ is continuous or m times continuously differentiable for $t \in \Upsilon$ *i.e.*, $\mathcal{P} \subset \mathbb{R}^n$, then the system is called *continuous* or a $C^m - smooth$ dynamical system, respectively.

For any arbitrary initial point $x \in \mathcal{P}$, $t \in \Upsilon$, the mapping $t \mapsto \psi^t(x)$, defines a *motion* of the dynamical system starting from x at time $t = 0$. The image $\gamma(x)$ of a motion starting at x is called the *orbit* (or called trajectory) through x, namely $\gamma(x) = \{\psi^t(x)\}_{t\in\Upsilon}$. In the similar fashion, the *positive semi-orbit* through x is defined by $\gamma^+(x) = \{\psi^t(x)\}_{t\geq 0}$, and if $\Upsilon \neq \mathbb{R}^+$ or $\Upsilon \neq \mathbb{Z}^+$, then the *negative semi-orbit* through x is defined by the notion $\gamma^-(x) = \{\psi^t(x)\}_{t\leq 0}$.

If $\gamma(x) = \{x\}$, then the orbit $\gamma(x)$ is called *steady state* also known as *stationary or equilibrium point*. If there exist a $T \in \Upsilon$, $T > 0$ such that $\psi^{t+T}(x) = \psi^t(x)$, $\forall\ t \in \Upsilon$, then it is called *T-periodic*. If $T \in \Upsilon$ is the smallest positive number with this property, T is called *period*.

In the following discussion, we will discuss discrete-, and continuous-time dynamical systems in detail and enlighten some attributes of these systems.

2.1.1 Continuous-time dynamical systems

Let $\mathcal{P} \subset \mathbb{R}^n$, $n \in \mathbb{N}$, $x = (x^1, x^2, \cdots, x^n) \in \mathcal{P}$ and $t \in \mathbb{R}$, then

$$\mathcal{F} : \mathcal{P} \to \mathcal{P}\,, \qquad \frac{\mathrm{d}x}{\mathrm{d}t} = \mathcal{F}(x(t)) = \mathcal{F}(x)\,, \tag{2.1}$$

is called *vector field*. It can be written as a system of n first order, autonomous (*i.e.*, not explicitly time-dependent), ordinary differential equations

$$\begin{cases} \dfrac{\mathrm{d}x^1}{\mathrm{d}t} = \mathcal{F}^1(x^1, x^2, \cdots, x^n), \\ \dfrac{\mathrm{d}x^2}{\mathrm{d}t} = \mathcal{F}^2(x^1, x^2, \cdots, x^n), \\ \qquad \vdots \\ \dfrac{\mathrm{d}x^n}{\mathrm{d}t} = \mathcal{F}^n(x^1, x^2, \cdots, x^n)\,. \end{cases} \tag{2.2}$$

If there exist a solution of Eq. (2.1), with the initial condition x_0, then

$$x(t) = \psi^t(x_0), \tag{2.3}$$

is called the *flow* of vector field. Here ψ^t is the transformation that we have encountered in Definition 2.1.1.

2.1.2 Discrete-time dynamical systems

Let $\mathcal{P} \subset \mathbb{R}^n$, $n \in \mathbb{N}$, $x_t \in \mathcal{P}$, $t \in \mathbb{Z}^+$, then the difference equation

$$\mathcal{B} : \mathcal{P} \to \mathcal{P}, \qquad x_{t+1} = \mathcal{B}(x_t), \tag{2.4}$$

is called *discrete-time map*. The map $x_{t+1} = \mathcal{B}(x_t)$ is also known as equation of motion of the dynamical system. The initial condition x_0 determines the outcomes of t discrete time steps in the following form

$$\begin{aligned} x_1 &= \mathcal{B}(x_0) = \mathcal{B}_1(x_0), \\ x_2 &= \mathcal{B}(x_1) = \mathcal{B}_1(\mathcal{B}(x_0)) = \mathcal{B}_2(x_0), \\ &\Rightarrow \mathcal{B}_m(x_0) := \mathcal{B} \circ \mathcal{B} \circ \cdots \mathcal{B}(x_0). \end{aligned} \tag{2.5}$$

In other words, for maps the situation is formally simpler than for differential equations: there is a unique solution to the equations of motion in form of $x_t = \mathcal{B}(x_{t-1}) = \cdots = \mathcal{B}_t(x_0)$. It represents the counterpart of the flow for continuous-time dynamical system.

Example 2.1.1 (**Invertible map**)**.** Consider the two-dimensional dynamical system on $\mathcal{P} = \mathbb{R}^2$

$$x_{t+1} = y_t + 1 - cx_t^2, \quad y_{t+1} = \mathrm{d}\, x_t, \quad \text{for} \;\; t \in \mathbb{Z}, \tag{2.6}$$

with the free parameter $c > 0$ and $d \neq 0$. It is called *Hénon mapping*. The mapping $\mathcal{B} : \mathbb{R}^2 \to \mathbb{R}^2$ corresponding to Eq. (2.6) is defined by $\mathcal{B}(x, y) = (1 + y - cx^2, \mathrm{d}x)$. It is infinitely often differentiable and invertible.

Example 2.1.2 (**Non-invertible map**)**.** Consider the dynamical system with the time evolution $x_{t+1} = \mathcal{B}(x)$, where

$$\begin{aligned} \mathcal{B} \;&:\; [-2, 2] \to [-2, 2], \\ \mathcal{B}(x) \;&=\; b - x_t^2\,, \qquad t \in \mathbb{N}. \end{aligned} \tag{2.7}$$

It is called the *logistic equation*, with phase space $\mathcal{P} = [-2, 2]$. Surely, $\mathcal{B}$ is infinitely many times differentiable, but not invertible. Thus one can conclude that

Eq. (2.7) defines a non-invertible dynamical system. This concept is more elaborated in Sec. (2.2.1).

Definition 2.1.2 (**Invariant measure**)**.** Let $\{\psi^t\}_{t\in\Upsilon}$ be a dynamical system on $\mathcal{P}\subset\mathbb{R}^n$. Suppose $\mathcal{A}$ is the σ-algebra of Borel sets on $\mathcal{P}$ and let $\mu:\mathcal{A}\to[0,+\infty]$ be a measure on $\mathcal{A}$. Every mapping ψ^t is supposed to be $\mu-$measurable. The measure μ is called *invariant measure* under $\{\psi^t\}_{t\in\Upsilon}$ if $\mu(\psi^{-t}(A))=\mu(A)$ holds for all $A\in\mathcal{A}$ and $t\in\Upsilon$.

Definition 2.1.3 (**Classical dynamical system**)**.** Let $\mathcal{B}:X\to X$ be a mapping of a metric space X. A probability measure μ is $\mathcal{B}-$invariant when $\mu\left(\mathcal{B}^{-1}(A)\right)=\mu(A)$ for all $A\in\mathcal{A}$ for which $\mu(X)=1$. In this case the triplet $(X,\mu,\mathcal{B})$ is called *classical dynamical system.*

Definition 2.1.4 (**Time-reversal invariant**)**.** The dynamics $\mathcal{B}$ on a phase space $\mathcal{P}$ is said to be *time-reversal invariant* if there exist an involution $i:\mathcal{P}\to\mathcal{P}$, such that $i\mathcal{B}(x)=\mathcal{B}^{-1}i(x)$ for all $x\in\mathcal{P}$.

An involution is a function $i:\mathcal{P}\to\mathcal{P}$, that is equal to its inverse, *i.e.*, which gives the identity when applied to itself.

2.2 Examples of discrete-time dynamical systems

2.2.1 Logistic map

In this section we elaborate more on non-invertible map in the sense of singularity, cobweb structure and representation of discrete time logistic map both geometrically and algebraically, which is defined in former example (2.1.2).

A continuous differentiable non-invertible 1-dimensional map has at least one point where its derivative vanishes. The simplest such maps are quadratic polynomials, which can always be brought to the form $f(x)=b-x_n^2$ under a suitable

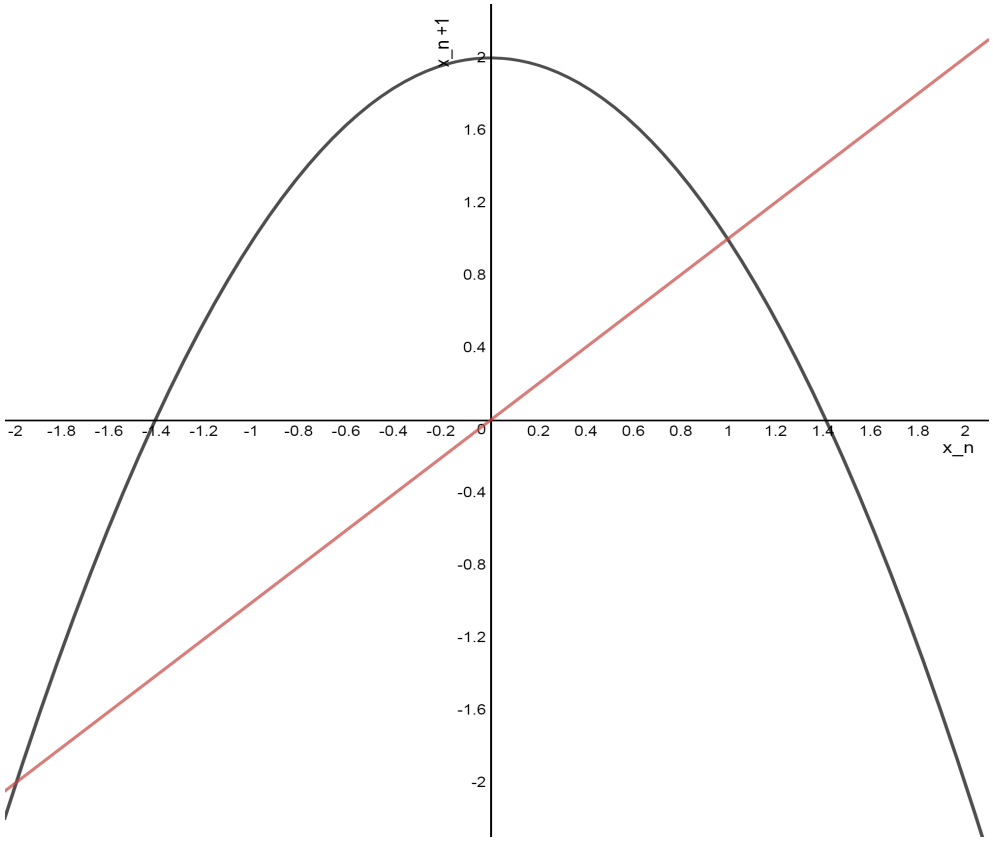

Figure 2.1: Illustration of logistic map represented in Eq. (2.8) with parameter $b = 2$. (Plot generated by *Desmos Graphing Calculator*).

change of variables. For the sake of simplicity we consider the 1-dimensional map[1]

$$x_{n+1} = b - x_n^2 \,, \tag{2.8}$$

which depend on a single parameter b. As seen in Fig. 2.1 the one-dimensional map displaying the singularity, one can also observe the singularity located at the critical point $x = 0$, which means that for every value in the range of map x_{n+1} has exactly two pre-images one is ranging on $-2 \leq x_n < 0$ and other $0 < x_n \leq 2$, this behaviour is a fundamental ingredient to generate chaos in one-dimensional maps. These maps are known as *unimodal*, if they have single critical point. *Unimodal* maps are fascinating for both physical and mathematical reasons. They produce a complicated chaos inspite of their simplicity in structure. With the varying degrees

[1]Another common variant of the logistic map is $x_{n+1} = \mu x_n(1 - x_n)$, with control parameter μ. This dynamics is equivalent for $\mu = 2b$.

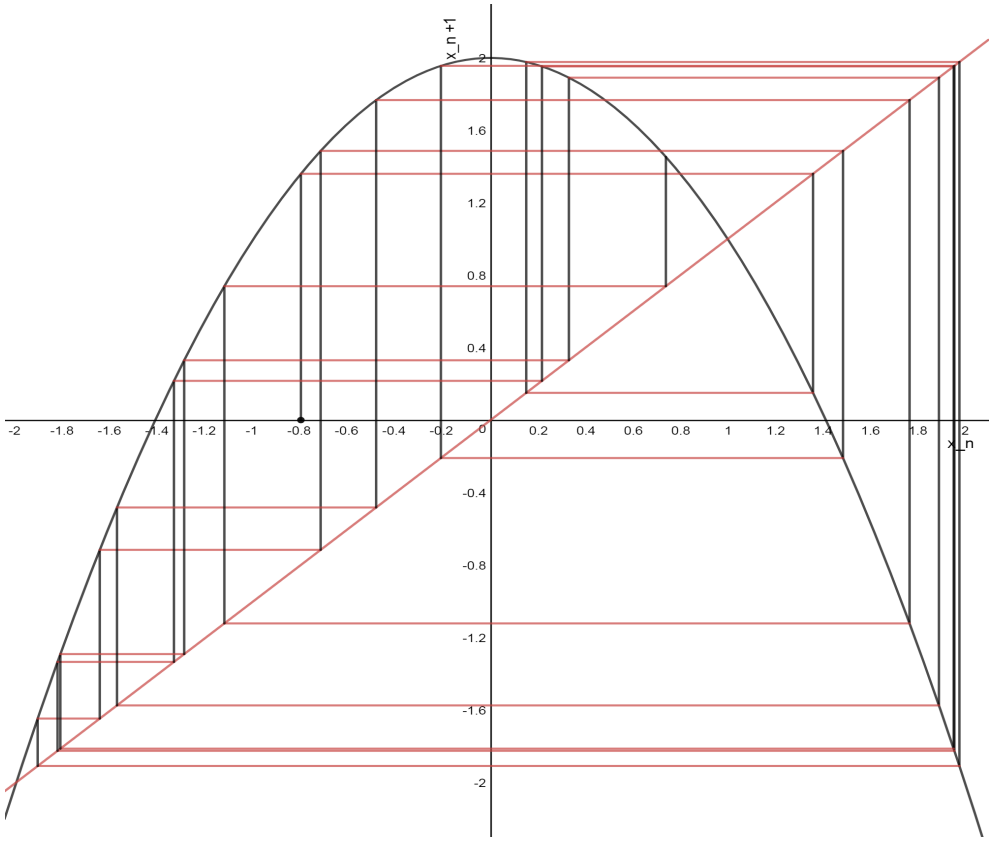

Figure 2.2: Graphical representation of iterating logistic map Eq. (2.8) with parameter $b = 2$. For the initial point $x_0 = -0.8$ we also show the cobweb structure along the diagonal $x_{n+1} = x_n$ and pre-images. (Plot generated by *Desmos Graphing Calculator*).

of success they have been used to model everything from insect populations to the on set of turbulence (see also [54]). As is frequently the case in dynamical frameworks theory, the evolution of the logistic map can be represented not only algebraically, as in Eq. (2.8), but also geometrically. Given a starting point x_n, the graph of the logistic map gives $x_{n+1} = f(x_n)$. To use x_{n+1} as the starting point of the next iteration, we must find the corresponding location in the x space. This is done simply by drawing the line from the point $[x_n, f(x_n)]$ to the diagonal. This simple construction is then repeated ad libitum, as illustrated in Fig. 2.2. What makes the study of the logistic map so important is not only that the organization in parameter space of these periodic and chaotic regimes can be completely understood with simple tools, but that, despite its simplicity, it displays the most important

features of low-dimensional chaotic behaviour. This map have that feature; first, it does not preserve the memory and second, if two trajectories start from their neighbourhood, after some point they differ.

2.2.2 Baker map

In Fig. 2.3 we geometrically define the well known baker map [45, 49], as a paradigmatic case of a two-dimensional area preserving chaotic dynamical system. The phase space is a unit square $M = [0,1] \times [0,1]$ in (x, y) plane. For $(x, y) \in M$. Let $(x, y) \to (x', y') = B(x, y)$, be

$$(x', y') = B(x, y) = \begin{cases} \left(2x, \frac{y}{2}\right), & \text{for} \quad 0 \leq x < \frac{1}{2}, \\ \left(2x - 1, \frac{y+1}{2}\right), & \text{for} \quad 1 \geq x \geq \frac{1}{2}. \end{cases} \tag{2.9}$$

The Baker map is measure preserving transformation that expands in the direction

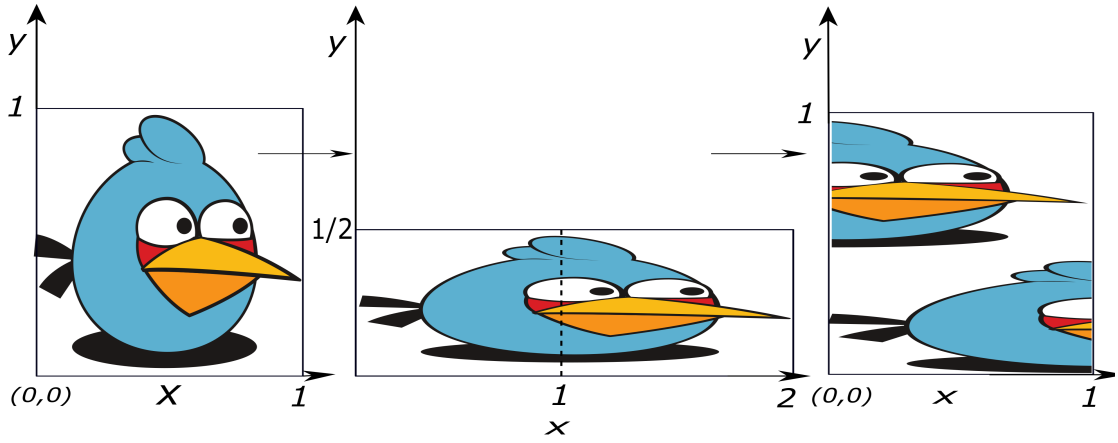

Figure 2.3: Baker's map transformation.

of x by factor 2, while it contracts in y direction by factor 1/2. The areas are arranged in such a way that the unit square is mapped onto itself at each unit of time (see figure 2.3).

The transformation consist of two steps: First the unit square is contracted in y-direction and stretched in the $x-$direction by a factor 2. This does not change the volume of any initial region. The unit square becomes a rectangle occupying the region $0 \leq x \leq 2$ and $0 \leq y \leq 1/2$. Next the rectangle is cut in the middle and the

right half is put on the top of the left half to recover a square. This does not change volume either. This transformation is reversible except on the lines where the area was chopped and glued back.

The Baker's map is invertible, thus the inverse of Baker's map $(x, y) \to (x', y') = B^{-1}(x, y)$ depends on whether transformation $y < 1/2$ or $y \geq 1/2$, thus we have:

$$(x', y') = B^{-1}(x, y) = \begin{cases} \left(\frac{x}{2},\, 2y\right), & \text{for} \quad y < \frac{1}{2}, \\ \left(\frac{x+1}{2},\, 2y-1\right), & \text{for} \quad y \geq \frac{1}{2}. \end{cases} \tag{2.10}$$

The Baker map $B(x, y)$ is mixing and ergodic [23]. It is worth mentioning that, due to the discontinuity in the map, the baker transformation is not a *diffeomorphism*. That is, it is not an example of continuously differentiable map with a continuous and continuously differentiable inverse. Still the discontinuity of the Baker's map poses no problems in many applications (see [18, 19, 62, 59, 41] Refs. are therein).

2.3 Deterministic normal and anomalous diffusion in one dimensional maps

In this section we review piecewise-linear maps for normal and anomalous diffusion. First we elaborate the concept of normal diffusion in section 2.3.1 by giving the well-known example of a drunken sailor [38], which is a random model. Then we explain how the same behaviour can be modeled a deterministic dynamics, called *box map*. Finally for anomalous diffusion, we study the *Pomeau-Manneville map* in section 2.3.2.

2.3.1 Normal diffusion

We start with revisiting the well-known example of a sailor who wants to go home, but is actually drunk so that he lost all control on his single steps. For sake of simplicity let us imagine that he moves in one dimension. He starts at a position $x = 0$ and then makes steps of a certain step length s to the left and to the right. Since he is completely drunk he looses all memory between any single steps, that is,

all steps are completely *uncorrelated* (pp. 20 of [38]). It resembles flipping a coin, to choose whether to go to one side or to the other at the next step. Now we look for the probability to find the sailor after t number of steps at position x *i.e.*, a distance $|x|$ away from the starting point.

For the sake of interest let us include a short historial note from literature: This "problem of considerable interest" was first formulated by *Karl Pearson* in a letter to the journal *Nature* in 1905. He asked for a solution, which was provided by Lord Rayleigh referring to older work by himself. *Pearson* concluded: "The lesson of *Lord Rayleigh's* solution is that in open country the most probable place to find a drunken man, who is at all capable of keeping on his feet, is somewhere near his starting point". This refers to the Gaussian probability distributions for the sailor's positions, which are obtained in a suitable scaling limit from a Gedankenexperiment with an "ensemble of sailor's" starting from their initial point. The mathematical reason behind the increasing Gaussianity of the probability distribution is the central limit theorem (pp. 21 of [38]).

Now let us quantify the speed by which a "droplet of sailors" starting at the initial point spreads out. This can be done by calculating the *diffusion coefficient* of this system, by which we can also extract the information of transport properties. Thus by Einstein formula (1905), the diffusion coefficient of 1-dimensional dynamics can be defined as [38]:

$$D := \lim_{t\to\infty} \frac{1}{2t}\langle x^2(t)\rangle, \tag{2.11}$$

where

$$\langle x^2(t)\rangle := \int \mathrm{d}x\, x^2 \rho_t(x), \tag{2.12}$$

is the second moment of the probability distribution $\rho_t(x)$ at each time step t, also known as *mean-square displacement* of the particles.

The spreading of the distribution of sailors is then quantified by the growth of the mean-square displacement in time. If this quantity grows linearly in time, which may not necessarily be the case but holds true in case our example [37], the magnitude of the diffusion coefficient D tells us how quickly our ensemble of sailors disperses. Of course, much more could be said about a statistical physics description

of diffusion, see [50] for further details.

In contrast to this well-known picture of diffusion as a stochastic random walk, the theory of dynamical systems makes it possible to treat diffusion as a *deterministic dynamical process*. Let us replace the sailor by a point particle. The orbit of such a particle starting at initial condition x_0 may then be generated by a chaotic dynamical system Eq. (2.4). Note that defining the one-dimensional map $\mathcal{B}(x)$ together with this equation yields the full microscopic equations of motion of the system. We may think of these equations as a caricature of Newton's equations of motion modeling the diffusion of a single particle (pp. 22 of [38]). Most importantly, in contrast to the drunken sailor with his memory loss after any time step here the complete memory of a particle is taken into account, that is, all steps are fully correlated. The decisive new fact that distinguishes this dynamical process from the one of a simple uncorrelated random walk is hence that x_{t+1} is uniquely determined by x_t, rather than having a random distribution of x_{t+1} for a given x_t. If the resulting dynamics of an ensemble of particles for given equations of motion has the property that a diffusion coefficient $D > 0$, Eq. (2.11), exists we speak of normal deterministic diffusion [18, 23, 36, 37]. When diffusion coefficient D is either zero or infinite we speak of anomalous diffusion. In Fig. 2.4 (right panel) we represent a simple piecewise-linear map of deterministic diffusion that we shall study, it depicts a *chain of boxes* of unit width, which continues periodically in both directions to infinity, and the orbit of a moving point particle. In each box the dynamics evolves according to the box map B_α [38]:

$$B_\alpha : (0,1) \to \left[1 - \frac{\alpha}{2}, \frac{\alpha}{2}\right),$$

$$B_\alpha(x) = \begin{cases} \alpha x, & \text{for} \quad 0 \le x < \frac{1}{2}, \\ \alpha x + 1 - \alpha, & \text{for} \quad \frac{1}{2} \le x < 1. \end{cases} \tag{2.13}$$

that is defined here on the unit interval. The slope $\alpha \geq 2$ defines a control parameter. For $\alpha = 2$ we recover the familiar *Bernoulli shift*, whereas for $\alpha > 2$ the map defines an open system. That is, whenever points are mapped into the escape region of width Δ these points are moved to a neighbouring unit interval. We may thus

periodically continue this box map onto the whole real line by defining

$$B_\alpha(x+1) = B_\alpha(x) + 1\,. \tag{2.14}$$

In physical terms, this means that $B_\alpha(x)$ continued onto the real line is translational

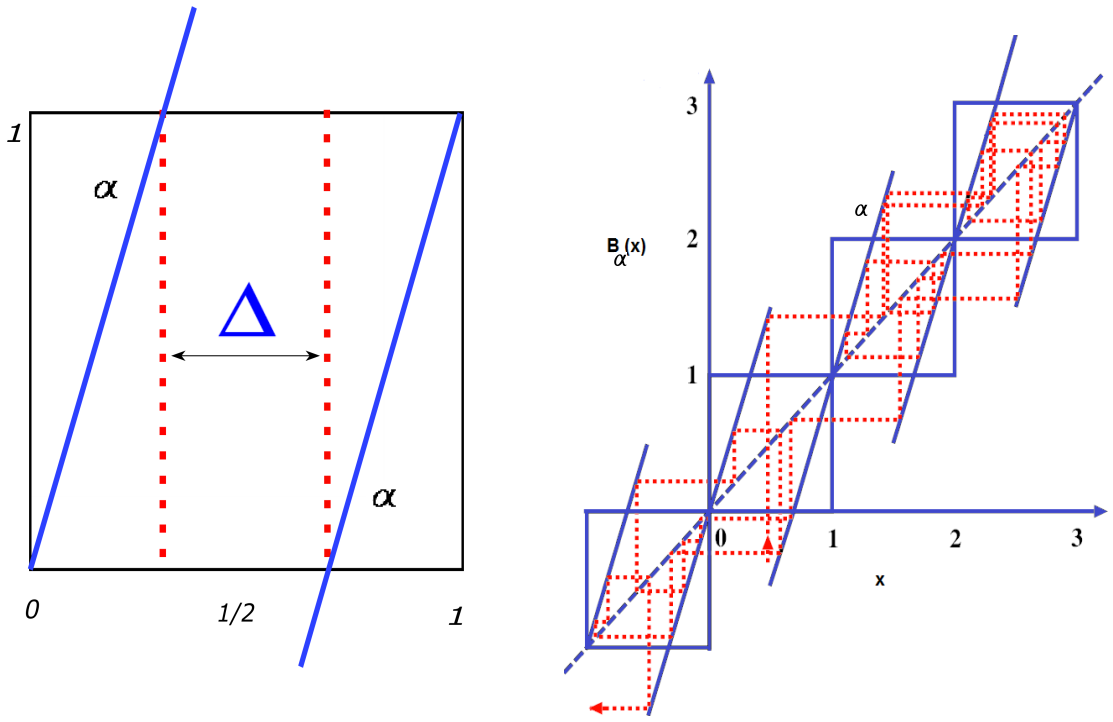

(a) The box map. (Plotted on Inkscape).

(b) The extended box map. (Fig. adapted from [38]).

Figure 2.4: (a) The box map $B_\alpha(x)$, defined in Eq. (2.13). The slope α defines the control parameter while Δ denotes the width of escape region. This is a generalization of the Bernoulli shift, defined as a parameter dependent map $B_\alpha(x)$ modeling an open system. (b) A simple model for deterministic diffusion. The dashed line depicts the orbit of a diffusing particle in form of a cobweb plot. The slope α serves as a control parameter for the periodically continued piece-wise linear map $B_\alpha(x)$.

invariant with respect to integers. Note furthermore that we have chosen a box map whose graph is point symmetric with respect to the center of the box at $(x, y) = \left(\frac{1}{2}, \frac{1}{2}\right)$ (pp. 23 of [38]). This implies that the graph of the full map $B_\alpha(x)$ is anti-

symmetric with respect to $x = 0$, *i.e.*,

$$B_\alpha(x) = -B_\alpha(-x), \tag{2.15}$$

so that there is no *drift*[2] in this chain of boxes [38]. Therefore this study generate unbiased random walk. Hence on the discrete level where we consider the integer part of $\lfloor x \rfloor$ Fig. 2.4b, it is equivalent to the binary random walk.

2.3.2 Anomalous diffusion

We now study anomalous diffusion by considering a variant of the piecewise-linear model. *Pomeau-Manneville*, introduced in 1980 [48], the following model

$$P_{\alpha,z} : [0,1] \to [0,1], \qquad P_{\alpha,z}(x) := x + \alpha\, x^z \bmod 1, \tag{2.16}$$

where again the dynamics is defined by $x_{n+1} = P_{\alpha,z}(x_n)$. The map has two control parameters, $\alpha \geq 1$ and the exponent of nonlinear behaviour $z \geq 1$. For $\alpha = z = 1$ the map reduces to the *Bernoulli shift*. However for $z > 1$ it provides a nontrivial nonlinear generalization: in this case the stability of the fixed point at $x = 0$ becomes marginal, $P'_{a,z}(0) = 1$. Since the map is smooth around $x = 0$, the dynamics resulting from the left lap of the map is largely determined by the stability of this fixed point, whereas the right lap is just of Bernoulli shift-type yielding ordinary chaotic dynamics [38].

Analogous to the discussion in Sec. 2.3.1 it is quite simple to define the spatially extended version of the Pomeau-Manneville map. For this we just continue

$$P_{\alpha,z}(x) = x + \alpha x^z, \qquad 0 \leq x < \frac{1}{2}, \tag{2.17}$$

onto the real line by the translation

$$P_{\alpha,z}(x+1) = P_{\alpha,z}(x) + 1\,, \tag{2.18}$$

under the symmetry $P_{\alpha,z}(-x) = -P_{\alpha,z}(x)$, (*cf.* Eqs. (2.14), (2.15)) and (2.16). The resulting dynamics is shown in Fig. 2.5. Analytical as well as numerical computation

[2]In general, when there is a higher probability to go one side the map is asymmetric. As a result the particles move in this direction on the average. This what we call drift.

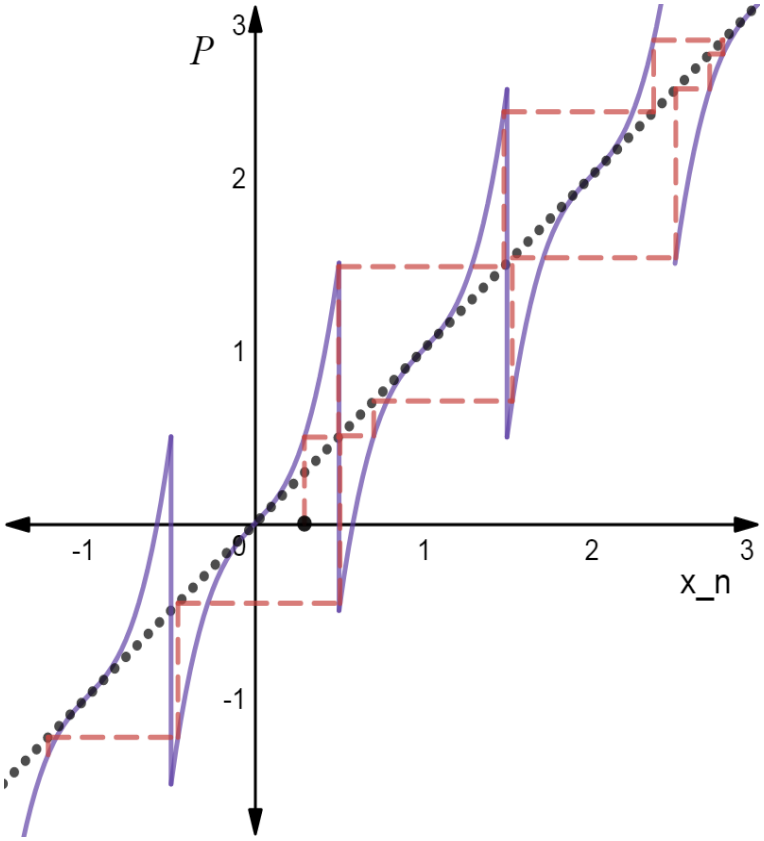

Figure 2.5: The extended Pomeau-Manneville map. (Plot generated by *Desmos Graphing Calculator*).

of the mean-square displacement for this map leads to subdiffusive behaviour, for $z > 2$

$$\langle x^2(n)\rangle = Kn^{\gamma}\,, \qquad \gamma < 1, \quad n \to \infty, \tag{2.19}$$

where K is the generalized diffusion coefficient. This implies that the diffusion coefficient D defined in Eq. (2.11) vanishes, despite the fact that particles can go anywhere on the real line as suggested by Fig. 2.5. Thus we encounter novel type of diffusion. The exponent $\gamma < 1$, in the mean square displacement Eq. (2.19) of an ensemble of particles, one says that there is sub-diffusion.

For sub-diffusive Pomeau-Manneville map Fig. 2.5 one can prove that

$$\gamma = \begin{cases} 1, & \text{for} \quad 1 \le z \le 2\,, \\ \dfrac{1}{z-1} < 1, & \text{for} \quad z > 2\,. \end{cases} \tag{2.20}$$

This finding can be obtained from stochastic continuous time random walk theory,

which yields a generalization of the drunken sailor's model, Fig. 2.4 to anomalous diffusion processes. For further discussion on this delicate topic we refer to the reader on Ref. [2].

2.4 Stochastic pathway

In this section we introduce Lévy walks and Lévy flights in the framework of continuous-time random walks (CTRW) [34, 27, 43, 55, 61].

Before going to the discussion we give definition of Lévy stable processes. We denote random variables by $X, X_1, X_2, \cdots$ and by $L_n = X_1 + X_2 + \cdots + X_n$ mutually independent random variables with a common distribution F and their sum [20].

Definition 2.4.1 (**Lévy stable processes**)**.** The distribution F, not concentrated at one point, is known as *stable* of for all $n \in \mathbb{N}$ there exists constants $k_n > 0$ and $\varkappa_n \in \mathbb{R}$, such that

$$L_n \stackrel{d}{=} k_n X + \varkappa_n \,, \tag{2.21}$$

where $\stackrel{d}{=}$ we mean that the random variables on the two side of the equality have the same distribution. If $\varkappa_n = 0$ the distribution is called *strictly stable*.

Let $P(x,t)$ be the probability distribution of being at position x at time t, and let $\Phi(x,t)$ be the probability distribution of making a step of length x in the time interval t to $t + \mathrm{d}t$. The total transition probability in this time interval is given by

$$\Phi(t) = \sum_x \Phi(x,t) = \Phi(j=0,t), \tag{2.22}$$

where $\Phi(j,t)$ is the Fourier transform $x \to j$ of $\Phi(x,t)$. If we denote by $\nu(x,t)$ the probability density of just arriving at x in the time interval t to $t+\mathrm{d}t$, then [27, 43, 61]

$$\nu(x,t) = \sum_{\bar{x}} \int_0^t \mathrm{d}\tau \; \nu(\bar{x},\tau)\, \Phi(x-\bar{x}, t-\tau) + \delta(t)\delta_{x,0}. \tag{2.23}$$

Here we assumed the initial condition of starting time at $t = 0$ from position x. The relation between $P(x,t)$ and $\nu(x,t)$ is given through

$$P(x,t) = \int_0^t \mathrm{d}\bar{\tau} \; \nu(x, t-\bar{\tau})\, \varrho(\bar{\tau}), \tag{2.24}$$

where

$$\varrho(t) = 1 - \int_0^t \mathrm{d}\tau\ \Phi(\tau), \tag{2.25}$$

is the probability of not having left the original site up to time t. The Laplace transform of $\varrho(t)$ yields

$$\varrho(u) = \left(1 - \Phi(u)\right)/u. \tag{2.26}$$

using Eq. (2.24) and changing the order of integration allows us to write Eq. (2.23) as an integral equation for $P(x,t)$ with Kernel $\Phi(x,t)$,

$$P(x,t) = \sum_{\bar{x}} \int_0^t \mathrm{d}\tau\ P(\bar{x},\tau)\,\Phi(x-\bar{x},t-\tau) + \varrho(t)\,\delta_{x,0}\,. \tag{2.27}$$

Reverting to the Fourier-Laplace space, we have

$$P(j,u) = P(j,u)\,\Phi(j,u) + \varrho(u), \tag{2.28}$$

with the solution

$$P(j,u) = \frac{1-\Phi(u)}{u}\,\frac{1}{1-\Phi(j,u)}\,, \tag{2.29}$$

this quantity is the key determination of $P(x,t)$ through Fourier-Laplace inversion. Before embarking on the discussion of Eq. (2.29), let us note that Eq. (2.27) is formally equivalent to generalized master equation [35]

$$\frac{\partial}{\partial t}P(x,t) = \sum_{\bar{x}} \int_0^t \mathrm{d}\tau\ K(x-\bar{x},t-\tau)\,P(\bar{x},\tau)\,, \tag{2.30}$$

when one takes in Fourier-Laplace space

$$K(j,u) = \frac{\Phi(j,u)-\Phi(u)}{1-\Phi(u)}\,u\,. \tag{2.31}$$

The equivalence is immediate when transforming Eq. (2.30) to (j,u) space and comparing to Eq. (2.31). Note that Eq. (2.30) is an integro-differential equation.

Now let us consider two different cases. First, when we take a distribution $\Phi(x,t)$ in which x and t are decoupled [13, 39], we have

$$\Phi(x,t) = \lambda(x)\Phi(t)\,. \tag{2.32}$$

From Eq. (2.29), we then get

$$P(j,u) = \frac{1-\Phi(u)}{u}\,\frac{1}{1-\lambda(j)\,\Phi(j,u)}\,. \tag{2.33}$$

Then assume $\Phi(t) = \delta(t-t_0)$ and let $\lambda(x)$ of Lévy stable form, with $\alpha \in (0,2)$. The resulting process in Markovian, but with diverging variance. The Fourier image of the associated probability density function is obtain from Eq. (2.33),

$$P(j,t) = e^{-D_\alpha |j|^\alpha\, t}, \tag{2.34}$$

where D_α is diffusion constant. Comparing this with Eq. (5.1) Chp. 5 of Ref. [39], we observe a characteristic function of a symmetric Lévy stable probability density function with the index of stability α. This type of random process is called *Lévy flight*.

As another example we consider a coupled form of $\Phi(x,t)$. A suitable function is of the form

$$\Phi(x,t) = A|x|^\eta \delta(|x| - t^\varsigma), \tag{2.35}$$

where, through the $\delta-$function, x and t are coupled. These processes are called *Lévy-walks*. Eq. (2.35) allows steps of arbitrary length as for Lévy flights, but long steps are penalized by the requiring longer time to be performed. Or, in other words, in a given time window only a finite shell of points may be reached: hierarchically nearer points are no more accessible and farther points are not yet accessible.

2.5 Auto-correlation functions

Correlations measure the relationship between two quantities, that are connected to each other. It allow us to determine the statistical relationship between them. Let us consider a dynamical system $\{\psi^t\}_{t\in\Upsilon}$ on the phase space $\mathcal{P}$ with ergodic[3] invariant measure μ. Let the mapping $\mathcal{H} : \mathcal{P} \to \mathbb{R}$, be an arbitrary continuous function, $\{\psi^t\}_{t\geq 0}$ be an arbitrary semi orbit and let the space average $\int_{\mathcal{P}} \mathcal{H}\,\mathrm{d}\mu$, [4] be

[3]Ergodicity entails that for almost all trajectories, the ensemble average and the time average produce the same result.

[4]Where $\mathcal{H}$ is integrable function $\mathcal{H} \in L^1(\mathcal{P},\mathcal{A},\mu)$ and $\int_{\mathcal{P}} \mathcal{H}\,\mathrm{d}\mu$ for μ-a.e. points $x \in \mathcal{P}$.

replaced by the time average $\widehat{\mathcal{H}}$, *i.e.*,

$$\lim_{T\to\infty}\frac{1}{T}\int_0^T \mathcal{H}(\psi^t(x))\,\mathrm{d}t\,, \qquad \text{and} \qquad \lim_{n\to\infty}\frac{1}{n}\sum_{i=0}^{n-1}\mathcal{H}(\psi^i(x))\,, \tag{2.36}$$

for continuous and discrete time systems respectively. With respect to $\mathcal{H}$ the *auto-correlation function* along with the semi orbit to a time point $\tau \geq 0$, is defined for flow as follows

$$C^{\mathcal{H}}(\tau) := \lim_{T\to\infty}\frac{1}{T}\int_0^T \mathcal{H}(\psi^{t+\tau}(x))\,\mathcal{H}(\psi^t(x))\,\mathrm{d}t - \widehat{\mathcal{H}}^2\,, \tag{2.37a}$$

and for a discreet system by

$$C^{\mathcal{H}}(\tau) := \lim_{n\to\infty}\frac{1}{n}\sum_{i=0}^{n-1}\mathcal{H}(\psi^{i+\tau}(x))\,\mathcal{H}(\psi^i(x)) - \widehat{\mathcal{H}}^2\,. \tag{2.37b}$$

2.6 Summary

We revisited the notion of dynamical system and presented some definitions and examples for continuous and discrete-time dynamical system. We revisited deterministic dynamics based on the examples of the logistic and the baker's map. Further we discussed a piece-wise linear map showing deterministic standard diffusion and a piece-wise nonlinear map that generates sub-diffusion. Under this discussion we will base some on our studies on deterministic maps in forthcoming chapters. Finally we briefly overview the continuous-time random-walk framework, with aim to investigate stochastic process. This general framework will be the base of our study of LLg model in forthcoming chapter.

Chapter 3

Moments and correlations in the Slicer Map

"Mathematics is the language with which GOD wrote the universe."

— Galileo Galilei

In this chapter, we consider a simple non-chaotic and deterministic map, which we call Slicer Map. Its dynamics exhibits a wide spectrum of diffusive behaviours *i.e.*, sub-, super- and normal under variation of a single parameter. Such analytically tractable deterministic maps are rare in the literature of anomalous transport but Salari *et al.* [53] introduced this map and calculated its moments of displacement. Here we compute moments of displacement in an alternate fashion and we go one step further in the characterization, computing the position auto-correlation function in a scaling form. We also compute the moments of velocity and the velocity auto-correlation function.

3.1 Definition of the SM

To define the SM we introduce the fundamental space unit $M := [0, 1]$, consisting of the interval of positions. Replicating M in a one dimensional lattice, we produce the infinite configuration space: $\widehat{M} := M \times \mathbb{Z}$. Each of its cells is identified by an

index $m \in \mathbb{Z}$: $\widehat{M}_m := [0,1] \times \{m\}$. Every cell $\widehat{M}_m$ contains two *"slicers"*,

$$\{\ell_m\} \times \{m\}\,, \quad \text{and} \quad \{1-\ell_m\} \times \{m\}\,,$$

with $0 < \ell_m < 1/2$. The slicers split each half of $\widehat{M}_m$ into two parts. Salari *et al.* [53] parameterised the value of ℓ_m by a positive number α as follows:

$$\ell_m(\alpha) = \frac{1}{(|m| + 2^{1/\alpha})^{\alpha}}\,, \qquad \text{with} \quad m \in \mathbb{Z}\,, \quad \alpha > 0\,. \tag{3.1}$$

The SM, $S_\alpha : \widehat{M} \to \widehat{M}$, is then defined on the configuration space $\widehat{M} := [0,1] \times \mathbb{Z}$ as follows:

$$S_\alpha(x,m) = \begin{cases} (x, m-1)\,, & \text{for} \quad 0 \le x \le \ell_m \text{ or } \frac{1}{2} < x \le 1-\ell_m, \\ (x, m+1)\,, & \text{for} \quad \ell_m < x \le \frac{1}{2} \text{ or } 1-\ell_m < x \le 1. \end{cases} \tag{3.2}$$

The map is neither injective nor surjective. It is nevertheless possible to define the inverse map when restricting to trajectories with initial conditions in cell $\widehat{M}_0$ [53].

The space $\widehat{M}$ can be enowed with a density of points that evolves under the action of S_α. In particular, we consider the initial density $\hat{\mu} := \lambda \times \delta_0$ on $\widehat{M}$, where λ is the Lebesgue measure on M and δ_0 is the Dirac measure on the integer 0. Then, S_α can be interpreted as describing the transport of non-interacting particles in a one-dimensional space.[1]

Let $\pi_{[0,1]}$ and $\pi_{\mathbb{Z}}$ be the projections of $\widehat{M}$ on its first and second factors, respectively. Taking $x \in [0,1]$ and $m \in \mathbb{Z}$, we denote by $\hat{\mathbf{x}} = (x,m)$ a point in $\widehat{M}$, so that $\pi_{[0,1]}\hat{\mathbf{x}} = x$ and $\pi_{\mathbb{Z}}\hat{\mathbf{x}} = m$. Following [53] we restrict our considerations to the initial distribution $\hat{\mu}$. We view $\widehat{M}$ as subdivided in two halves that are invariant for the SM:

$$\widehat{M}^+ := ([1/2,1] \times \{0\}) \cup ([0,1] \times \mathbb{Z}^+),$$

and

$$\widehat{M}^- := ([0,1/2) \times \{0\}) \cup ([0,1] \times \mathbb{Z}^-).$$

[1]The "particles" are the points moved by S_α. Analogously to the particles of systems such as the extended box map defined in Fig. 2.4b they do not interact with each other, since there is no coupling term connecting various particles in their equations of motion.

The dynamics in the two intervals are the mirror images of each other. Indeed, since at $m = 0$ the two slicers coincide with the single $\ell_0 = 1/2$, *cf.* Eq. (3.1). The points that lie initially in $[1/2, 1]$ never reach negative m, and those initially in $[0, 1/2)$ never reach positive m. Therefore, without loss of generality we restrict the following analysis to the positive part of the chain, $\widehat{M}^+$. The sequence of integers $\pi_{\mathbb{Z}}(S^j(\hat{\mathtt{x}}))$, $j \in \mathbb{N}$, will be called the *coarse-grained trajectory* of $\hat{\mathtt{x}}$. A crucial aspect

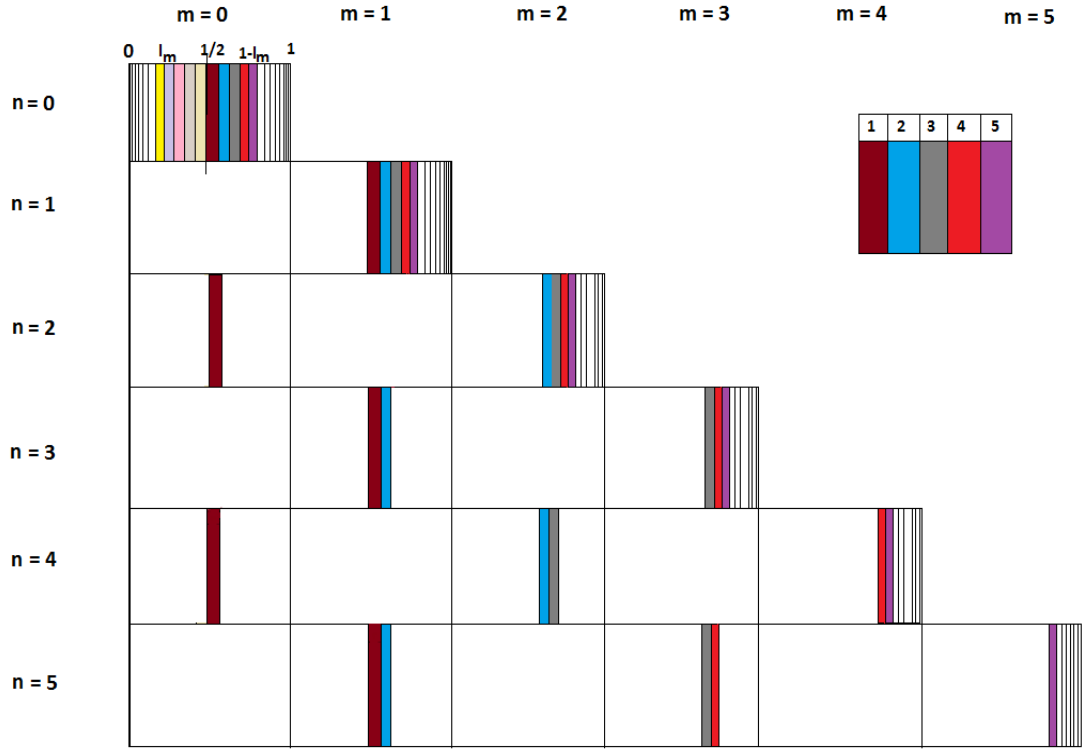

Figure 3.1: Dynamics of the SM illustrated by a space-time plot where m's and n's denote space and time respectively. The colors guide the eye, identifying the motion of points with different position $x \in [0, 1]$.

of the dynamics S_α is, analogous to polygonal billiards and its Lyapunov exponents vanish. Different trajectories in $\widehat{M}$ neither converge nor diverge from each other in time, except when they are separated by a slicer. In that case their distance jumps discontinuously. However, the set of separation points is discrete, it has zero $\hat{\mu}$-measure. Hence the Lyapunov exponent vanishes.

3.2 Dynamics of the SM

To illustrate some fundamental properties of the slicer dynamics, let us introduce the symbols

$$\ell_m^+(\alpha) := 1 - \ell_m(\alpha) = 1 - \frac{1}{(m + 2^{1/\alpha})^\alpha}, \qquad \text{with} \quad m \in \mathbb{N} \cup \{0\}\,. \tag{3.3}$$

They obey

$$\frac{1}{2} = \ell_0^+(\alpha) < \ell_1^+(\alpha) < \cdots < \ell_k^+(\alpha) < \ell_{k+1}^+(\alpha) < \cdots < 1, \quad \text{and} \quad \lim_{k\to\infty} \ell_k^+(\alpha) = 1\,. \tag{3.4}$$

Hence, there is a unique natural number $\overline{m} = \overline{m}_\alpha(x) > 0$ for any $x \in [1/2, 1)$ such that

$$\ell_{\overline{m}-1}^+(\alpha) < x \leq \ell_{\overline{m}}^+(\alpha)\,. \tag{3.5}$$

In other words:

$$\overline{m}_\alpha(x) = \min\{m \in \mathbb{N} : \ell_m^+(\alpha) \geq x\}, \qquad \text{for } x \in [1/2, 1)\,. \tag{3.6}$$

Inspection of Eq. (3.2) and the definition (3.3) reveals that $\overline{m}_\alpha(x)$ is the maximum travelled distance for trajectories starting in the interval, Eq. (3.5):

Lemma 3.2.1.: *Given $x \in [1/2, 1)$, let $\overline{m}(x)$ be the integer that satisfies Eq. (3.5). Then,*

$$S_\alpha(x, \overline{m}_\alpha(x)) = (x, \overline{m}_\alpha(x) - 1), \qquad S_\alpha(x, \overline{m}_\alpha(x) - 1) = (x, \overline{m}_\alpha(x)). \tag{3.7}$$

Proof. This is a straightforward consequence of Eqs. (3.2) and (3.5). □

This means that all trajectories become periodic with period 2 after the a number $\overline{m}_\alpha(x)$ of steps. The description of the trajectory

$$\{S_\alpha^j(\hat{\mathtt{x}})\}_{j=0}^\infty,$$

with initial condition $\hat{\mathtt{x}} \in \widehat{M}_0$ is completed by the following Proposition.

Proposition 3.2.2.: *For $x \in [1/2, 1)$, let $\hat{\mathtt{x}}_0 = (x, 0) \in \widehat{M}_0$ and $\overline{m}_\alpha(x)$ as defined by Eq.* (3.6)*. Then the iterations of the trajectory starting at $\hat{\mathtt{x}}_0$ obey:*

$$S^k_\alpha(x,0) = \begin{cases} (x,k)\,, & \text{for} \quad 0 \quad \leq k < \overline{m}_\alpha(x)\,, \\ (x, \widetilde{m}_{\alpha,k}(x))\,, & \text{for} \quad \overline{m}_\alpha(x) \leq k\,, \end{cases} \tag{3.8a}$$

where

$$\widetilde{m}_{\alpha,k}(x) = \begin{cases} \overline{m}_\alpha(x)\,, & \text{for} \quad (k - \overline{m}_\alpha(x)) \ \textit{is even}\,, \\ \overline{m}_\alpha(x) - 1\,, & \text{for} \quad (k - \overline{m}_\alpha(x)) \ \textit{is odd}\,. \end{cases} \tag{3.8b}$$

Proof. This is a consequence of Lemma 3.2.1 and Eq. (3.2). As long as $k < \overline{m}_\alpha(x)$, the forthcoming iteration with S_α increases the cell index by one. For $k \geq \overline{m}_\alpha(x)$ the trajectory alternates between the cells $\overline{m}_\alpha(x)$ and $\overline{m}_\alpha(x) - 1$. □

Remark 3.2.3. *Lemma 3.2.1 and Proposition 3.2.2 imply that every trajectory starting at $\hat{\mathtt{x}}$ with $\pi_{[0,1]}(\hat{\mathtt{x}}) \in [1/2, 1)$ is ballistic for a finite time. Eventually, it gets localised, turning periodic of period* 2*.*

Remark 3.2.4. *The trajectories starting at $\hat{\mathtt{x}}$ with $\pi_{[0,1]}(\hat{\mathtt{x}}) = 1/2$ or $\pi_{[0,1]}(\hat{\mathtt{x}}) = 1$ do not satisfy Eq.* (3.5)*. Hence, they are forever ballistic, but they constitute a set of zero measure.*

To investigate the transport properties of the SM, we observe that the function

$$\overline{m}_\alpha(x) : (1/2,\ 1) \to \mathbb{N}, \tag{3.9}$$

is a step function with unitary jumps at the points $\ell^+_m(\alpha)$, such that

$$x \in (\ell^+_{k-1}(\alpha), \ell^+_k(\alpha)] \mapsto \overline{m}_\alpha(x) = k\,. \tag{3.10}$$

Then, the following properties are satisfied:

1. $\overline{m}_\alpha(x)$ is not decreasing: $x_1 < x_2$ implies $\overline{m}_\alpha(x_1) \leq \overline{m}_\alpha(x_2)$,
2. $\overline{m}_\alpha(x)$ is left continuous: $\lim_{h\to 0^-} \overline{m}_\alpha(\ell^+_k(\alpha) + h) = \overline{m}_\alpha(\ell^+_k(\alpha)) = k$,
3. $\lim_{x\to 1/2^+} \overline{m}_\alpha(x) = 1,\ \lim_{x\to 1^-} \overline{m}_\alpha(x) = \infty$,

4. $\alpha_1 < \alpha_2$ implies $\overline{m}_{\alpha_1}(x) \geq \overline{m}_{\alpha_2}(x)$, since $\ell_j^+(\alpha_1) > \ell_j^+(\alpha_2)$ for $j > 0$.

The points belonging to a strip $(\ell_{k-1}^+(\alpha), \ell_k^+(\alpha)] = \overline{m}_\alpha^{-1}(k)$ share the same fate. Hence, the transport properties of the SM depend on the rate at which such strips shrink with growing k.

Indeed, an ensemble of initial conditions

$$\widehat{E}_0 \subset (1/2, x_0) \times \{0\} \subset \widehat{M}_0, \qquad \text{with} \quad x_0 < 1,$$

represents a coarse-grained version of the Dirac δ initial distribution, as commonly considered in diffusion theory. This ensemble reaches localisation: the set

$$\{\pi_{\mathbb{Z}}(S_\alpha^j(\widehat{E}_0)),\, j \in \mathbb{N}_0\},$$

is bounded. After all, the travelled distance does not exceed $\overline{m}_\alpha(x_0)$, which is finite. Consequently, non-trivial transport properties *necessarily* require the initial ensemble $\widehat{E}_0$ to obey the condition:

$$\sup_{x \in \pi_{[0,1]}(\widehat{E}_0)} \overline{m}_\alpha(x) = \infty, \tag{3.11a}$$

or, equivalently, to accumulate at $x = 1$:

$$\sup(\pi_{[0,1]}(\widehat{E}_0)) = 1\,. \tag{3.11b}$$

The condition (3.11a) (or (3.11b)) is not sufficient for non-trivial behaviour. To understand this fact, take an ensemble of *uniformly distributed* initial conditions in $\widehat{E}_0 \subset (1/2, 1) \times \{0\}$ —analogous to the setting in [10]—and characterise the transport properties of the SM by computing the corresponding ensemble averages. Then, $\overline{m}_\alpha(x)$ is the distance travelled by the point $\hat{\mathbf{x}} \in \widehat{E}_0$, with $\pi_{[0,1]}(\hat{\mathbf{x}}) = x$. Consequently, the *mean maximum displacement* and the *mean maximum square displacement* are given by

$$\langle \Delta \hat{\mathbf{x}} \rangle = \frac{1}{\lambda(\pi_{[0,1]}(\widehat{E}_0))} \int\limits_{\pi_{[0,1]}(\widehat{E}_0)} \overline{m}_\alpha(x)\, \mathrm{d}x, \tag{3.12}$$

and

$$\langle \Delta \hat{\mathbf{x}}^2 \rangle = \frac{1}{\lambda(\pi_{[0,1]}(\widehat{E}_0))} \int\limits_{\pi_{[0,1]}(\widehat{E}_0)} \overline{m}_\alpha^2(x)\, \mathrm{d}x, \tag{3.13}$$

respectively, where $\lambda(\pi_{[0,1]}(\widehat{E}_0)) \leq 1/2$ is the Lebesgue measure of the projection of $\widehat{E}_0$ on $[0,1]$.

These averages do not depend on time. However, they indicate what can be expected for the time evolution of the average travelled distance and mean-square distance. To understand this point, we observe that in each interval $(\ell^+_{k-1}(\alpha), \ell^+_k(\alpha)]$, $k \in \mathbb{N}$ the function $\overline{m}_\alpha(x)$ takes the constant value k. We denote the length of these intervals by:

$$\Delta_k(\alpha) := \ell^+_k(\alpha) - \ell^+_{k-1}(\alpha)\,. \tag{3.14a}$$

By construction their length adds up to $1/2$,

$$\sum_{k=1}^{\infty} \Delta_k(\alpha) = \frac{1}{2}\,, \tag{3.14b}$$

and to leading order in k, we have:

$$\Delta_k(\alpha) = \frac{\alpha}{k^{\alpha+1}} \left(1 - \frac{\tilde{c}(\alpha)}{k} + \mathcal{O}(k^{-2})\right), \tag{3.14c}$$

with

$$\tilde{c}(\alpha) = (1+\alpha)\,\left(2^{1/\alpha} - \frac{1}{2}\right).$$

Then, for $\widehat{E}_0 = (1/2, 1) \times \{0\}$, one finds

$$\langle \Delta\hat{\mathrm{x}} \rangle = 2\int_{1/2}^{1} \overline{m}_\alpha(x)\; \mathrm{d}x = 2\sum_{k=1}^{\infty} k\,\Delta_k(\alpha) = 2\sum_{k=1}^{\infty} \frac{\alpha}{k^\alpha}\,\left(1 + \mathcal{O}(k^{-1})\right), \tag{3.15a}$$

where Eqs. (3.10) and (3.14c) have been used. Thus, $\langle \Delta\hat{\mathrm{x}} \rangle$ converges for $\alpha > 1$, and it diverges otherwise. Analogously, the mean maximum square displacement is

$$\langle \Delta\hat{\mathrm{x}}^2 \rangle = 2\int_{1/2}^{1} \overline{m}^2_\alpha(x)\; \mathrm{d}x = 2\sum_{k=1}^{\infty} k^2\Delta_k(\alpha) = 2\sum_{k=1}^{\infty} \frac{\alpha}{k^{\alpha-1}}\,\left(1 + \mathcal{O}(k^{-1})\right). \tag{3.15b}$$

For $\alpha > 2$ the square displacement, $\langle \Delta\hat{\mathrm{x}}^2 \rangle$, is finite. This corresponds to the localisation phenomenon described in Remark 6 of [53]. It arises from the fact that $\ell^+_k(\alpha)$ tends to 1 faster, and the transport of the SM is slower, for larger α. On the other hand, for $0 < \alpha < 2$ the mean maximum square displacement diverges, and it is of interest to explore the rate at which this divergence takes place, *i.e.* to determine the *transport exponent* γ.

3.3 Time evolution of the displacement moments

Under the SM each particle moves by exactly one step in each time step. Hence, trajectories reach at most site n in n time steps, and the distance $\Delta\hat{\mathtt{x}}_n$ travelled by $\hat{\mathtt{x}} = (x, 0)$ at time n is given by

$$\min\{\widetilde{m}_{\alpha,n}(x), n\}\,, \tag{3.16}$$

cf. Eq. (3.8). Moreover, for even and odd times n the displacement $\Delta\hat{\mathtt{x}}_n$ also takes even and odd values, respectively. The corresponding (time-dependent) mean-square displacement can be written as:

$$\begin{aligned}\langle\Delta\hat{\mathtt{x}}_n^2\rangle &= 2\int_{1/2}^{1}\min\{\widetilde{m}_{\alpha,n}(x), n\}^2\,\mathrm{d}x,\\ &= \begin{cases} 2\sum\limits_{i=1}^{(n/2)-1}(2i)^2\left(\Delta_{2i}(\alpha)+\Delta_{2i+1}(\alpha)\right)+2n^2\sum\limits_{k=n}^{\infty}\Delta_k(\alpha)\,, & \text{for n even}\,,\\ 2\sum\limits_{i=1}^{(n-1)/2}(2i-1)^2\left(\Delta_{2i-1}(\alpha)+\Delta_{2i}(\alpha)\right)+2n^2\sum\limits_{k=n}^{\infty}\Delta_k(\alpha)\,, & \text{for n odd}\,. \end{cases}\end{aligned} \tag{3.17a}$$

The sums involving terms $k \geq n$ collect the particles that make n steps to the right and never turned back. Salari *et al.* [53] denoted this as the travelling area. It is the same in both cases. The other sum accounts for particles that turn back at least once. Consequently, the particles get localised within n time steps. This represents sub-travelling area in [53]. To leading order this contribution to the mean-square displacement takes the same for odd and even n. Hence, we write:

$$\begin{aligned}\langle\Delta\hat{\mathtt{x}}_n^2\rangle &= 2\int_{1/2}^{1}\min\{\widetilde{m}_{\alpha,n}(x), n\}^2\,\mathrm{d}x,\\ &= 2\sum_{k=1}^{n-1}k^2\Delta_k(\alpha)\,\left(1+\mathcal{O}(k^{-1})\right)+2n^2\sum_{k=n}^{\infty}\Delta_k(\alpha)\,.\end{aligned} \tag{3.17b}$$

The asymptotic behaviour of the first sum is:[2]

$$\begin{aligned}2\sum_{k=1}^{n-1}k^2\Delta_k(\alpha) &= 2\sum_{k=1}^{n-1}\frac{\alpha}{k^{\alpha-1}}\,\left(1+\mathcal{O}(k^{-1})\right),\\ &\sim \begin{cases} \frac{2\,\alpha}{2-\alpha}n^{2-\alpha}\,, & \text{for}\quad 0<\alpha<2\,,\\ 4\,\ln n\,, & \text{for}\quad \alpha=2\,,\\ \text{const}\,, & \text{for}\quad \alpha>2\,. \end{cases}\end{aligned} \tag{3.18a}$$

[2]By $f_1(n) \sim f_2(n)$ we mean $f_1(n)/f_2(n) \to 1$ as $n \to \infty$.

The form of this scaling can be guessed by interpreting the sum as a Riemann-sum approximation of the integral $\int_1^n x^{1-\alpha}\,\mathrm{d}x$. A formal derivation is given in Appendix A. The second sum can be evaluated based on the definition of $\Delta_k(\alpha)$,

$$2\,n^2\sum_{k=n}^{\infty}\Delta_k(\alpha) = 2\,n^2\,\ell_{n-1}(\alpha) = 2\,n^2\,n^{-\alpha}\left(1-\frac{\alpha\,2^{1/\alpha}}{n}+\mathcal{O}(n^{-2})\right)\sim 2\,n^{2-\alpha}\,. \tag{3.18b}$$

Remark 3.3.1. *According to Eqs.* (3.18a) *and* (3.18b) *the travelling and the sub-travelling areas have the same asymptotic scaling.*

Altogether, we find that the mean-square displacement scales like

$$\langle\Delta\hat{\mathrm{x}}_n^2\rangle \sim \begin{cases} \frac{4}{2-\alpha}\,n^{2-\alpha}\,, & \text{for} \quad 0<\alpha<2\,,\\ 4\,\ln n\,, & \text{for} \quad \alpha=2\,,\\ \text{const}\,, & \text{for} \quad \alpha>2\,. \end{cases} \tag{3.19}$$

The computation of other moments $\langle|\Delta\hat{\mathrm{x}}_n|^p\rangle$, with $p>\alpha$, can be obtained in the same way, based on the same integral representation:

$$\begin{aligned} \langle|\Delta\hat{\mathrm{x}}_n|^p\rangle &= 2\int_{1/2}^{1}\min\{\widetilde{m}_{\alpha,n}(x),n\}^p\,\mathrm{d}x,\\ &\sim 2\sum_{k=1}^{n-1}k^p\Delta_k(\alpha)\left(1+\mathcal{O}(k^{-1})\right)+2n^p\sum_{k=n}^{\infty}\Delta_k(\alpha),\\ &\sim \begin{cases} \frac{2p}{p-\alpha}\,n^{p-\alpha}\,, & \text{for} \quad 0<\alpha<p\,,\\ 2\,p\,\ln n\,, & \text{for} \quad \alpha=p\,,\\ \text{const}\,, & \text{for} \quad \alpha>p\,, \end{cases} \end{aligned} \tag{3.20}$$

because

$$\sum_{k=1}^{n-1}k^p\Delta_k(\alpha) = 2\sum_{k=1}^{n-1}\frac{\alpha}{k^{\alpha-p+1}}\left(1+\mathcal{O}(k^{-1})\right)\sim\begin{cases} \frac{2\alpha}{p-\alpha}\,n^{p-\alpha}\,, & \text{for} \quad 0<\alpha<p\,,\\ 2\,p\,\ln n\,, & \text{for} \quad \alpha=p\,,\\ \text{const}\,, & \text{for} \quad \alpha>p\,. \end{cases} \tag{3.21}$$

We hence reproduced central results of [53] in a formalism that is suitable to compute correlation functions. These findings are summarised by the following theorem.

Theorem 3.3.2.: *Given $\alpha \geq 0$, the transport coefficient of the Slicer Dynamics with uniformly distributed initial condition in $\widehat{M}_0$ takes the value $\gamma = 2 - \alpha$, and the the dynamics is:*

1. *ballistic if $\alpha = 0$,*
2. *super-diffusive if $0 < \alpha < 1$,*
3. *diffusive if $\alpha = 1$,*
4. *sub-diffusive if $1 < \alpha < 2$,*
5. *with logarithmic growth of the mean-square displacement, $\langle \Delta\hat{\mathrm{x}}_n^2 \rangle \sim \ln n$, for $\alpha = 2$,*
6. *with localisation in mean-square displacement, $\langle \Delta\hat{\mathrm{x}}_n^2 \rangle \sim const(\alpha)$, if $\alpha > 2$.*

Furthermore, for $p > \alpha$ the moments satisfy $\langle |\Delta\hat{\mathrm{x}}_n|^p \rangle \sim n^{p-\alpha}$.

Remark 3.3.3.: *The behaviour described above for a given α is not universal. It depends on the initial distribution.*

For instance, suppose that the x-component of the initial conditions has got density ρ with respect to the uniform measure $\mathrm{d}x$ in the interval $(1/2, 1)$. Then, we have

$$\langle \Delta\hat{\mathrm{x}}_n^2 \rangle_\rho = 2 \int_{1/2}^{1} \min\{\widetilde{m}_{\alpha,n}(x), n\}^2 \, \rho(x) \, \mathrm{d}x, \tag{3.22}$$

in place of Eq. (3.17). If the support of ρ does not contain a (left) neighbourhood of 1, then $\langle \Delta\hat{\mathrm{x}}_n^2 \rangle \to$ const as $n \to \infty$ even for $\alpha < 1$. Moreover, different asymptotic behaviours arise from different distributions supported in a neighbourhood of 1. For instance, take $\rho(x) = \mathcal{O}((1-x)^r)$ as $x \to 1^-$ with $r > -1$. Then, different values of r produce different kinds of diffusion, even at fixed α.

To see this we work out the specific example

$$\rho(x) = \begin{cases} r\, 2^{r-1} \left(\frac{1}{2} - x\right)^{r-1}, & \text{for} \quad 0 \leq x \leq \frac{1}{2}, \\ r\, 2^{r-1} \, (1-x)^{r-1}, & \text{for} \quad \frac{1}{2} < x \leq 1. \end{cases} \tag{3.23}$$

Analogously to the treatment of Eq. (3.17) the expression Eq. (3.22) can be split into the sums

$$\langle \Delta\hat{\mathrm{x}}_n^2 \rangle_\rho = 2 \int_{1/2}^{1} \min\{\widetilde{m}_{\alpha,n}(x), n\}^2 \, \rho(x) \, \mathrm{d}x \;\; \sim \;\; 2 \sum_{k=1}^{n} k^2 \int_{x_{k-1}}^{x_k} \rho(x) \, \mathrm{d}x + 2n^2 \int_{x_n}^{1} \rho(x) \, \mathrm{d}x \,, \tag{3.24}$$

because $\widetilde{m}_{\alpha,k}(x) = k + \mathcal{O}(1)$ in the interval $(x_{k-1}, x_k] \equiv (\ell_{k-1}^+(\alpha), \ell_k^+(\alpha)]$. Previously, we found that

$$\Delta_k(\alpha) = \int_{x_{k-1}}^{x_k} \mathrm{d}x.$$

For the power-law form of $\rho(x)$ this result changes to

$$2^{r-1} \, \Delta_k(\alpha; r) = \int_{x_{k-1}}^{x_k} \rho(x) \, \mathrm{d}x,$$

with

$$\Delta_k(\alpha; r) := (k - 1 + 2^{1/\alpha})^{-\alpha r} - (k + 2^{1/\alpha})^{-\alpha r}.$$

Since $\Delta_k(\alpha \, ; r) \sim \Delta_k(r \, \alpha)$, the evaluation of Eq. (3.22) is analogous to the one of Eq. (3.17). Equation (3.22) can therefore be worked out along the same lines as Eq. (3.17), after substituting $\Delta_k(\alpha)$ by $2^{r-1} \, \Delta_k(r \, \alpha)$. One thus finds that

$$\langle \Delta\hat{\mathrm{x}}_n^2 \rangle_\rho \sim \begin{cases} \frac{2^{r+1}}{2-r\alpha} \, n^{2-r\alpha} \,, & \text{for} \quad 0 < r \, \alpha < 2 \,, \\ 2^{r+1} \, \ln n \,, & \text{for} \quad r \, \alpha = 2 \,, \\ \text{const} \,, & \text{for} \quad r \, \alpha > 2 \,. \end{cases} \tag{3.25}$$

The transport exponent $\gamma = 2 - r \, \alpha$ depends continuously on r, and only for $r = 1$ (the case of the uniform distribution treated so far) does Eq. (3.25) reduce to Eq. (3.19). In general, different initial distributions lead the SM to different transport properties, as already observed in other frameworks, such as those of Lévy walks [10]. However, the dynamical mechanisms underlying these two evolutions are rather different. Indeed, the properties of the moments suffice to draw the following conclusions.

Remark 3.3.4.: *The anomalous behaviour of the SM with $\alpha \neq 1$ is related to the presence of memory: the initial state is not forgotten, and correlations persist in time. This is in line with the common observation that rapid correlation decay is*

associated with normal diffusion, while memory effects lead to persistent correlations and anomalous transport. Interestingly, the SM enjoys normal diffusion also for $\alpha = 1$*, despite having memory as in the cases with* $\alpha \neq 1$*. (This observation will further be supported by the discussion of correlations in Subsection 3.4.)*

Remark 3.3.5.: *In agreement with the observations of [58], the SM illustrates how equality of moments (even of all moments) of a given random variable does not guarantee full equivalence of the processes that share such moments. Diffusion in the SM arises from dynamical mechanisms that substantially differ even from those of simple deterministic or stochastic particle systems, such as the Lorentz gas with finite horizon or random walks on a line.*

In the following, we explore whether correlations might help to distinguish the SM from the LLg. To this end we analytically compute various scaling limits of the position-position correlations generated by the SM. In Sec. 4.3 we compare them with numerically computed correlations of the LLg with the same exponent γ.

3.4 Position auto-correlations function

In this section we investigate the properties of various versions of the position-position correlation functions, for the dynamics of the SM. This requires knowledge of the relative motion of two points, $\hat{\mathtt{x}} = (x, 0)$ and $\hat{\mathtt{y}} = (y, 0)$ in $\widehat{M}$. There are two possible cases: either there exists an interval $(\ell^+_{j-1}(\alpha), \ell^+_j(\alpha)]$ such that $x, y \in (\ell^+_{j-1}(\alpha), \ell^+_j(\alpha)]$, or such interval that does not exist.

a. When the interval exist the coarse-grained trajectories of $\hat{\mathtt{x}}$ and $\hat{\mathtt{y}}$, $x(n) := \pi_{\mathbb{Z}}(S^n_\alpha(\hat{\mathtt{x}}))$ and $y(n) := \pi_{\mathbb{Z}}(S^n_\alpha(\hat{\mathtt{y}}))$, coincide for all times n: the particles have the maximum degree of correlation.

b. In the second case, suppose that $x < y$. Hence, we have

$$x \in (\ell^+_{\overline{m}_\alpha(x)-1}(\alpha), \ell^+_{\overline{m}_\alpha(x)}(\alpha)]\,, \qquad \text{and} \qquad y \in (\ell^+_{\overline{m}_\alpha(y)-1}(\alpha), \ell^+_{\overline{m}_\alpha(y)}(\alpha)]\,,$$

with

$$(\ell^+_{\overline{m}_\alpha(x)-1}(\alpha), \ell^+_{\overline{m}_\alpha(x)}(\alpha)] \cap (\ell^+_{\overline{m}_\alpha(y)-1}(\alpha)\,, \ell^+_{\overline{m}_\alpha(y)}(\alpha)] = \varnothing, \quad \text{and} \quad \overline{m}_\alpha(x) < \overline{m}_\alpha(y)\,.$$

This means that the two points have the same coarse grained trajectory up to time $\overline{m}_\alpha(x)$, when $\hat{\mathbf{x}}$ enters its periodic orbit, while $\hat{\mathbf{y}}$ continues its ballistic motion up to time $\overline{m}_\alpha(y)$. At times larger than $\overline{m}_\alpha(y)$, the distance between the two particles will either be $\overline{m}_\alpha(y) - \overline{m}_\alpha(x)$ or $\overline{m}_\alpha(y) - \overline{m}_\alpha(x) \pm 1$. For all the points with $(x, y) \in (0, 1)$, the distance become periodic after a finite time; after an initial transient.

The larger the difference $\overline{m}_\alpha(y) - \overline{m}_\alpha(x)$ the smaller is the correlation between the particle positions at the different times. In any case, the difference $\overline{m}_\alpha(y) - \overline{m}_\alpha(x)$ should say something about the strength of the correlation between the two particles. Considering 1 negligible with respect to $\overline{m}_\alpha(y) - \overline{m}_\alpha(x)$, we can classify the pair of initial conditions according to this distance.

Let us introduce the notation

$$I_j(\alpha) := (\ell^+_{j-1}(\alpha), \ell^+_j(\alpha)] \ , \quad \text{and} \quad R := (1/2, 1) \times (1/2, 1) \ . \tag{3.26}$$

Then we can write:

$$R = \cup_{i,j} R_{i,j}(\alpha) \, , \qquad \text{with} \quad R_{i,j}(\alpha) := I_i(\alpha) \times I_j(\alpha) \, . \tag{3.27}$$

The pairs (x, y) belonging to the diagonal elements $R_{i,i}(\alpha)$ have the same trajectory, whose length grows with i, while $R_{i,i}(\alpha)$ gets closer to the corner $(1, 1)$ of R when i grows. Moving away from the diagonal, $|\overline{m}_\alpha(y) - \overline{m}_\alpha(x)|$ gets larger and larger. Nevertheless, memory persists and there is no sensitive dependence on initial conditions, consistently with the absence of a positive Lyapunov exponent, *cf.* Sec. 3.1.

Let us introduce the position-position auto-correlation function as:

$$\phi(n, m) := \langle \pi_{\mathbb{Z}}(S^n(\hat{\mathbf{x}})) \, \pi_{\mathbb{Z}}(S^m(\hat{\mathbf{x}})) \rangle := \langle \Delta\hat{\mathbf{x}}_n \, \Delta\hat{\mathbf{x}}_m \rangle \tag{3.28a}$$

$$= 2 \int_{1/2}^{1} \min\{\widetilde{m}_{\alpha,m}(x), m\} \, \min\{\widetilde{m}_{\alpha,n}(x), n\} \, \mathrm{d}x, \quad \text{with } m \leq n. \tag{3.28b}$$

The integration interval $\mathrm{I} := (1/2, 1]$ can be subdivided in three parts,

$$\mathrm{I} = E^<_m \cup E_{m,n} \cup E^>_n \ ,$$

defined by

$$\begin{cases} E_m^< = \{x \in \mathrm{I} \,:\, \widetilde{m}_{\alpha,m}(x) \le m\}, \\ E_{m,n} = \{x \in \mathrm{I} \,:\, m < \widetilde{m}_{\alpha,n}(x) \le n\}, \\ E_n^> = \{x \in \mathrm{I} \,:\, n < \widetilde{m}_{\alpha,n}(x)\}. \end{cases} \tag{3.29a}$$

Thus each sub-interval corresponds to following quantity

$$\Rightarrow \begin{cases} \min\{\widetilde{m}_{\alpha,m}(x), m\}\ \min\{\widetilde{m}_{\alpha,n}(x), n\} = \widetilde{m}_{\alpha,m}(x)\,\widetilde{m}_{\alpha,n}(x)\,, \\ \min\{\widetilde{m}_{\alpha,m}(x), m\}\ \min\{\widetilde{m}_{\alpha,n}(x), n\} = m\,\widetilde{m}_{\alpha,n}(x)\,, \\ \min\{\widetilde{m}_{\alpha,m}(x), m\}\ \min\{\widetilde{m}_{\alpha,n}(x), n\} = m\,n\,, \end{cases} \tag{3.29b}$$

respectively. Rewriting the resulting integrals in terms of sums over the intervals where $\overline{m}_\alpha(x)$ takes the constant value k (*cf.* Eq. (3.17)), for $m \le n$ one has:

$$\phi(n,m) = 2\int\limits_{E_m^<} \widetilde{m}_{\alpha,n}(x)\,\widetilde{m}_{\alpha,m}(x)\,\mathrm{d}x + 2\,m\int\limits_{E_{m,n}} \widetilde{m}_{\alpha,n}(x)\,\mathrm{d}x + 2\,m\,n\int\limits_{E_n^>} \mathrm{d}x, \tag{3.30a}$$

$$\sim\ 2\sum_{k=1}^{m} k^2\,\Delta_k(\alpha) + 2\,m\sum_{k=m+1}^{n} k\,\Delta_k(\alpha) + 2\,m\,n\sum_{k=n+1}^{\infty}\Delta_k(\alpha)\,. \tag{3.30b}$$

The first and the third sum have been evaluated in Eqs. (3.18a) and (3.18b), respectively. The asymptotic behaviour of the second term depends on the value of α and on the relation between m and n. In the following, we discuss the following examples:

1. $n \to \infty$ with m fixed,
2. $n, m \to \infty$ with fixed $h = n - m$,
3. $n, m \to \infty$ with $n = m + \ell\, m^q$, where ℓ, q are positive constants.

3.4.1 Scaling of $\phi(n,m)$ for $n \to \infty$ with m fixed

In order to evaluate the second sum in Eq. (3.30b) we observe that

$$2\,m\sum_{k=m+1}^{n} k\,\Delta_k(\alpha) = 2\,m\sum_{k=0}^{n} k\,\Delta_k(\alpha) - 2\,m\sum_{k=0}^{m} k\,\Delta_k(\alpha)\,. \tag{3.31}$$

For fixed m, the latter sum takes a constant value, and for $n \to \infty$ the former sum scales as (*cf.* Eq. (3.21) or the formal derivation provided in Appendix A)

$$2\,m \sum_{k=0}^{n} k\,\Delta_k(\alpha) \sim \begin{cases} \frac{2\,\alpha\,m}{1-\alpha}\,n^{1-\alpha}\,, & \text{for} \quad 0 < \alpha < 1\,, \\ 2\,m\,\ln n\,, & \text{for} \quad \alpha = 1\,, \\ \text{const}\,, & \text{for} \quad \alpha > 1\,. \end{cases} \tag{3.32}$$

The leading-order scaling of the three sums in Eq. (3.30b) is summarised in the following lemma:

Lemma 3.4.1.: *For $n \to \infty$ with fixed m the auto-correlation function, $\phi(n,m)$, defined in Eq.* (A.17a)*, asymptotically scales as:*

$$\phi(n,m) \sim \begin{cases} \frac{2\,m}{1-\alpha}\,n^{1-\alpha}\,, & \textit{for} \quad 0 < \alpha < 1\,, \\ 2\,m\,\ln n\,, & \textit{for} \quad \alpha = 1\,, \\ \textit{const}\,, & \textit{for} \quad \alpha > 1\,. \end{cases} \tag{3.33}$$

Proof. The first sum in (3.30b) has a finite number of terms that all take finite positive values. Hence, it adds to a finite positive number. For $0 < \alpha < 1$ the leading-order contributions of the second and the third sum have the same scaling, $n^{1-\alpha}$, which diverges for $n \to \infty$. From Eqs. (3.32) and (3.18b) we have

$$\phi(n,m) \sim 2\,m\,\left(\frac{\alpha}{1-\alpha} + 1\right)\,n^{1-\alpha} = \frac{2\,m}{1-\alpha}\,n^{1-\alpha} \qquad \text{for } 0 < \alpha < 1\,.$$

For $\alpha = 1$ the exponent $1 - \alpha = 0$ such that the third term also takes a finite value. In that case the leading-order scaling is provided by the second sum, Eq. (3.32). Finally, for $\alpha > 1$ all sums contributing to Eq. (A.17a) take constant values. □

The dashed lines in Figure 3.2a show the asymptotic behaviour, Eq. (3.33), for $\alpha = 1/2$ and different fixed values of m. They provide an excellent description of the asymptotic behaviour of the numerical evaluation of the definition, Eq. (A.17a) (solid lines). The lower panel of the figure demonstrates that the ratio of the correlation function and the prediction of its asymptotic behaviour approaches one for a vast range of different values of m.

3.4.2 Scaling of $\phi(m+h,m)$ for $m \to \infty$ with $h > 0$ fixed

In this case, the second sum in Eq. (3.30a) involves a finite number of positive terms. The sum can be bounded from above by

$$\begin{aligned} 2\,m \sum_{k=m+1}^{m+h} k\,\Delta_k(\alpha) &= 2\,\alpha\,m \sum_{k=m+1}^{m+h} k^{-\alpha} \left(1 - \frac{\tilde{c}(\alpha)}{k} + \mathcal{O}(k^{-2})\right), \\ &< 2\,\alpha\,h\,m^{1-\alpha} \left(1 - \frac{\tilde{c}(\alpha)}{m+h} + \mathcal{O}(m^{-2})\right), \\ &< \begin{cases} 2\,\alpha\,h\,(m+h)^{1-\alpha}, & \text{for} \quad 0 < \alpha < 1, \\ 2\,\alpha\,h, & \text{for} \quad 1 \leq \alpha. \end{cases} \end{aligned}$$

and from below by

$$\begin{aligned} 2\,m \sum_{k=m+1}^{m+h} k\,\Delta_k(\alpha) &> 2\,\alpha\,h\,m\,(m+h)^{-\alpha} \left(1 + \mathcal{O}(m^{-1})\right), \\ &> \begin{cases} 2\,\alpha\,h\,m^{1-\alpha}, & \text{for} \quad 0 < \alpha < 1, \\ 0, & \text{for} \quad 1 \leq \alpha. \end{cases} \end{aligned}$$

Noting that constant h implies $(m+h)^{1-\alpha} = m^{1-\alpha}\,(1+h/m)^{1-\alpha} \sim m^{1-\alpha}$ we find that the second sum scales as

$$2\,m \sum_{k=m+1}^{m+h} k\,\Delta_k(\alpha) \sim \begin{cases} 2\,\alpha\,h\,m^{1-\alpha}, & \text{for} \quad 0 < \alpha < 1, \\ \mathcal{O}(1), & \text{for} \quad 1 \leq \alpha. \end{cases} \tag{3.34}$$

Hence, the leading-order scaling of the auto-correlation function takes the form:

Lemma 3.4.2.: *For $m \to \infty$ with fixed $n - m = h = const$ the auto-correlation function, $\phi(m+h,m)$, asymptotically scales as:*

$$\phi(m+h,m) \sim \begin{cases} \frac{4}{2-\alpha}\,m^{2-\alpha}, & \textit{for} \quad 0 < \alpha < 2, \\ 4\,\ln(m), & \textit{for} \quad \alpha = 2, \\ const, & \textit{for} \quad \alpha > 2. \end{cases} \tag{3.35}$$

Proof. For $0 < \alpha < 2$ the leading-order contributions of the first and third term in Eq. (3.30b) have the same scaling, $m^{2-\alpha}$. These terms dominate the scaling of

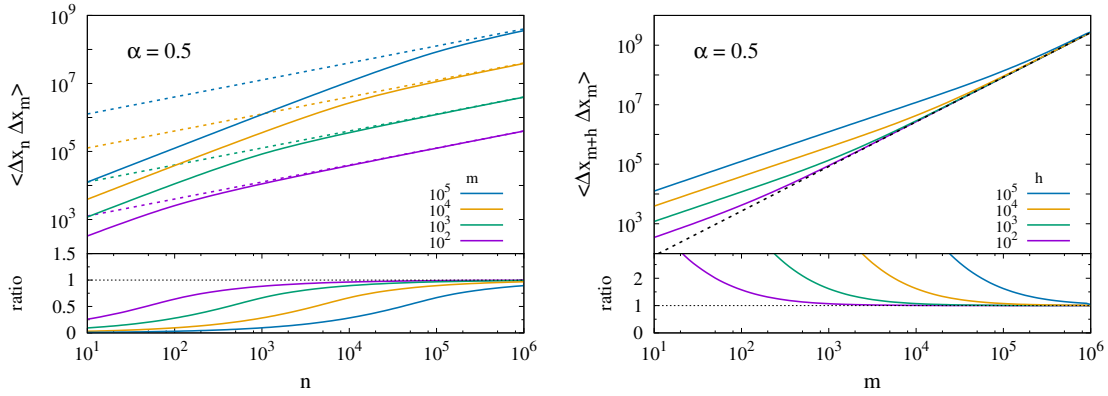

(a) Correlations for fixed time m.

(b) Correlations for fixed time lag $h = n - m$.

Figure 3.2: Comparison of the auto-correlation function, $\phi(n, m)$, and expressions for its asymptotic scaling, for $\alpha = 1/2$ in two different cases. The functions $\phi(n, m)$ obtained from the sums of Eq. (3.30b) are plotted as solid lines. The respective asymptotic expressions are indicated by dashed lines. (a) The limit of large n for a for fixed value of m. The values of m are provided in the figure legend in the order of the lines from top to bottom. The asymptotic scaling is provided by Eq. (3.33). (b) The large-m limit for a fixed time lag $h = n - m$. The values of h are provided in the figure legend in the order of the lines from top to bottom. The asymptotic scaling is provided by Eq. (3.35). In the lower panels we show the ratio of the auto-correlation function and the respective asymptotic expressions. (Figures adapted from Ref. [25]).

the second sum, Eq. (3.34). In this range one hence recovers the scaling of the mean-square displacement in Eq. (3.19).

For $\alpha = 2$ the second and third terms in Eq. (3.30b) take constant values, while the first one diverges logarithmically according to Eq. (3.18a). Finally, for $\alpha > 2$ all sums contributing to Eq. (3.30b) take constant values. □

The dashed lines in Figure 3.2b show the asymptotic behaviour, Eq. (3.35), for $\alpha = 1/2$, and different time lags $h = n - m$. They provide an excellent description of the asymptotics of the numerical evaluation of the definition, Eq. (A.17a) (solid lines). The lower panel of the figure demonstrates that the ratio of the auto-correlation

function and the prediction of its asymptotic behaviour approaches 1 for a vast range of values of h.

3.4.3 Scaling of $\phi(m + \ell m^q, m)$ for $m \to \infty$ with $\ell > 0$

For $q < 1$, $q = 1$, and $q > 1$ the auto-correlation function shows different scalings.

Scaling for $q < 1$. In this case bounds for the second sum in Eq. (3.30b) can be provided by a calculation fully analogous to the derivation of Eq. (3.34). This provides the scaling

$$2\,m \sum_{k=m+1}^{m+h} k\,\Delta_k(\alpha) \sim \begin{cases} 2\,\alpha\,\ell\,m^{1-q-\alpha}\,, & \text{for} \quad 0 < \alpha < 1\,, \\ \mathcal{O}(1)\,, & \text{for} \quad 1 \leq \alpha\,. \end{cases}$$

This scaling is always sub-dominant with respect to those of the other two sums in Eq. (3.30b). As far as the asymptotic scaling is concerned we have the same situation as for fixed $n - m = h$, and the auto-correlation function has the same scaling in these two limits.

Lemma 3.4.3.: *For $q < 1$, $\ell > 0$, and $m \to \infty$ the auto-correlation function, $\phi(m+\ell m^q, m)$ follows the same asymptotic scaling, Eq.* (3.35)*, as for the case where the time difference between the arguments is constant,*

$$\phi(m + \ell\,m^q, m) \sim \phi(m + h, m)\,, \qquad \textit{for} \quad \ell, h > 0 \quad \textit{and} \quad q < 1\,. \tag{3.36}$$

Scaling for $q = 1$. In this case we have $n = m + \ell\,m^q = (1 + \ell)m$, *i.e.* n is proportional to m. In order to find the scaling for large m, we start from Eq. (3.31). For $\alpha \neq 1$ the two sums on the right-hand side scale like a power law with exponent $1 - \alpha$ and a constant offset that is relevant when $\alpha > 1$. The constant drops out when taking the difference, so that we obtain

$$2\,m \sum_{k=m+1}^{n} k\,\Delta_k(\alpha) \;\sim\; \frac{2\,m\,\alpha}{1-\alpha}\left(n^{1-\alpha} - m^{1-\alpha}\right)\,, \tag{3.37a}$$

$$\;=\; \frac{2\,\alpha}{1-\alpha}\left((\ell+1)^{1-\alpha} - 1\right) m^{2-\alpha} \qquad \text{for} \quad \alpha \neq 1\,. \tag{3.37b}$$

Moreover, for $\alpha = 1$ the sum diverges logarithmically:

$$2\,m \sum_{k=m+1}^{n} k\,\Delta_k(\alpha) \sim 2\,m\,\alpha\,\ln\frac{n}{m} = 2\,m\,\ln(1+\ell), \qquad \text{for} \quad \alpha = 1\,. \tag{3.37c}$$

Hence, the leading-order scaling of the auto-correlation function is given by:

Lemma 3.4.4.: *For any $\ell > 0$ the auto-correlation function, $\phi((1+\ell)\,m, m)$, asymptotically scales as:*

$$\phi((1+\ell)\,m, m) \sim \begin{cases} \frac{2}{1-\alpha}\left((1+\ell)^{1-\alpha} - \frac{\alpha}{2-\alpha}\right) m^{2-\alpha}\,, & \textit{for} \quad 0<\alpha<2, \quad \alpha \neq 1\,, \\ (4 + 2\,\ln(1+\ell))\;m\,, & \textit{for} \quad \alpha = 1\,, \\ 4\,\ln(m)\,, & \textit{for} \quad \alpha = 2\,, \\ \textit{const}\,, & \textit{for} \quad \alpha > 2\,. \end{cases} \tag{3.38}$$

Proof. The cases $\alpha \geq 2$ are obtained as in Lemma 3.4.1. For $0 < \alpha < 2$ the leading-order contributions to all three sums in Eq. (3.30a) scale like $m^{2-\alpha}$. The case $\alpha = 1$ is special, however, because the second sum takes a different prefactor, Eq. (3.37c), rather the one obtained in Eq. (3.37b). For $0 < \alpha < 2$ and $\alpha \neq 1$ we have

$$\phi((1+\ell)\,m, m) \sim \left(\frac{2\,\alpha}{2-\alpha} + \frac{2\,\alpha}{1-\alpha}\,\left((1+\ell)^{1-\alpha} - 1\right) + 2\,(1+\ell)^{1-\alpha}\right)\,m^{2-\alpha}\,,$$

while for $\alpha = 1$ we have

$$\phi((1+\ell)\,m, m) \sim (2 + 2\,\ln(1+\ell) + 2)\;m\,.$$

The result indicated in Eq. (3.38) is obtained after collecting terms. □

Scaling for $q > 1$. In this case Eq. (3.37a) still applies, but $n^{1-\alpha}$ is the dominating term in the bracket for $\alpha > 1$, while $m^{1-\alpha}$ is the dominating term in the bracket for $\alpha < 1$. Moreover, the logarithm in the scaling provided in Eq. (3.37c) now scales as $\ln(n/m) = \ln(1 + \ell\,m^{q-1}) \sim (q-1)\,\ln(m)$. When we further observe that $n \sim \ell\,m^q$, this implies

$$2\,m \sum_{k=m+1}^{n} k\,\Delta_k(\alpha) \;\sim\; \begin{cases} \frac{2\,\ell\,\alpha}{1-\alpha}\,m^{1+q\,(1-\alpha)}\,, & \text{for} \quad 0<\alpha<1\,, \\ 2\,(q-1)\;m\;\ln(m)\,, & \text{for} \quad \alpha = 1\,, \\ \frac{2\,\alpha}{\alpha-1}\,m^{2-\alpha}\,, & \text{for} \quad \alpha > 1\,. \end{cases} \tag{3.39}$$

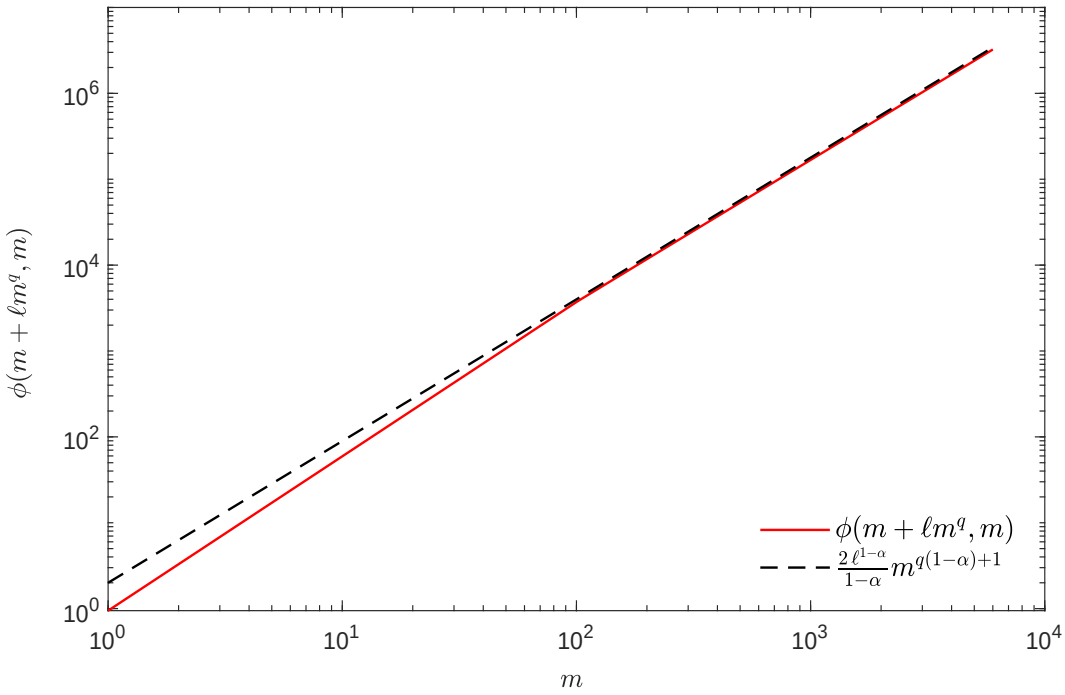

Figure 3.3: Comparison of auto-correlation function $\phi(n, m)$ represented by solid line with their respective asymptotic scaling in Eq. (3.40). The large-m limit for $\phi(m + \ell m^q)$ with $\alpha = 0.5$ and fixed $q = 1.4$.

Hence, the leading-order scaling of the auto-correlation function obeys the following:

Lemma 3.4.5.: *For $q > 1$, $\ell > 0$, and $m \to \infty$ the auto-correlation function, $\phi(m + \ell\, m^q, m)$ asymptotically scales as:*

$$\phi(m+\ell\, m^q, m) \sim \begin{cases} \frac{2}{1-\alpha}\, \ell^{1-\alpha}\, m^{1+q\,(1-\alpha)}\,, & \textit{for} \quad 0 < \alpha < 1\,, \\ 2\,(q-1)\, m\, \ln(m)\,, & \textit{for} \quad \alpha = 1\,, \\ \frac{2\,\alpha}{(2-\alpha)\,(\alpha-1)}\, m^{2-\alpha}\,, & \textit{for} \quad 1 < \alpha < 2\,, \\ 4\, \ln(m)\,, & \textit{for} \quad \alpha = 2\,, \\ \textit{const}\,, & \textit{for} \quad \alpha > 2\,. \end{cases} \tag{3.40}$$

Proof. The cases $\alpha \geq 2$ are obtained as in Lemma 3.4.1. For $1 < \alpha < 2$ the leading-order contributions scale like $m^{2-\alpha}$. They appear in the first and in the second

sum on the right-hand-side of Eq. (3.30b). Collecting the corresponding terms in Eqs. (3.18a) and (3.39) we obtain

$$\phi(m+\ell\, m^q, m) \sim \left(\frac{2\,\alpha}{2-\alpha}+\frac{2\,\alpha}{\alpha-1}\right)\, m^{2-\alpha} = \frac{2\,\alpha}{(2-\alpha)\,(\alpha-1)}\, m^{2-\alpha}\,.$$

For $\alpha = 1$ the leading-order scaling contribution to the auto-correlation function is provided in Eq. (3.39).

For $0 < \alpha < 1$ the leading-order contributions scale like $m\, n^{1-\alpha} \sim \ell^{1-\alpha}\, m^{1+q\,(1-\alpha)}$. Collecting these terms in Eqs. (3.18b) and (3.39) provides

$$\phi(m+\ell\, m^q, m) \sim \left(\frac{2\,\alpha}{1-\alpha}+2\right)\, \ell^{1-\alpha}\, m^{1+q\,(1-\alpha)} = \frac{2}{1-\alpha}\, \ell^{1-\alpha}\, m^{1+q\,(1-\alpha)}\,.$$

□

3.5 Moments of velocity

The velocity of any point of the SM is either $+1$ or -1 and moments of the velocity can be determined by evaluating

$$\langle v^p(n)\rangle = 2\sum_{k=1}^{n} v_k^p(n)\Delta_k(\alpha) + 2\sum_{k=n+1}^{\infty} v_k^p(n)\Delta_k(\alpha)\,, \tag{3.41}$$

where $v_k(n)$ is the velocity at time n of particle with $x \in [\ell_{k-1}^+, \ell_k^+)$. The velocity of the particle is given by

$$v_k(n) = I_{\{n<k\}} - (-1)^{n-k} I_{\{n\geq k\}}, \tag{3.42}$$

where I_A is the indicator of the event A. Then by using Eq. (3.42) in (3.41), one finds

$$\langle v^p(n)\rangle = 2(-1)^{p(n+1)}\sum_{k=1}^{n}(-1)^{pk}\Delta_k(\alpha) + 2\sum_{k=n+1}^{\infty}\Delta_k(\alpha)\,, \tag{3.43}$$

In the following we give the separate expression(s) for the even and odd moments of velocity.

The even moments of velocity are

$$\langle v^p(n)\rangle = 2\sum_{k=1}^{n}\Delta_k(\alpha) + 2\sum_{k=n+1}^{\infty}\Delta_k(\alpha)\,, \qquad \text{even } p \geq 2\,. \tag{3.44}$$

In order to compute expression of odd moments, first we split the sum in Eq. (3.43) into two cases and simplify, in following proposition

Proposition 3.5.1. *For $\alpha > 0$ and odd $p \geq 1$, the following result holds*

$$2(-1)^{p(n+1)} \sum_{k=1}^{n} (-1)^{pk} \Delta_k(\alpha) = \begin{cases} -1 - 4 \sum\limits_{k=1}^{n/2} \Delta_{2k}(\alpha) + 2\ell_n^+(\alpha)\,, & \textit{for} \quad \textit{even}\, n\,, \\ 1 + 4 \sum\limits_{k=1}^{(n-1)/2} \Delta_{2k}(\alpha) - 2\ell_n^+(\alpha)\,, & \textit{for} \quad \textit{odd}\, n\,, \end{cases} \tag{3.45}$$

where $\ell_0^+(\alpha) = 1/2$ and $\Delta_{2k}(\alpha)$ expressed in Eq. (A.16).

Proof. See appendix A.3. □

Substituting Eq. (3.45) in to (3.43), the odd $p \geq 1$ moments of velocity are

$$\langle v^p(n) \rangle = \begin{cases} -1 + 2\ell_n^+(\alpha) - 4 \sum\limits_{k=1}^{n/2} \Delta_{2k}(\alpha) + 2 \sum\limits_{k=n+1}^{\infty} \Delta_k(\alpha)\,, & \text{for} \quad \text{even}\, n\,, \\ 1 - 2\ell_n^+(\alpha) + 4 \sum\limits_{k=1}^{(n-1)/2} \Delta_{2k}(\alpha) + 2 \sum\limits_{k=n+1}^{\infty} \Delta_k(\alpha)\,, & \text{for} \quad \text{odd}\, n\,. \end{cases} \tag{3.46}$$

3.5.1 Asymptotic scaling

The asymptotic scaling for the even moments of velocity is found as a straightforward consequence of the definition of $\Delta_k(\alpha)$, *cf.* Eq. (3.14b), such that the sum

$$2 \sum_{k=n+1}^{\infty} \Delta_k(\alpha) = 2\,\ell_{n-1} = 2\,n^{-\alpha} \left(1 - \frac{\alpha 2^{1/\alpha}}{n} + O(n^{-2}) \right) \sim 2\,n^{-\alpha}, \quad n \to \infty. \tag{3.47}$$

converges for $\alpha > 0$.

Therefore the even moments of velocity scale asymptotically like

$$\langle v^p(n) \rangle \;\sim\; 1, \qquad \text{even}\;\; p \geq 2, \quad n \to \infty\,. \tag{3.48}$$

Theorem 3.5.2. *For $\alpha > 0$ and $n \to \infty$, the odd $p \geq 1$ moments of velocity $\langle v^p(n) \rangle$ scales asymptotically as:*

$$\langle v^p(n) \rangle \sim \begin{cases} \;\;3 - 4\ln(2)\,, & \textit{for} \quad \textit{even}\, n,\, \alpha = 1, \\ -3 + 4\ln(2)\,, & \textit{for} \quad \textit{odd}\, n,\, \alpha = 1, \\ \;\;1 - 4L(\alpha)\,, & \textit{for} \quad \textit{even}\, n,\, 0 < \alpha < 2, \\ -1 + 4L(\alpha)\,, & \textit{for} \quad \textit{odd}\, n,\, 0 < \alpha < 2\,, \end{cases} \tag{3.49}$$

where

$$L(\alpha) = \sum_{k=1}^{\infty} \Delta_{2k}(\alpha).$$

Proof. The asymptotic behaviour of the series in Eq. (3.46) can be evaluated by recalling the definition of $\Delta_k(\alpha)$ (*cf.* Eq. (3.14c)). The asymptotic scaling of the sum $\sum_{k=n+1}^{\infty}\Delta_k(\alpha)$ is computed in Eq. (3.47).

We now find the scaling for $\alpha = 1$.

Scaling for $\alpha = 1$. In this case the first sum in Eq. (3.46), recalling definition of Δ_{2k} (*cf.* Eq. (A.16)) can be written as

$$4\sum_{k=1}^{n/2}\Delta_{2k}(\alpha) := 4\sum_{k=1}^{n/2}\left(\frac{1}{(2k-1+2^{1/\alpha})^{\alpha}} - \frac{1}{(2k+2^{1/\alpha})^{\alpha}}\right) = 4\sum_{k=1}^{n/2}\left(\frac{1}{2k+1} - \frac{1}{2k+2}\right). \tag{3.50}$$

Lemma 3.5.3. *For $\alpha = 1$, the series in Eq.* (3.50) *has the following representation*

$$\sum_{k=1}^{n/2}\frac{1}{(2k+1)(2k+2)} = \frac{1}{2}\left(H_{\frac{n+1}{2}} - H_{\frac{n}{2}+1} - 1 + \ln(4)\right), \tag{3.51}$$

for $n = 2, 4, 6, \cdots$, where $H_n = \sum_{k=1}^{n} k^{-1}$ is the n^{th} harmonic number.

Proof. See appendix A.2. □

The n-th harmonic number H_n, is as large as the natural logarithm of n, because the sum $\sum_{k=1}^{n} k^{-1}$ is approximated by the integral $\int_1^n 1/x \ \mathrm{d}x = \ln n$. As $n \to \infty$ the sequence $(H_n - \ln n)$ decreases monotonically towards the limit:

$$\lim_{n\to\infty}(H_n - \ln n) = \gamma\,,$$

where γ is the Euler-Mascheroni constant, which has the value $\gamma \equiv 0.57722$. The asymptotic expansion for $n \to \infty$ is

$$H_n = \ln n + \gamma + \frac{1}{2n}\sum_{k=1}^{\infty}\frac{B_{2k}}{2kn^{2k}} = \ln n + \gamma + \frac{1}{2n} - \frac{1}{12n^2} + \frac{1}{120n^4} - \cdots, \tag{3.52}$$

where B_k are the Bernoulli numbers (see for instance [29]).
Hence we can write

$$H_{\frac{n+1}{2}} - H_{\frac{n}{2}+1} \sim \ln\left(\frac{n+1}{2}\right) - \ln\left(\frac{n}{2}+1\right) \sim -\frac{1}{n}\,. \tag{3.53}$$

Therefore the sum reported in Eq. (3.50), asymptotically scales as

$$4\sum_{k=1}^{n/2}\Delta_{2k}(\alpha) \sim 4\ln 2 - 2 - \frac{2}{n}\,. \tag{3.54}$$

It turns to $\sim 4\ln 2 - 2$, as $n \to \infty$. The results indicated in Eq. (3.49) for $\alpha = 1$, are obtained after collecting terms from Eqs. (3.47) and (3.54).

Scaling for $0 < \alpha < 2$. Recalling Δ_{2k} (*cf.* Eq. (A.16)), the sum in Eq. (3.46) can be written as

$$\sum_{k=1}^{n/2}\Delta_{2k}(\alpha) = \sum_{k=1}^{n/2}\frac{\alpha}{(2k)^{\alpha+1}}\left(1 - f_\alpha(k)\right)\,, \quad \text{and} \quad f_\alpha(k) := \frac{\widetilde{c}(\alpha)}{2k} + \mathcal{O}\left(k^{-2}\right)\,. \tag{3.55}$$

Thus the sums

$$L(\alpha) := \sum_{k=1}^{n/2}\Delta_{2k}(\alpha) + \sum_{k=n/2+1}^{\infty}\Delta_{2k}(\alpha)\,. \tag{3.56a}$$

will converge for $\alpha > 0$, and they can be estimated as

$$\sum_{k=1}^{n/2}\Delta_{2k}(\alpha) \sim L(\alpha) - \mathcal{O}\left(n^{-\alpha}\right)\,, \tag{3.56b}$$

where $L(\alpha)$ is the sum all the way to infinity.

The results of Eq. (3.49) for $0 < \alpha < 2$ are obtained after collecting terms from Eqs. (3.47) and (3.56b). □

3.6 1-time velocity auto-correlation $\langle v(0)v(n)\rangle$

The velocity of any point of the SM is either $+1$ or -1 and its auto-correlation is defined by

$$\langle v(0)v(n)\rangle = 2\sum_{k=1}^{n} v(0)v_k(n)\Delta_k(\alpha) + 2\sum_{k=n+1}^{\infty} v(0)v_k(n)\Delta_k(\alpha)\,, \tag{3.57}$$

where $v_k(n)$ is the velocity at time n of a particle with $x \in [\ell^+_{k-1}, \ell^+_k)$ and $v(0) = 1$. Then by using Eq. (3.42) in (3.57), one finds:

$$\langle v(0)v(n)\rangle = 2\sum_{k=1}^{n}\left\{-(-1)^{n-k}I_{\{n\geq k\}}\right\}\Delta_k(\alpha) + 2\sum_{k=n+1}^{\infty}\left\{I_{\{n<k\}}\right\}\Delta_k(\alpha). \tag{3.58}$$

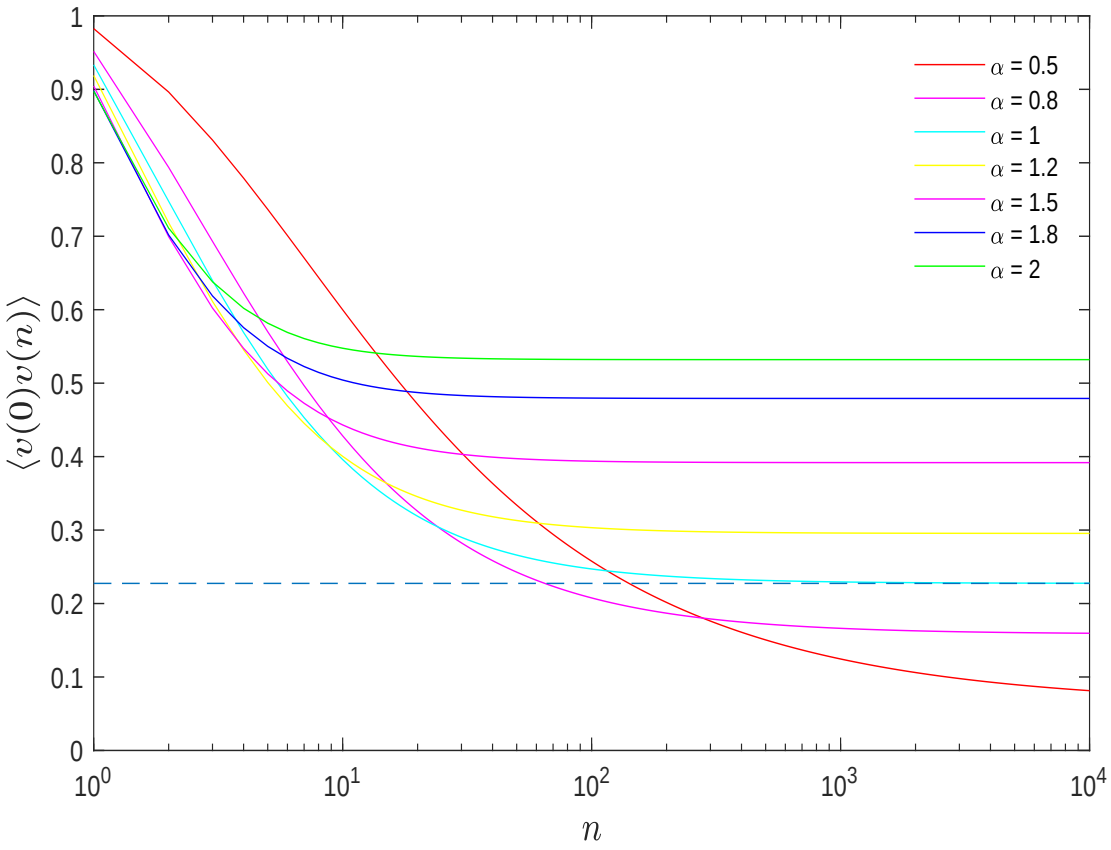

Figure 3.4: Representation of Eq. (3.60) for even time n with different values of α. All curves converge to finite value. In particular, the dashed line mark the asymptotic behaviour computed in Eq. (3.49) for $\alpha = 1$.

Therefore the VACF can be expressed as follows

$$\langle v(0)v(n)\rangle = 2(-1)^{n+1}\sum_{k=1}^{n}(-1)^k\Delta_k(\alpha) + 2\sum_{k=n+1}^{\infty}\Delta_k(\alpha). \tag{3.59}$$

The first sum of this expression has same contribution as in proposition 3.5.1 with $p = 1$. Then substituting Eq. (3.45) in to (3.59), we find the (time dependent) VACF of the SM

$$\langle v(0)v(n)\rangle = \begin{cases} -1 + 2\ell_n^+(\alpha) - 4\sum\limits_{k=1}^{n/2}\Delta_{2k}(\alpha) + 2\sum\limits_{k=n+1}^{\infty}\Delta_k(\alpha)\,, & \text{for} \quad \text{even } n\,, \\ 1 - 2\ell_n^+(\alpha) + 4\sum\limits_{k=1}^{(n-1)/2}\Delta_{2k}(\alpha) + 2\sum\limits_{k=n+1}^{\infty}\Delta_k(\alpha)\,, & \text{for} \quad \text{odd } n\,. \end{cases} \tag{3.60}$$

Remark 3.6.1. *For $\alpha > 0$, the 1-time velocity auto-correlation functions behave*

like the odd $p \geq 1$ moments of the velocity i.e., $\langle v(0)v(n)\rangle = \langle v^p(n)\rangle$, cf. Eqs. (3.60) *and* (3.46).

Lemma 3.6.2. *For $\alpha > 0$ and $n \to \infty$, the 1-time velocity auto-correlation function $\langle v(0)v(n)\rangle$ has the same asymptotic scaling, Eq.* (3.49)*, as for the odd moments of the velocity $\langle v^p(n)\rangle$ i.e.,*

$$\langle v(0)v(n)\rangle \sim \langle v^p(n)\rangle, \qquad for \quad odd \;\; p \geq 1. \tag{3.61}$$

3.7 2-times velocity auto-correlation $\langle v(m)v(n)\rangle$

In this section, we look for the expression of the VACF of the SM for times m and n. Adopting $m \leq n$, and recalling Eq. (3.42) we have:

$$v_k(n)v_k(m) = (-1)^{m-k}(-1)^{n-k} I_{\{n\geq k\}} I_{\{m\geq k\}} - (-1)^{n-k} I_{\{n\geq k\}} I_{\{m<k\}} + I_{\{n<k\}} I_{\{m<k\}}. \tag{3.62}$$

Multiplying by $\Delta_k(\alpha)$ and summing over k, yields

$$\begin{aligned}\langle v(n)v(m)\rangle &= 2\sum_{k=1}^{m}(-1)^{n-k}(-1)^{m-k}\Delta_k(\alpha) - 2\sum_{k=m+1}^{n}(-1)^{n-k}\Delta_k(\alpha) + 2\sum_{k=n+1}^{\infty}\Delta_k(\alpha)\,, \\ &= 2(-1)^{n+m}\sum_{k=1}^{m}\Delta_k(\alpha) - 2(-1)^{n}\sum_{k=m+1}^{n}(-1)^{k}\Delta_k(\alpha) + 2\sum_{k=n+1}^{\infty}\Delta_k(\alpha)\,.\end{aligned} \tag{3.63}$$

We evaluate this for the following cases

(i) m and n are even,

(ii) m and n are odd ,

(iii) m even and n odd,

(iv) m odd and n even .

Here we consider the simplest case, when $n - m = h = \text{const}$.

Case 1. m **and** n **both either even or odd.** According to the definition of velocity $v_k(n)$, presented in Eq. (3.42), the VACF in Eq. (3.63) has the following contribution: The first sum represents those trajectories that start oscillating between $+1$ and -1 because $k < m < n$, so when m and n, are even-even or odd-odd, the velocity $v_k(m)v_k(n)$ will remain $+1$. The second sum refers to trajectories which got stuck between $+1$ and -1 for $m < k < n$ (*i.e.*, $v_k(n)$), while it is still travelling with velocity $+1$. In the third sum thee trajectories are flying with velocity $+1$ at both times $m < n < k$. We called this the travelling area. In the case a and b, Eq. (3.63) turns to:

$$\langle v(n)v(m)\rangle = 2\sum_{k=1}^{m}\Delta_k(\alpha) - 2(-1)^n\sum_{k=m+1}^{n}(-1)^k\Delta_k(\alpha) + 2\sum_{k=n+1}^{\infty}\Delta_k(\alpha)\,. \tag{3.64}$$

Case 2. m **even and** n **odd or vice versa.**

$$\langle v(n)v(m)\rangle = -2\sum_{k=1}^{m}\Delta_k(\alpha) - (-1)^n\sum_{k=m+1}^{n}(-1)^k\Delta_k(\alpha) + 2\sum_{k=n+1}^{\infty}\Delta_k(\alpha)\,. \tag{3.65}$$

Lemma 3.7.1. *Given $\alpha \geq 0$, the velocity auto-correlation function of the Slicer dynamics for uniformly distributed initial condition in $\widehat{M}_0$ has the following expressions*

$$\langle v(m)v(n)\rangle =$$

$$\begin{cases} -2\ell_m^+(\alpha) + 2\ell_n^+(\alpha) + 2\sum\limits_{k=1}^{m}\Delta_k(\alpha) - 4\sum\limits_{k=m+1}^{n/2}\Delta_{2k}(\alpha) + 2\sum\limits_{k=n+1}^{\infty}\Delta_k(\alpha), & \textit{for} \quad m,n \textit{ even}, \\ 2\ell_m^+(\alpha) - 2\ell_n^+(\alpha) + 2\sum\limits_{k=1}^{m}\Delta_k(\alpha) + 4\sum\limits_{k=m+1}^{(n-1)/2}\Delta_{2k}(\alpha) + 2\sum\limits_{k=n+1}^{\infty}\Delta_k(\alpha), & \textit{for} \quad m,n \textit{ odd}, \\ 1 - 4\ell_m^+(\alpha) + 2\ell_n^+(\alpha) - 4\sum\limits_{k=m+1}^{n/2}\Delta_{2k}(\alpha) + 2\sum\limits_{k=n+1}^{\infty}\Delta_k(\alpha), & \textit{for} \quad m \textit{ odd}, n \textit{ even}, \\ 1 - 2\ell_n^+(\alpha) + 4\sum\limits_{k=m+1}^{(n-1)/2}\Delta_{2k}(\alpha) + 2\sum\limits_{k=n+1}^{\infty}\Delta_k(\alpha), & \textit{for} \quad m \textit{ even}, n \textit{ odd}. \end{cases} \tag{3.66}$$

Proposition 3.7.2. *For $m \to \infty$ with $n = m + h$, $h > 0$ finite, the velocity auto-correlation function, $\langle v(m)v(n)\rangle$, defined in Eq.* (3.66)*, scales asymptotically as:*

$$\langle v(m)v(n)\rangle \sim \begin{cases} 1, & \textit{for} \quad m,\, n;\ \textit{even or odd}, \\ -1, & \textit{for} \quad m,\, n;\ \textit{even-odd, or odd-even}. \end{cases} \tag{3.67}$$

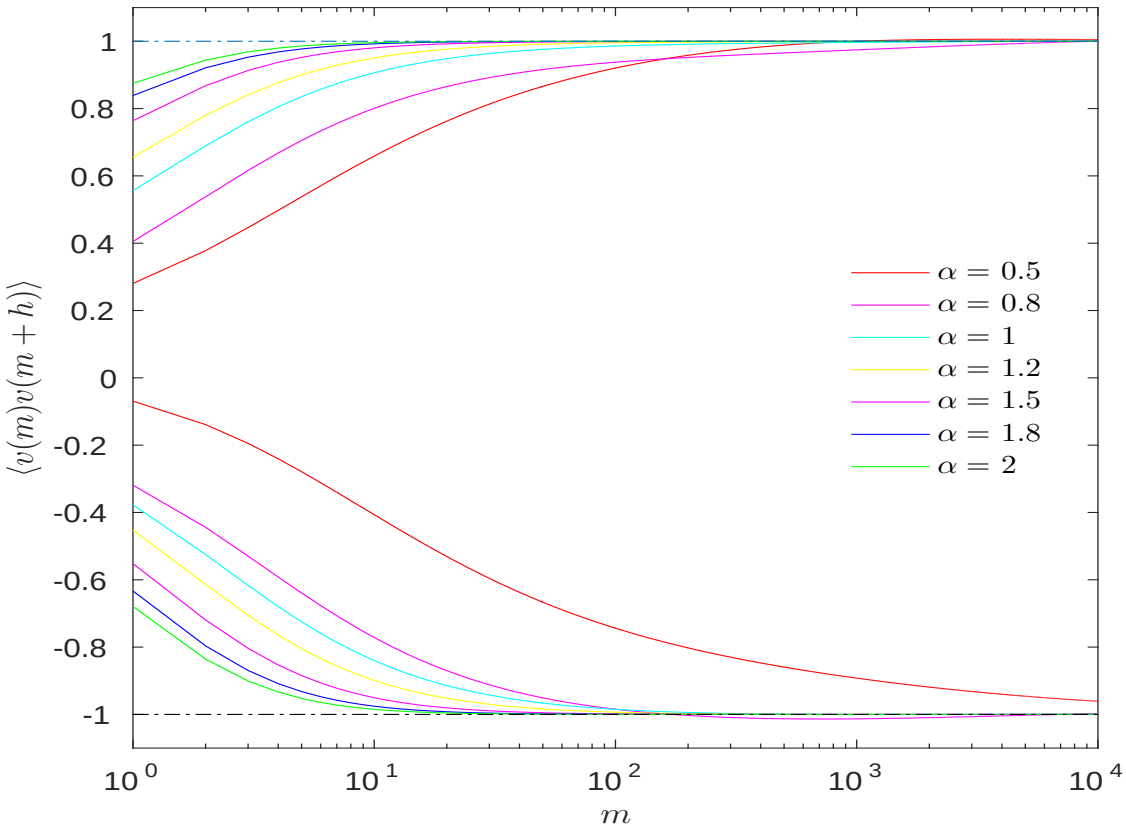

Figure 3.5: Illustration of VACF, Eq. (3.66), for $n - m = h = 10^3$, along with their respective asymptotic behaviour coumputed in Eq. (3.67). Irrespective of α all curves eventually converges to $+1$ or -1 with different convergence rate.

Proof. We start by Eq. (3.66). Recalling Eq. (3.14b), we have

$$\sum_{k=1}^{m} \Delta_k(\alpha) = \frac{1}{2}\,, \qquad \text{as} \quad m \to \infty\,. \tag{3.68}$$

While the sum $\sum_{k=m+1}^{n=m+h} \Delta_{2k}(\alpha)$, in Eq. (3.66), can be evaluated as follows

$$\sum_{k=m+1}^{n} \Delta_{2k}(\alpha) = \sum_{k=m+1}^{n} \frac{\alpha}{(2k)^{\alpha+1}} - \frac{\alpha\tilde{c}(\alpha)}{2^{\alpha+2}} \sum_{k=m+1}^{n} \frac{1}{k^{\alpha+2}} + \sum_{k=m+1}^{n} \mathcal{O}\left(\frac{1}{k^{\alpha+3}}\right), \tag{3.69}$$

and $\tilde{c}(\alpha)$ represented in Eq. (A.1b).

Thus the bound of the first sum of the previous expression is

$$\frac{h}{(m+h)^p} \leq \sum_{k=m+1}^{m+h} \frac{1}{k^p} \leq \frac{h}{m^p}\,, \tag{3.70}$$

similar bounds of remaining terms can be written as

$$\sum_{k=m+1}^{n=m+h} \frac{\alpha}{k^{\alpha+1}} \sim \alpha\, h\, m^{-(\alpha+1)}\,, \qquad \sum_{k=m+1}^{n=m+h} \frac{\alpha}{k^{\alpha+2}} = \mathcal{O}\left(m^{-(\alpha+2)}\right)\,,$$
$$\sum_{k=m+1}^{n=m+h} \mathcal{O}\left(\frac{\alpha}{k^{\alpha+3}}\right) = \mathcal{O}\left(m^{-(\alpha+3)}\right)\,. \tag{3.71}$$

Hence

$$\sum_{k=m+1}^{n=m+h} \Delta_{2k}(\alpha) \sim \alpha\, h\, m^{-(\alpha+1)}\,, \qquad h>0,\ \alpha>0\,,\ m\to\infty\,. \tag{3.72}$$

The results shown in Eq. (3.67) are obtained after collecting the terms. □

Remark 3.7.3. *For $m = 0$ the 2-times velocity auto-correlation functions presented in Eq.* (3.66) *reduces to the 1-time velocity auto-correlation, Eq.* (3.60).

3.8 Summary

Dynamical systems that exhibit all possible diffusion regimes in the field of anomalous transport are rare in literature, although in the realm of deterministic dynamics several authors [30, 31, 32] investigated anomalous diffusion. In [53] the SM moments of displacement were computed analytically. In this chapter (see also [25]) we performed a more daring task the computation of the position auto-correlation functions. In [53] it has also been proven that the SM and the LLg are asymptotically indistinguishable at the level of moments. This gives rise to the more challenging task to establish the equivalence also for the correlation functions. In chapter 4 we will show the statistical equivalence of the moments and the position auto-correlation functions of the SM and the LLg.

Chapter 4

Equivalence of position correlations: SM and LLg

"If you're going to Limit you dreams $\lim_{x\to\infty} f(x) = \infty$*,*
at least tend them to infinity."

— Plato Poster

In this chapter we establish the equivalence of the position auto-correlation functions of the Slicer Map [53] (deterministic process) and the Lévy-Lorentz gas [10] (stochastic process). We start with a brief introduction of the LLg and its analytical derivation for the moments of displacement. First we compare the analytical results of moments with numerically computed moments. Then, we compare the SM position auto-correlation functions which we have computed analytically in chapter 3, with the LLg position auto-correlation functions which are determined numerically. We will find that the position auto-correlations of the SM and to the LLg agree, at least in the low scatterers density of the LLg.

4.1 Lévy walks in quenched disordered media

The Lévy-Lorentz gas deals with the motion of a point particle in a one-dimensional random environment [4]. It moves ballistically (with velocity $\pm v$) between static point scatterers arranged on a line from which it is either transmitted or reflected

with probability 1/2. The distances r between two consecutive scatterers are random variables drawn independently from a Lévy distribution with density:

$$\lambda(r) \equiv \beta r_0^{\beta} \frac{1}{r^{\beta+1}}\,, \qquad r \in [r_0, +\infty). \tag{4.1}$$

Here $\beta > 0$ and r_0 is a cutoff fixing the characteristic length scale of the system. The setup is sketched in Fig. 4.1.

A subtle effect of quenched disorder is the dependence of the observables on the choice of the walker starting site. In particular, on in-homogeneous structures, the averages over different starting points can provide different results with respect to the corresponding local quantities [9, 11]. Thus there is an intricate dependence on initial condition. In what follows my computation refers to the non-equilibrium initial condition, where all particles start on the same scatterrer (*i.e.*, δ-function localized on a scatter.)

Under the hypothesis of *single long jumps*, Burioni *et al.* [10] derive an analytical expression for asymptotic behaviour of the characteristics scale length $\ell(t)$ of probability distribution $P(r,t)$ for the mean-square displacement $\langle r^2(t)\rangle$, when averaged over the scattering points. For large t it scales as follows

$$\ell(t) \sim \begin{cases} t^{1/(1+\beta)}\,, & \text{for} \quad 0 < \beta < 1\,, \\ \\ t^{1/2}\,, & \text{for} \quad \beta \geq 1\,. \end{cases} \tag{4.2}$$

First we define the most general scaling hypothesis for $P(r,t)$ in a one dimensional system:

$$P(r,t) = \ell^{-1}(t) f\left(\frac{r}{\ell(t)}\right) + g(r,t)\,, \tag{4.3}$$

where $\ell^{-1}(t) f(r/\ell(t))$ is the leading and $g(r,t)$ is subleading contribution. For convergence in probability for the leading term it is assumed that

$$\lim_{t\to\infty} \int_0^{vt} \mathrm{d}r \left| P(r,t) - \ell^{-1}(t) f\left(\frac{r}{\ell(t)}\right)\right| = 0\,, \tag{4.4}$$

while for convergence in probability of the subleading contribution they require

$$\lim_{t\to\infty} \int_0^{vt} \mathrm{d}r\, |g(r,t)| = 0\,. \tag{4.5}$$

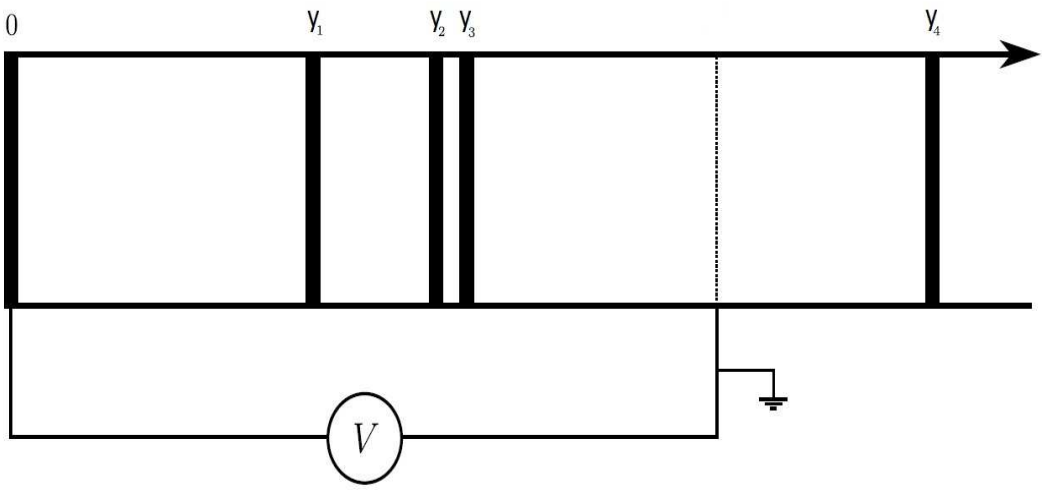

Figure 4.1: The one dimensional Lévy-Lorentz lattice gas model is equivalent electric problem (see [5]). Scatterers are placed randomly at positions $0, Y_1, Y_2, \cdots$. The spacing $|Y_{i+1} - Y_i|$ between scatterers are Lévy distributed according to the probability density Eq. (4.1).

The integration cut off is provided by the fact that the walker (a point particle) covers at most the distance vt in time t where $v = \pm 1$ is the velocity of the walker. The leading term $\ell^{-1}(t) f(r/\ell(t))$ is significantly different from zero for $r \lesssim \ell(t)$. The subleading term with the condition Eq. (4.5) leads to $\ell(t) \ll r < t$. Hence, it describes the behaviour at large distances. Since $g(r,t)$ is a subleading term, even it can give an essential contribution to the mean-square displacement $\langle r^2(t) \rangle$ if it does not vanish rapidly. The explicit analytical expression of the mean-square displacement now reads:

$$\langle r^2(t) \rangle = \int_0^{vt} \mathrm{d}r\, \ell^{-1}(t) f\left(\frac{r}{\ell(t)}\right) r^2 + \int_0^{vt} \mathrm{d}r\, g(r,t) r^2. \tag{4.6}$$

Anomalies for the standard behaviour $\langle r^2(t) \rangle \sim \ell^2(t)$, can be present for two significant reasons. Firstly, the second term in Eq. (4.6) can be dominant with respect to the first one (this happen *e.g.,* while averaging over any initial site [3]). Secondly, a more subtle anomaly shows up if the scaling function $f(x)$ decays gradually for $x \to \infty$, as observed in the annealed model described in [24, 56, 64]. Depending on the choice of β the process presents both behaviours [10].

Since the anomalies are determined by the regime where $r \gg \ell(t)$, we expect that the mean-square displacement is dominated by a *single long jump* of length r. Expectations over starting sites the probability of *"long jump"* is considerably higher at the initial step. Thus the single long range events appears at $t = 0$. On the other hand, it can happen, with equal probability, at any scattering site. Specifically, neglecting the multiple *"long jumps"*. We eventually get, for $r \gg \ell(t)$

$$P(r,t) \sim \frac{N(t)}{r^{1+\beta}} \ll 1\,, \tag{4.7}$$

where $N(t)$ is the number of scattering events visited by the particle at time t, and $1/r^{1+\beta}$ is the probability for a scatterer to be followed by the jump of length r. Discarding the single long jump, the distance crossed by the walker in time t is of order $\ell(t)$. According to Ref. [5], the number of scattering sites visited in this time is the resistance of a segment of length $\ell(t)$, *i.e.*, $\ell(t)^\beta$ for $\beta < 1$, and $\ell(t)$ for $\beta > 1$. This implies that $N(t) \sim t^{\beta/(1+\beta)}$ for $\beta < 1$ and $N(t) \sim t^{1/2}$ for $\beta \geq 1$. Now summarize our assumptions, we estimate $P(r,t)$ for $\beta < 1$ and $r \gg \ell(t)$ as

$$P(r,t) \sim t^{\beta/(\beta+1)} \frac{1}{r^{\beta+1}} \sim \frac{1}{\ell(t)} \left(\frac{r}{\ell(t)}\right)^{-(\beta+1)}\,. \tag{4.8}$$

The scaling function $f(x)$ features a long tail for large x decaying as $x^{-(\beta+1)}$.
We note that the contribution to $\langle r^2(t)\rangle$ of lengths $r \lesssim \ell(t)$ is always of order $\ell(t)^2$, while at larger distances, the dominant contribution is provided by previously stated probability distributions Eq. (4.8). The contribution coming from these tails are, for $\beta < 1$

$$\int_{\ell(t)}^{vt} \mathrm{d}r\, t^{\beta/(1+\beta)} \frac{r^2}{r^{1+\beta}} \sim t^{(2+2\beta-\beta^2)/(1+\beta)}\,. \tag{4.9}$$

On the other hand we also estimate $P(r,t)$ for $\beta \geq 1$ and $r \gg \ell(t)$, we have

$$P(r,t) \sim t^{1/2} \frac{1}{r^{\beta+1}} \sim \frac{1}{t^{(\beta-1)/2}\ell(t)} \left(\frac{r}{\ell(t)}\right)^{-(\beta+1)} \sim g(r,t)\,. \tag{4.10}$$

We discussed previously that $g(r,t)$ contributes a subleading term and converges in probability as defined by Eq. (4.5). Thus for $\beta > 1$, the dominant contribution provided by Eq. (4.10) to $\langle r^2(t)\rangle$ is:

$$\int_{\ell(t)}^{vt} \mathrm{d}r\, t^{1/2} \frac{r^2}{r^{1+\beta}} \sim t^{5/2-\beta}\,. \tag{4.11}$$

The contribution Eq. (4.9) for large times is always greater than $\ell^2(t)$, while Eq. (4.11) is dominant with respect $\ell^2(t)$ only for $\beta < 3/2$.

Barkai *et al.* [4] calculated bounds for the mean-square displacement for equilibrium and non-equilibrium initial conditions. Subsequently, Burioni *et al.* [10] adopted some simplifying assumptions expand this argument in order to find the asymptotic form for non-equilibrium conditions of all moments $\langle |r(t)|^p \rangle$ with $p > 0$

$$\langle |r(t)|^p \rangle \sim \begin{cases} t^{\frac{p}{1+\beta}}, & \text{for} \quad \beta < 1,\ p < \beta, \\ t^{\frac{p(1+\beta)-\beta^2}{1+\beta}}, & \text{for} \quad \beta < 1,\ p > \beta, \\ t^{\frac{p}{2}}, & \text{for} \quad \beta > 1,\ p < 2\beta - 1, \\ t^{\frac{1}{2}+p-\beta}, & \text{for} \quad \beta > 1,\ p > 2\beta - 1. \end{cases} \tag{4.12}$$

4.2 Comparison of the SM and the LLg

The similarities and differences between the LLg and the SM have been enlightened in [53]. The LLg shares basic similarities with the SM in that both systems deal with non-interacting particles and the initial condition plays an important role. On the other hand, the differences are evident: the LLg is a continuous-time stochastic system, while the SM is discrete-time and deterministic. In particular, the LLg dependence on the initial condition is much more intricate than in the SM: the LLg transport properties depend on whether a walker starts anywhere on the line, which means typically between two scatterers, called equilibrium initial condition, or exactly at a scatterer, called non-equilibrium initial condition [4, 10]. In the following we always consider non-equilibrium initial condition. In Ref. [4], the bounds for the mean-square displaccement have been calculated in both cases, while in [10], simplifying assumptions led to analytic expressions Eq. (4.12) for non-equilibrium conditions.

4.2.1 Moments of the displacement

For the mean-square displacement, $p = 2$, Eq. (4.12) implies

$$\langle r(t)^2 \rangle \sim t^\gamma \,, \quad \text{with} \quad \gamma = \begin{cases} 2 - \frac{\beta^2}{(1+\beta)} \,, & \text{for} \quad \beta < 1 \,, \\ \frac{5}{2} - \beta \,, & \text{for} \quad 1 \leq \beta < 3/2 \,, \\ 1 \,, & \text{for} \quad 3/2 \leq \beta \,. \end{cases} \tag{4.13}$$

Unlike the SM case, that enjoys sub-diffusive transport for $\alpha > 1$, non-equilibrium initial conditions for the LLg only lead to super-diffusive ($0 < \beta < 3/2$) or diffusive ($\beta \geq 3/2$) regimes: sub-diffusion is not expected.

Salari *et al.* [53] observed that the moments of the SM in its super-diffusive regime ($0 < \alpha < 1$) can be mapped to those of the LLg. They proved that all moments of the SM, Eq. (3.20), scale like those conjectured and numerically validated for the LLg, Eq. (4.12), once the second moments do. This is the case if the following holds, *cf.* Eqs. (3.19) and (4.13):

$$\alpha = \begin{cases} \frac{\beta^2}{(1+\beta)} \,, & \text{for} \quad 0 < \beta \leq 1 \,, \\ \beta - \frac{1}{2} \,, & \text{for} \quad 1 < \beta \leq \frac{3}{2} \,, \\ 1 \,, & \text{for} \quad \frac{3}{2} < \beta \,. \end{cases} \tag{4.14}$$

When adopting this mapping also all other moments of the SM agree with those of the LLg, Eq. (4.12). The (α, β) correspondence is represented in the inset of Fig. 4.3.

Adopting the relation Eq. (4.14) makes the SM and the LLg asymptotically indistinguishable from the viewpoint of moments, provided the assumptions of [10] hold. This equivalence is by no means trivial. In particular, the relation takes different functional forms in different parameters ranges, because the LLg has different scaling regimes for super-diffusive transport, while the SM has only one regime for all kinds of transport. The moments carry only partial information on the properties of the (anomalous) transport, and this information is not sufficient to distinguish the substantially different dynamics of the SM and the LLg. We now explore whether the position auto-correlations of the two dynamics differ. The correlations were calculated analytically for the SM in Sec. 3.4. This prediction will now be compared

to numerical data for the LLg. For correlations in the LLg there are no analytic results such as those of [10] for the moments.

4.2.2 Numerical implementation of the LLg

The non-equilibrium initial conditions for the LLg are implemented by starting each particle in the origin $x_0 = 0$, where a scatterer is assumed to be present in all realisations of the scatterers distribution. Moreover, trajectories that return to the origin provide a minor contribution to the moments for super-diffusive transport. For numerical efficiency we slightly modify the original dynamics of the LLg, placing a reflecting barrier at $x = 0$ and giving an initial positive velocity to each LLg walker. The resulting system, that evolves in $\mathbb{R}_0^+$, will be denoted LLg$^+$.

More precisely, let $(L_0, L_1, L_2, \ldots)$ be a sequence of i.i.d. random variables with density Eq. (4.1), and let $Y_{i+1} = Y_i + L_i$, $i = 0, 1, 2, \ldots$, with $Y_0 \equiv 0$. Denote by $\mathtt{Y}$ a given realisation of the sequence $(Y_0 \equiv 0, Y_1, Y_2, \ldots)$, that represents one set of random scatterers distribution in $\mathbb{R}_0^+$. We introduce the discrete-time process that represents the LLg$^+$at the scattering events. Let $\omega = (\omega_0, \omega_1, \omega_2, \ldots)$ be a random walk on $\mathbb{Z}_0^+$ with the conditions that $\omega_0 \equiv 0$ and $\omega_n - \omega_{n-1}$, $n = 1, 2, \ldots$ are i.i.d. dicotomic variables with $P(\omega_n - \omega_{n-1} = +1 \,|\, \omega_{n-1} \neq 0) = P(\omega_n - \omega_{n-1} = -1 \,|\, \omega_{n-1} \neq 0) = 1/2$, and $P(\omega_n - \omega_{n-1} = +1 \,|\, \omega_{n-1} = 0) = 1$. These conditions mean that the walk starts at 0 and whenever it returns there, it is reflected to the right. Away from 0, each walker follows a simple symmetric random walk. Then, the process that represents the position of the moving particle at the scattering events will be given by $\mathcal{W} = (Y_{\omega_0}, Y_{\omega_1}, Y_{\omega_2}, \ldots)$. From knowledge of $\mathcal{W}$, the continuous-time position $r(t)$ of the corresponding moving particle of LLg$^+$can be unambiguously reconstructed, because the velocity between any two scattering events is constant. This procedure has been implemented in a FORTRAN code by introducing a truncation in the sequence of scattering events $\bar{\omega} = (\omega_0, \omega_1, \omega_2, \ldots, \omega_N)$ that corresponds to a time $T = T(\bar{\omega}, \mathtt{Y})$ at which the process $r(t)$ stops. The stopping time $T(\bar{\omega}, \mathtt{Y})$ is random,

[1]Best fit to data estimated from the simple linear regression algorithm by using curve fitting tool box of MATLAB.

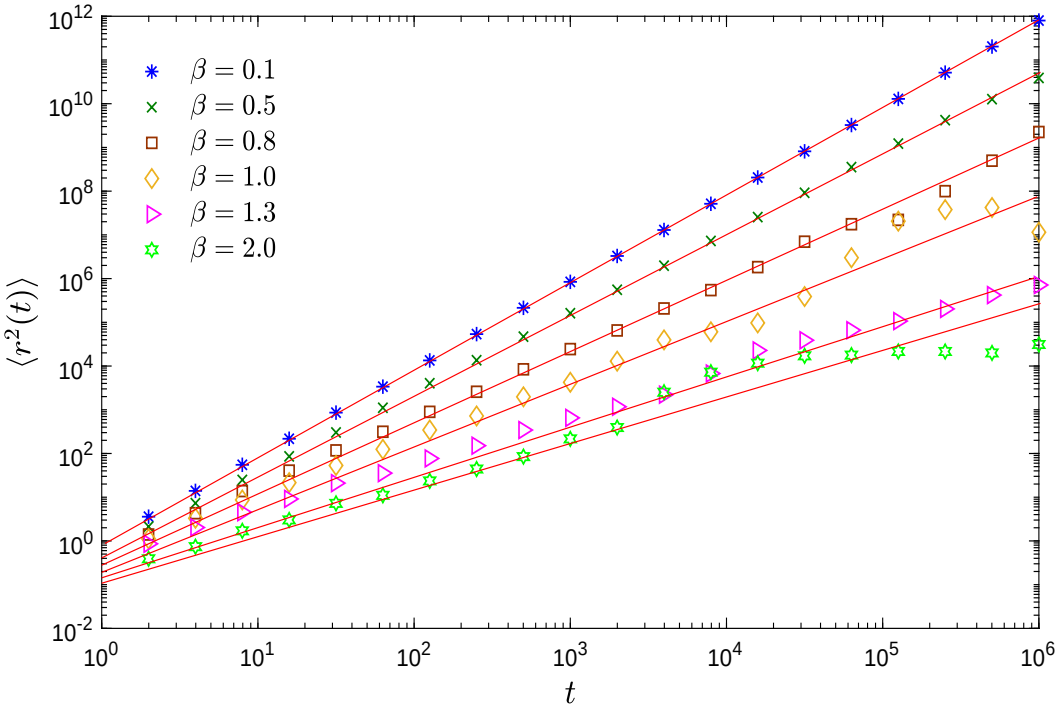

Figure 4.2: Data of the mean-square displacement of the LLg$^+$ are presented by symbols as a function of time t for different values of β. The thin (red) lines provide the best fit to the data[1]. In Fig. 4.3 and Tab. 4.1 we compare the fit results to the theoretical predictions.

and typically large if the scatterers are placed at large distances from one another, *i.e.*, for small β. In contrast, for large β, the distances are on average approximately equal r_0.[2] Therefore, one expects typically smaller and smaller $T(\bar{\omega}, \mathtt{Y})$ for larger and larger β, with the risk of under-sampling the large-time behaviour of LLg$^+$in numerical estimates of statistical properties. We took care that this problem does not arise in the data shown here.

The process $r(t)$ is affected by two sources of stochasticity: the environment $\mathtt{Y}$ and the scattering ω. Hence, averages can be taken in two different fashions. Let us denote by $\mathbb{E}_\omega$ the average w.r.t. the process ω, *i.e.*, the average over particles

[2]More precisely, if L is distributed according to Eq. (4.1), then $\mathbb{E}[L] = +\infty$ if $\beta \leq 1$ and $\mathbb{E}[L] = \frac{\beta r_0}{\beta - 1}$ if $\beta > 1$. Moreover the variance is $\frac{\beta\, r_0^2}{(\beta-2)(\beta-1)^2}$ for $\beta > 2$ and $+\infty$ for $\beta \leq 2$. For $\beta \gg 1$ the expected distance is therefore $\mathbb{E}[L] \simeq r_0$ with relative deviations of the order of β^{-1}.

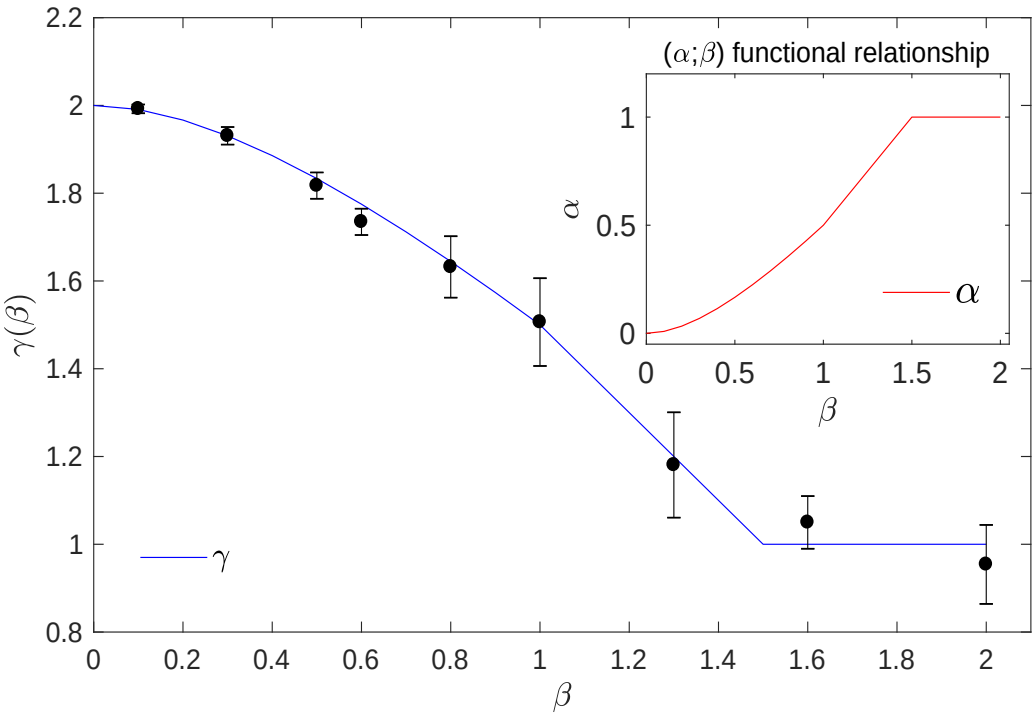

Figure 4.3: Theoretical values of the exponent γ in Eq. (4.13) compared with the fitted values as a function of β with their confidence bounds. The inset shows the (α, β) functional relationship, represented by Eq. (4.14).

that can be identified with their scattering sequences in a given realisation of the environment. Analogously, let $\mathbb{E}_Y$ denote the average over the random scatterers realisations. Then, the average of $r^2(t)$ at fixed scatterers configuration $\mathtt{Y}$, is denoted by $\mathbb{E}_\omega(r^2(t)|\mathtt{Y})$. This is a random quantity because $\mathtt{Y}$ is random. Averaging this quantity over the ensemble of scatterers yields the mean-square displacement of the LLg$^+$:

$$\langle r^2(t)\rangle_\beta = \mathbb{E}_Y[\mathbb{E}_\omega(r^2(t)|\mathtt{Y})]\,. \tag{4.15}$$

The subscript β indicates that the distribution of scatterers, Eq. (4.1), depends on β. Our choice of r_0 and v in the numerical simulations of the LLg$^+$ follows [10]. We set the characteristic length r_0 to 0.1, and the velocity v of the ballistic motion is always 1. The number of simulated scattering events is $N = 2.5\cdot 10^6$. We tested the

[3]The 95% confidence intervals are computed by simple linear regression model, which are presented in fourth column of Tab. 4.1, as the 0.975 quantile of data t-distribution with 18 degrees

β	γ		
	Eq. (4.13)	fit to data	C.I.[3] 95%
0.1	1.99	1.99	$\pm$0.01
0.3	1.93	1.93	$\pm$0.02
0.5	1.83	1.82	$\pm$0.03
0.6	1.77	1.73	$\pm$0.03
0.8	1.64	1.63	$\pm$0.07
1.0	1.50	1.51	$\pm$0.1
1.3	1.20	1.18	$\pm$0.1
2.0	1.00	0.95	$\pm$0.1

Table 4.1: Comparison of numerical values for the scaling exponent γ of the mean-square displacement in the LLg$^+$(third column) vs. the prediction of Eq. (4.13) (second column). The numerical estimate of γ agrees with the expressions derived and tested in [10], while confidence interval of fit data are presented in fourth column.

code by calculating the mean-square displacement of the LLg$^+$, in order to verify the power-law behaviour, Eq. (4.13). Table 4.1 and Fig. 4.3 show that our numerical results for the mean-square displacement for the LLg$^+$accurately reproduce the exponent given in Eq. (4.13) for the LLg, at least for not too large values of β. We attribute the slightly decreasing accuracy for increasing β to poorer statistics of the numerical estimates, as suggested above. Therefore, in the following we mainly focus on the cases with $\beta \lesssim 1$.

of freedom is $t^*_{18} = 2.101$.

4.3 Comparison of correlations of the LLg$^+$and SM

For $t, s \geq 0$, we define the position-position correlation function for the LLg$^+$as follows:

$$\varphi(t,s) = \langle r(t)\, r(s)\rangle_\beta = \mathbb{E}_Y[\mathbb{E}_\omega(r(t)r(s)|\mathtt{Y})]. \tag{4.16}$$

We aim at comparing the asymptotic behaviour of $\varphi(t,s)$ with that of the SM correlation function $\phi(n,m)$, Eq. (A.17a). Following the scaling adopted in Sec. 3.4.1, 3.4.2, and 3.4.3 for the SM we consider three cases:

1. $\varphi(t,s)$ for $t \to \infty$ at a fixed value of s.
2. $\varphi(t+\tau,t)$ for $t \to \infty$ at a fixed value of τ.
3. $\varphi(t+\ell\, t^q,t)$ for $t \to \infty$ at fixed q and $\ell > 0$.

Note that there is no free fit parameter in this comparison of the exponents, when one assumes the relation Eq. (4.14) between α and β.

We test the asymptotic scaling form of the mean-square displacement of the SM and the LLg$^+$when α and β obey Eq. (4.14). Here, we now verify with some scaling form of position auto-correlation function that α and β obey same relation Eq. (4.14).

4.3.1 Correlation $\langle r(t)\, r(s)\rangle_\beta$ with $s > 0$ constant

In Sec. 3.4.1, we provided the scaling of the auto-correlation function for the SM, Eq. (3.33), when one of its times is fixed. For $0 < \alpha < 1$ we have:

$$\langle \Delta x_n\, \Delta x_m\rangle_\alpha \sim \frac{2\,m}{1-\alpha}\, n^{1-\alpha}, \quad \text{as } n \to \infty. \tag{4.17}$$

Here and in the following we denote by $\langle\cdot\rangle_\alpha$ the ensemble average of the trajectories of the SM with parameter α. In analogy to the scaling, Eq. (4.17), we propose the following

Conjecture 4.3.1. a: The auto-correlation function of the LLg$^+$asymptotically scales as the one of the SM. When the time s is fixed, the correlation function $\langle r(t)\, r(s)\rangle_\beta$ obeys:

$$\lim_{t\to\infty} \frac{\langle r(t)\, r(s)\rangle_\beta}{\frac{2s}{w_1}\, t^{w_1}} \;=\; C_1 \neq 0\,, \tag{4.18a}$$

$$\text{with} \qquad w_1 = 1-\alpha(\beta) = \gamma(\beta) - 1\,. \tag{4.18b}$$

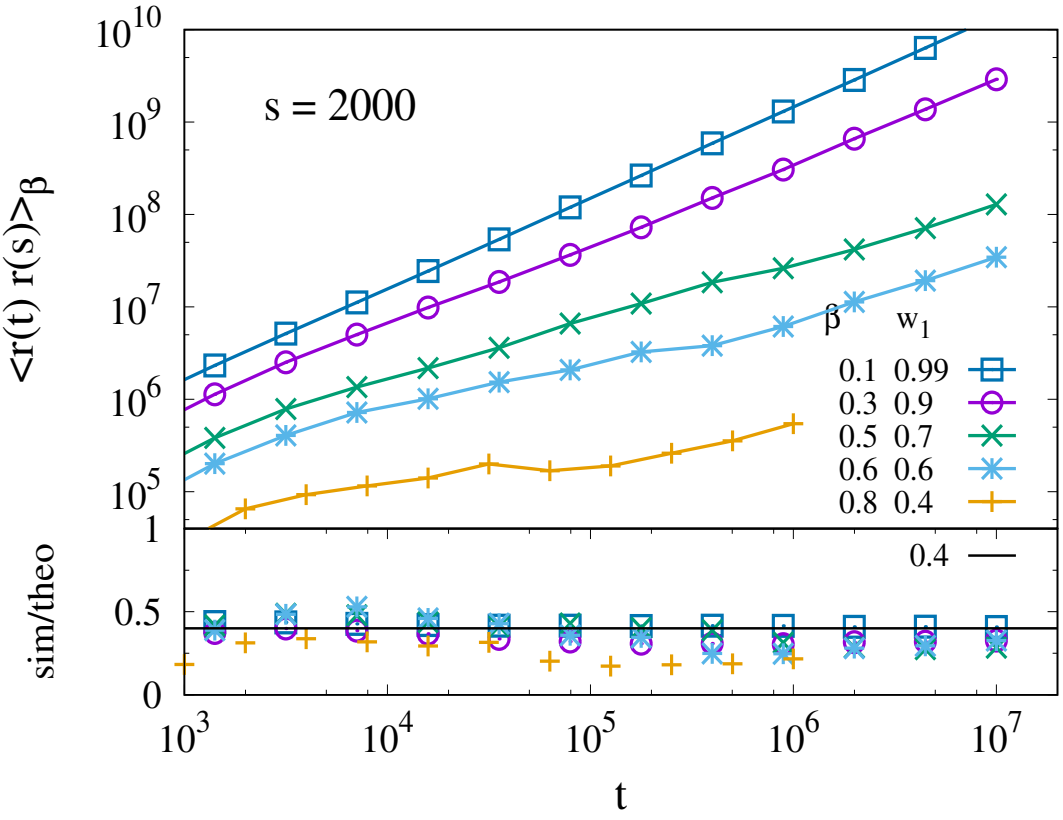

Figure 4.4: Log-log plot of the correlation $\langle r(t)\, r(s)\rangle_\beta$ as a function of time t, for different values of β and fixed s. The respective values for β are specified in the figure legend. In this figure we also specify the values for the exponents w_1 that provide the best fit to the data. The approach of the data towards the solid line in the bottom panel demonstrates that Eq. (4.18a) provides a faithful asymptotic scaling, with $C_1 = 0.4$. (Figure adapted from Ref. [25]).

Numerical Evidence. The LLg$^+$correlations $\langle r(t) r(s)\rangle_\beta$ have been computed for several values of s. Numerical results for fixed $s = 2000$ and different values of β

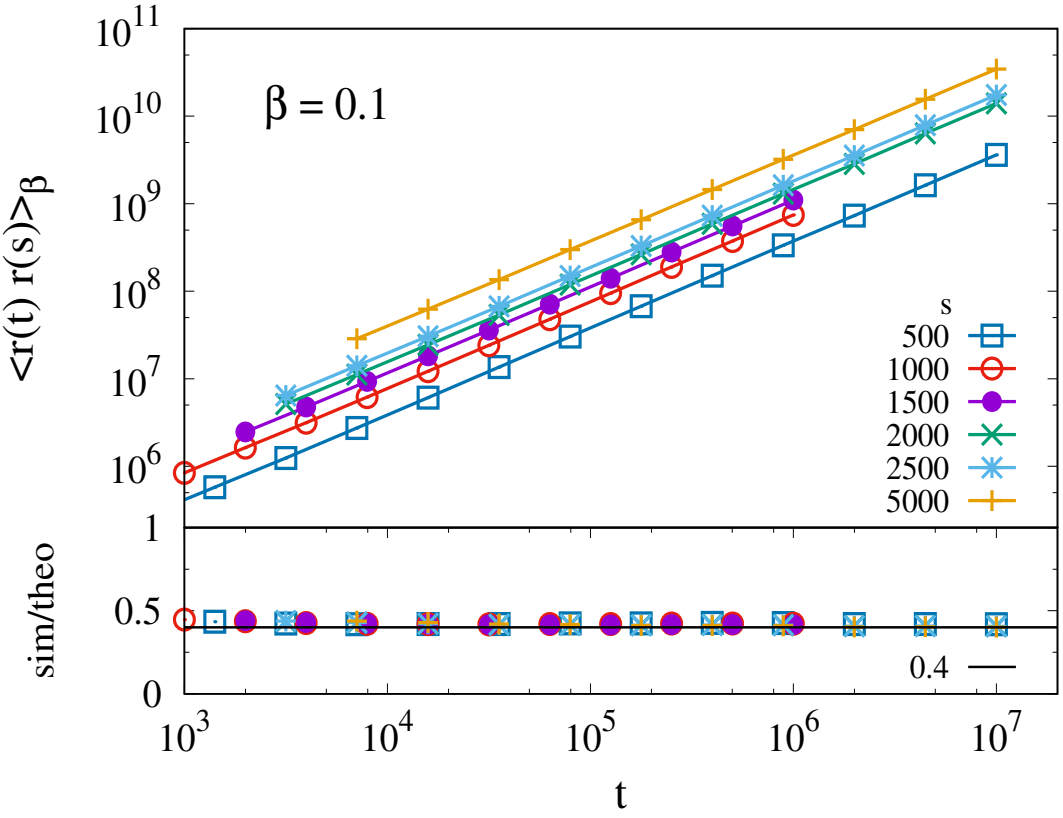

Figure 4.5: Log-log plot of the correlation $\langle r(t)\, r(s)\rangle_\beta$ as a function of time t, for different values of s with fixed β, the respective values are mentioned in legend of figure. The approach of the data towards the solid line in the bottom panel demonstrates that Eq. (4.18a) provides a faithful asymptotic scaling, with $C_1 = 0.4$. (Figure adapted from Ref. [25]).

between 0.1 and 0.8 are shown in the upper panel of Figure 4.4. Moreover, in the upper panel of Figure 4.5 we show data for $\beta = 0.1$ and six values of s in the range between 500 and 5000.

The respective lower panels show the time dependence of the ratio of Eq. (4.18a), in order to test its asymptotic convergence. For small β and different s this ratio provides a perfect data collapse (Figure 4.5). For larger β the data collapse is still fair in view of the numerical accuracy of our data (Figure 4.4). Moreover, the scaling exponents w_1 adopted to achieve the collapse depend on β and they are independent of s. The β-dependence agrees with the values $w_1 = 1 - \alpha(\beta) = \gamma(\beta) - 1$ suggested by the SM (*cf.* the values for $\gamma(\beta)$ provided in Table 4.1). Consequently, the SM

provides a faithful description of the LLg$^+$auto-correlation function, both as far as the exponents and the the parameter-dependence of the prefactor is concerned.

4.3.2 Correlation $\langle r(t+\tau)\, r(t)\rangle_\beta$ with $\tau > 0$ constant

In Sec. 3.4.2, we provided the scaling of the auto-correlation function for the SM, Eq. (3.35),when the difference h between the times is fixed. For $0 < \alpha < 2$ and fixed h, one has

$$\langle \Delta x_{m+h}\, \Delta x_m\rangle_\alpha \sim \frac{4}{2-\alpha} m^{2-\alpha}, \quad \text{as } m \to \infty\,. \tag{4.19}$$

In analogy to this scaling we propose the following conjecture

Conjecture 4.3.1. b: The auto-correlation function of the LLg$^+$asymptotically scales like the one of the SM. When the time lag h is fixed, the correlation function $\langle r(t)\, r(t+\tau)\rangle_\beta$ obeys:

$$\lim_{t\to\infty} \frac{\langle r(t+\tau)\, r(t)\rangle_\beta}{\frac{4}{w_2}\, t^{w_2}} \;=\; C_2 \neq 0\,, \tag{4.20a}$$

$$\text{with} \qquad w_2 = 2 - \alpha(\beta) = \gamma(\beta)\,. \tag{4.20b}$$

Numerical Evidence. In Figure 4.6 we show numerical data for a fixed value $\tau = 500$ and β in the range between 0.1 and 0.8, and Figure 4.7 represents a fixed value $\beta = 0.1$ and τ in the range between 100 and 8000. The lower panels show the ratio of the numerical data and the theoretical prediction, Eq. (4.20a). The curves are not globally linear in the log-log plot. However, they approach a power law for sufficiently large values of t, and in that range they nicely follow the asymptotic scaling, Eq. (4.20a), with $C_2 = 0.45$. The coefficient and the exponent of the asymptotic law are independent of τ and the dependence of w_2 faithfully agrees with the expected value $2 - \alpha(\beta) = \gamma(\beta)$, as provided in Table 4.1.

4.3.3 Correlation $\langle r(t+\ell\, t^q)\, r(t)\rangle_\beta$ with $\ell = 1$ and $0 < q < 1$ constant

In Sec. 3.4.3, we derived the auto-correlation for the SM, Eq. (3.33). For $0 < q < 1$

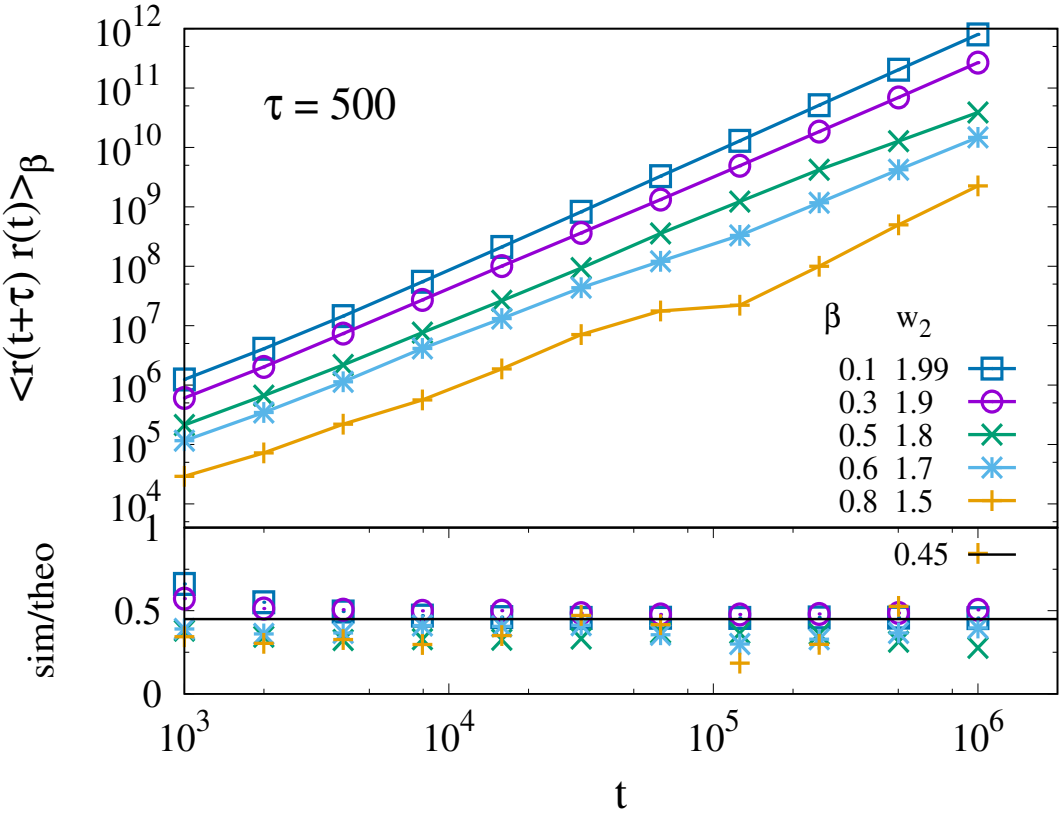

Figure 4.6: Log-log plots of the correlation $\langle r(t+\tau)\, r(t)\rangle_\beta$ as a function of time t for various values of β and any fixed τ. The respective values for β and τ are specified in the figure legends. This figure also specifies the values for the exponents w_2 that provide the best fit to the data. The approach of the data towards the solid line in the bottom panel demonstrates that Eq. (4.20a) provides a faithful asymptotic scaling, with $C_2 = 0.45$. (Figure adapted from Ref. [25]).

and $0 < \alpha < 1$, one has:

$$\langle \Delta x_{m+m^q}\, \Delta x_m \rangle_\alpha \sim \frac{4}{2-\alpha}\, m^{2-\alpha}, \quad \text{as } m \to \infty\,. \tag{4.21}$$

In analogy to this scaling, we propose the following

Conjecture 4.3.1. c: The auto-correlation function of the LLg$^+$asymptotically scales like the SM. For the time time lag ℓt^q with $0 < q < 1$ between its two

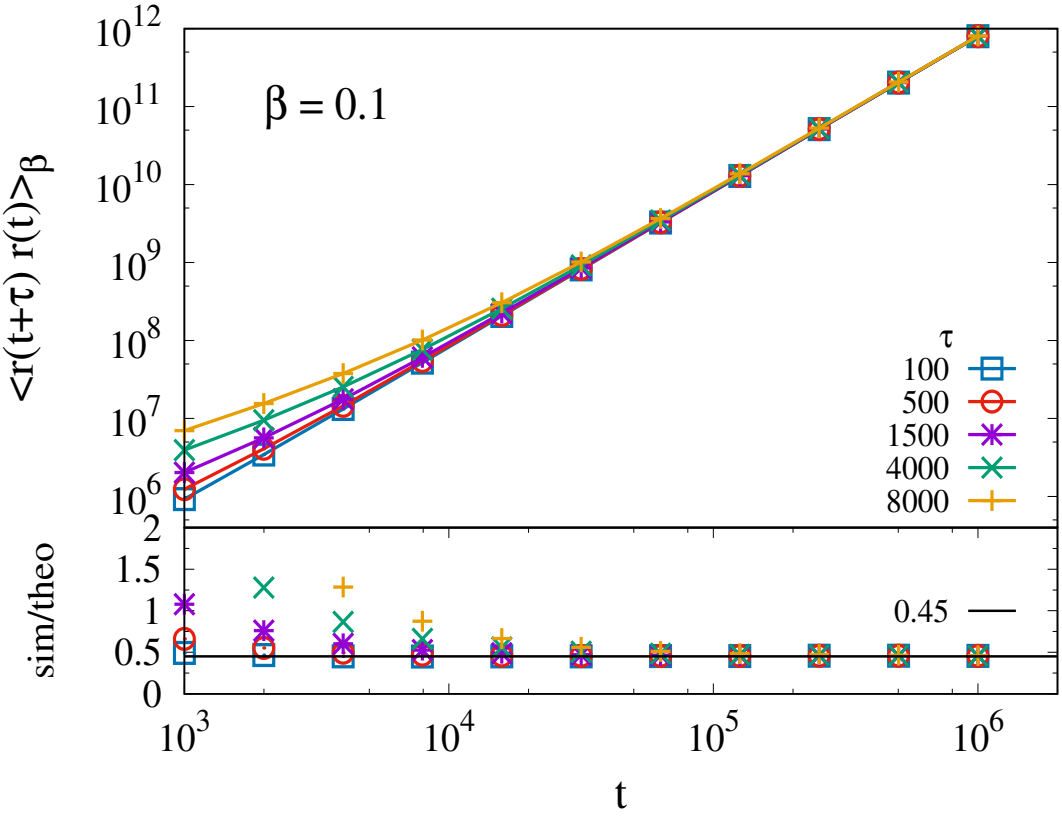

Figure 4.7: Log-log plots of the correlation $\langle r(t+\tau)\, r(t)\rangle_\beta$ as a function of time t for various values of *tau* and fixed β. The respective values for β and τ are specified in the figure legends. This figure also represent for different choice of τ values all curves converge to the same line. The approach of the data towards the solid line in the bottom panel demonstrates that Eq. (4.20a) provides a faithful asymptotic scaling, with $C_2 = 0.45$. (Figure adapted from Ref. [25]).

times, the auto-correlation function $\langle r(t)\, r(t+\ell\, t^q)\rangle_\beta$ obeys:

$$\lim_{t\to\infty} \frac{\langle r(t+\ell\, t^q)\, r(t)\rangle_\beta}{\frac{4}{w_3}\, t^{w_3}} \quad = \quad C_3 \neq 0\,, \tag{4.22a}$$

$$\text{with} \qquad w_3 = 2 - \alpha(\beta) = \gamma(\beta)\,. \tag{4.22b}$$

Numerical Evidence. In Figure 4.8, we show numerical data for a fixed value $q = 0.7$ and β in the range between 0.1 and 0.8, and Figure 4.9 represents a fixed value $\beta = 0.1$ and q in the range between 0.1 and 0.9. The lower panels show the ratio of the numerical data and expected scaling, Eq. (4.22a). Also in this case there is an excellent agreement between the data and the proposed asymptotic scaling.

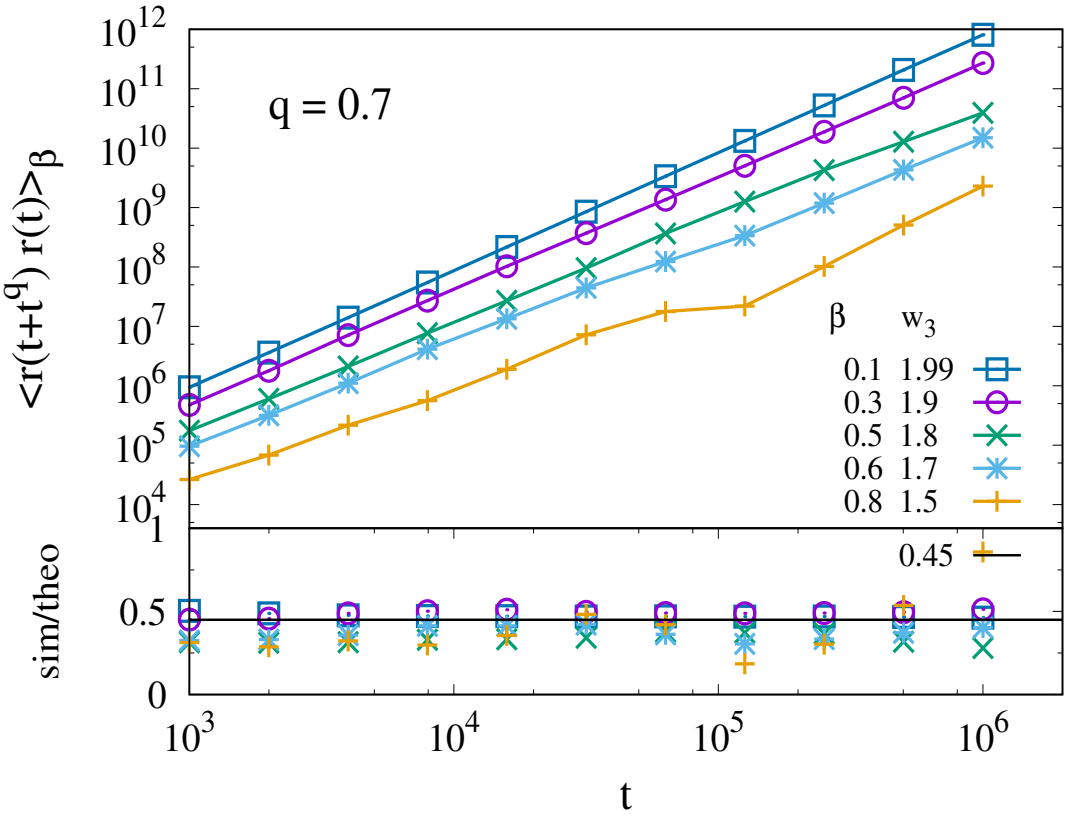

Figure 4.8: Log-log plot of the correlation $\langle r(t)r(t+t^q)\rangle_\beta$ as a function of time t for various values of β and of h. The respective values for β and fixed q are specified in the figure legends. This figure also specifies the values for the exponents w_3 that provide the best fit to the data. Also in this case the dependence of w_3 agrees faithfully with the expected value $\gamma(\beta)$ that has been provided in Table 4.1. Further, the approach of the data towards the solid line in the bottom panel demonstrates again that Eq. (4.22a) provides a faithful asymptotic scaling, with $C_3 = 0.45$. (Figure adapted from Ref. [25]).

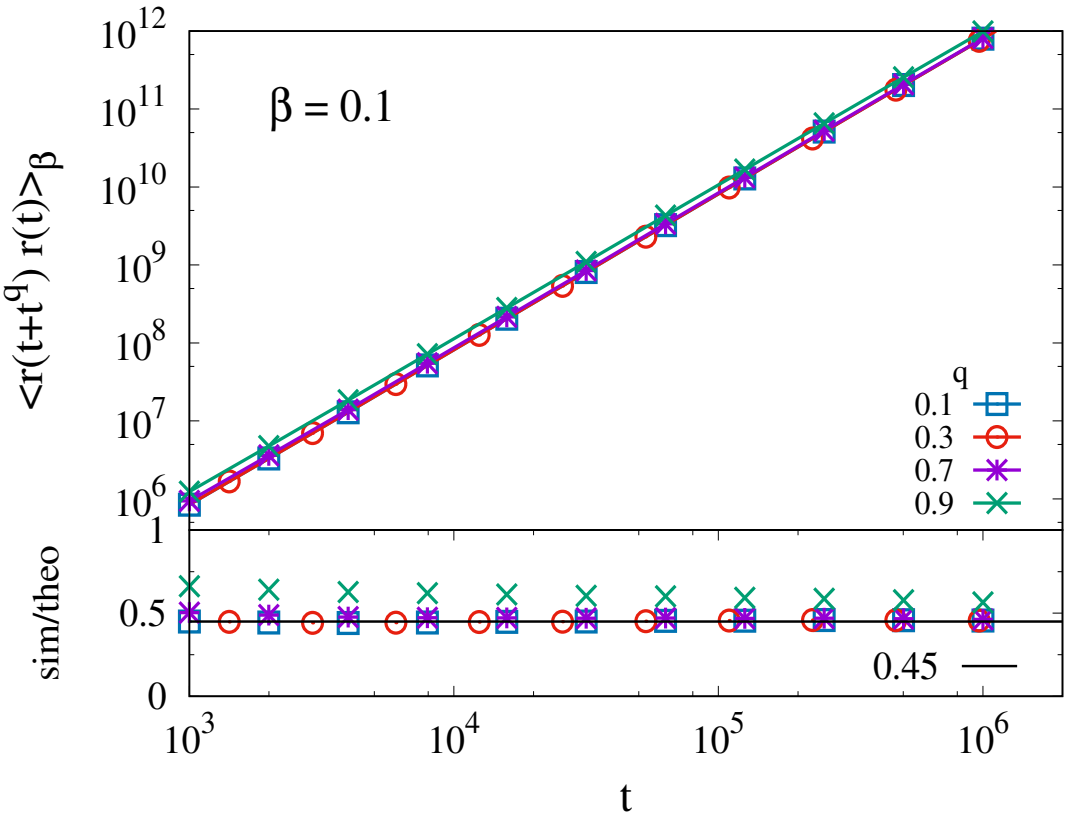

Figure 4.9: Log-log plot of the correlation $\langle r(t)r(t+t^q)\rangle_\beta$ as a function of time t for various values of q and of fixed β. The respective values for β and h are specified in the figure legends. Further, the approach of the data towards the solid line in the bottom panel demonstrates again that Eq. (4.22a) provides a faithful asymptotic scaling, with $C_3 = 0.45$. (Figure adapted from Ref. [25]).

4.4 Quantitative comparison of the LLg$^+$and SM correlations function

In the previous section we explicitly compared the position auto-correlation function of the SM and the LLg$^+$. Now we shed some light on linear representation and the detailed quantitative analysis of correlation functions. The asymptotic exponents mapping of the correlations provides a faithful agreement between the SM and the LLg$^+$. We also provide numbers in brackets $(\cdot)$ that are error[4] in the trailing digits of the exponents which strengthen our argument with the SM exponents.

Different cases of correlations are considered for asymptotic scaling to gain insight in the properties of SM and LLg$^+$.

Correlation $\langle r(t)r(h)\rangle_\beta$ with $h > 0$ constant

The correlation for the SM is, see Sec. 3.4.1,

$$\langle x(n)x(h)\rangle_\alpha \sim \frac{2h}{1-\alpha}\, n^{1-\alpha}, \quad n \to \infty. \tag{4.23}$$

The LLg$^+$correlations $\langle r(t)r(h)\rangle_\beta$ have been computed for several values of h and the asymptotic form

$$\langle r(t)r(h)\rangle_\beta \sim d(h)\, t^{w(h)}\,, \tag{4.24}$$

has been fitted to the data. The results, for $h = 10^3, 10^4$ and several values of β are reported in Tab. 4.2. The exponents are quite close, at least $\beta \lesssim 1$. To corroborate this result, in Figs. 4.10 we report the log-log plot of $\langle r(t)r(h)\rangle_\beta$ vs t for some β's and varying h. The lines are parallel, indicating that $w(h)$ is independent of h, as in the case of SM. In Tab. 4.3, for h ranging from 500 up to 5000, with $\beta = 0.1$, that agrees with exponent Eq. (4.23). The pre-factors $d(h)$ in Eq. (4.24) and $c(h) = 2h/(1-\alpha)$ in Eq. (4.23) are computed. Again, the correlations $\langle x(n)x(h)\rangle_\alpha$ of the SM reproduce quite well the asymptotic behaviour of the corresponding correlation function in LLg$^+$. In Figs. 4.10(d-f), the correlations $\langle r(t)r(h)\rangle_\beta$ for the same values of h,

[4]We compute errors while fitting data by simple linear regression model on curve fitting tool (cftool) of MATLAB. These are with 95% confidence bounds.

β	$1-\alpha$ Eq. (4.23)	$w(h)$ $h=10^3$	$w(h)$ $h=10^4$
0.1	0.991	0.994(3)	0.996(3)
0.3	0.93	0.93(2)	0.93(2)
0.5	0.83	0.80(4)	0.84(5)
0.6	0.77	0.73(6)	0.78(6)
0.8	0.64	0.65(8)	0.64(9)
1.3	0.2	0.28(9)	0.22(15)

Table 4.2: The 3rd and 4th column provides the exponent $w(h)$ of the asymptotic relation (4.24) for the LLg$^+$, as β is varied (1st column). We provide data for $h = 10^3$ and $h = 10^4$, where the numbers in brackets provide the error in the trailing digits of the exponents. These values should be compared to the prediction of $1-\alpha$, Eq. (4.23), that are given in the second column.

h	$1-\alpha$	$w(h)$	$\log_{10}(c(h))$	$\log_{10}(d(h))$
500	0.991	0.991(3)	3.00	2.62(1)
1000	0.991	0.994(3)	3.31	2.92(1)
1500	0.991	0.995(3)	3.48	3.08(1)
2000	0.991	0.993(3)	3.61	3.21(1)
2500	0.991	0.993(3)	3.70	3.31(1)
5000	0.991	0.993(4)	4.00	3.60(1)

Table 4.3: The exponent $w(h)$ (3rd column) provide the asymptotic estimate of Eq. (4.24) is compared with the corresponding exponent $1-\alpha$ of the SM, Eq. (4.23), for various values of h with $\beta = 0.1$. The logarithm of the pre-factors in Eqs. (4.23) and (4.24) are also shown. The number in brackets $(\cdot)$ are the error in the trailing digits.

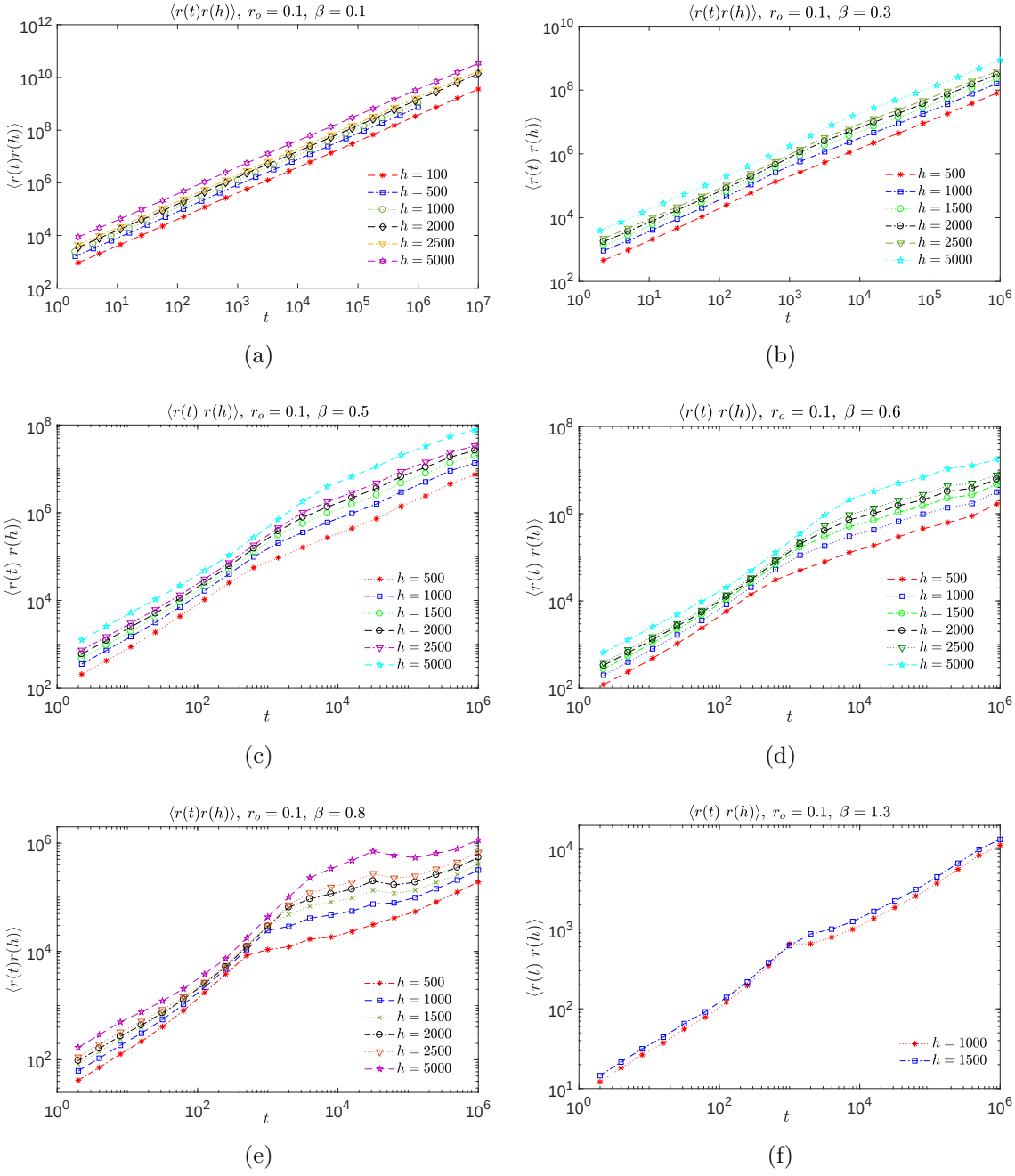

Figure 4.10: Log-log plot of the correlation $\langle r(t)r(h)\rangle_\beta$ as a function of time t with different fixed h for varying β's in sub-figures. The parallel lines show the strong dependence on finite h, while the parallelization is gradually lost as β increases.

but with $\beta = 0.6, 0.8, 1.3$, are reported. The difference with the cases $\beta \leq 0.3$, are striking since the behaviour of correlations is not uniform over the time interval of our simulations and, in particular, non-linear (in the log-log plot). For the largest times, say $t > 10^5$, the parallel linear behaviour already observed in Fig. 4.10a, seems to be restored. Unfortunately, we do not have enough statistics for large times to give further support to this observation.

Correlation $\langle r(t)r(t+h)\rangle_\beta$ with $h > 0$ constant

In this case the SM has the following asymptotic behaviour, see Sec. 3.4.2

$$\langle x(n)x(n+h)\rangle_\alpha \sim \frac{4}{2-\alpha} n^{2-\alpha}, \quad \text{as } n \to \infty, \tag{4.25}$$

which will again be compared with

$$\langle r(t)r(t+h)\rangle_\beta \sim d(h)\, t^{w(h)}. \tag{4.26}$$

We remark that the coefficient and the exponent of the asymptotic law of the SM are independent of h. The log-log plots of $\langle r(t)r(t+h)\rangle_\beta$ vs t for several values of h with some β ranging 0.1 to 1.3 are given in Fig. 4.11. We observe that the curves are not globally linear in the log-log plot. They are linear for sufficiently large values of t, and for such t's, the curves with different h superimpose quite well. This indicates that the LLg$^+$ exponents $w(h)$ and the factor $d(h)$ are in fact independent of h, as in the case of the SM. The crossover between pre-asymptotic (non power-law) and asymptotic (power-law) behaviours can be roughly placed at h. The dashed line in all subplots of Fig. 4.11, represents the fit of the largest t's. For $\beta = 0.1$ the fit gives $w(h) \approx 1.9905$, while $2 - \alpha \approx 1.9909$; the figures suggest that the asymptotic behaviour Eq. (4.26) is reached with $d(h)$ and $w(h)$ independent of h, as in Eq. (4.25). More details are given in Tab. 4.4, which shows that the SM exponent $2 - \alpha$ constitutes a good approximation of $w(h)$ up to moderately large values of β.

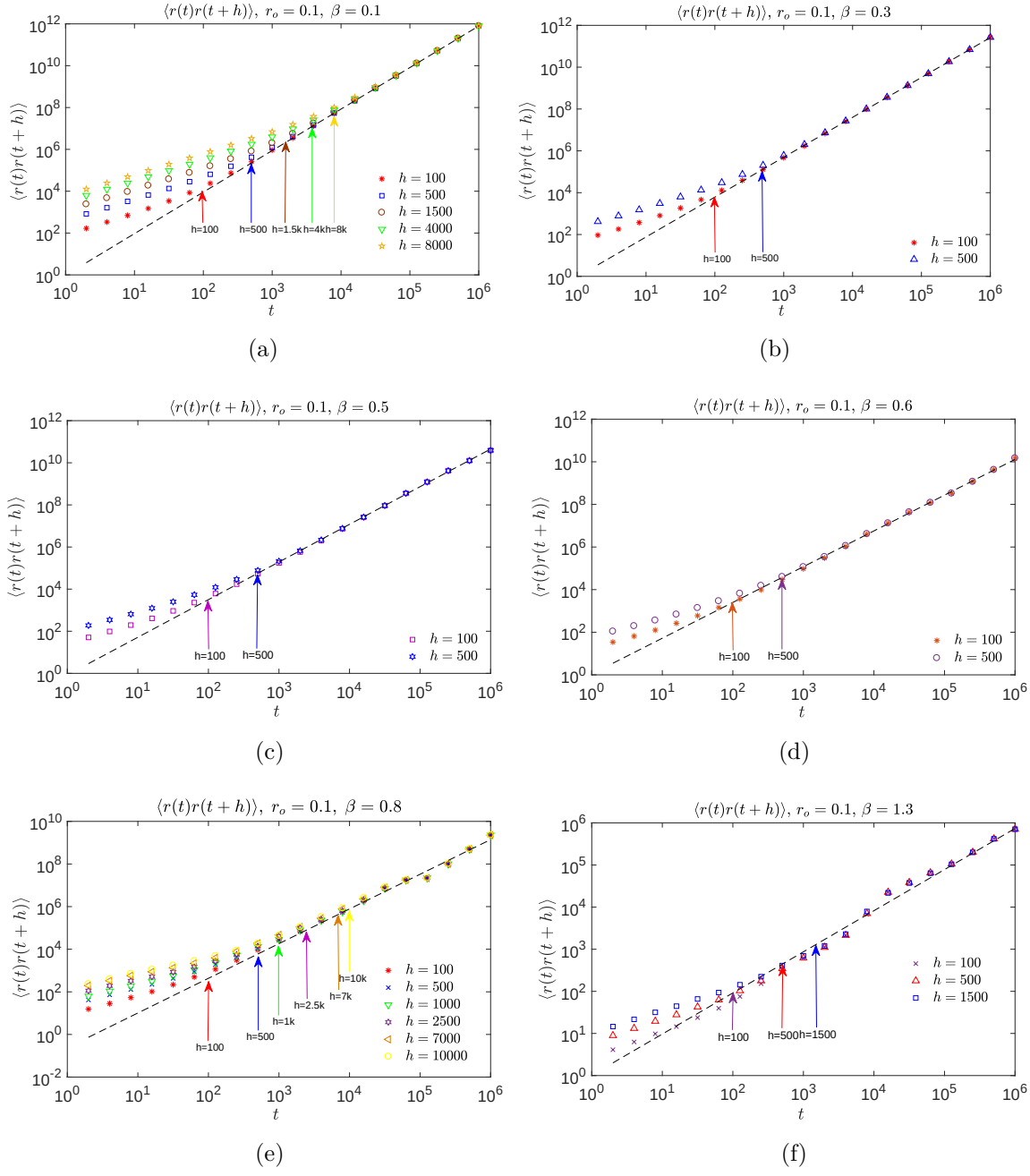

Figure 4.11: Log-log plot of the correlation $\langle r(t)r(t+h)\rangle_\beta$ as a function of time t for some finite values of h with different β. The vertical arrow heads at $\log_{10} h$ identify the crossover between the pre-asymptotic and asymptotic behaviours. The dashed lines represent the best fit of the largest values of t.

β	$2-\alpha$ Eq. (4.25)	$w(h)$ $h=100$	$w(h)$ $h=500$
0.1	1.991	1.993(2)	1.986(5)
0.3	1.931	1.93(3)	1.93(3)
0.5	1.833	1.81(3)	1.79(4)
0.6	1.775	1.76(14)	1.76(14)
0.8	1.644	1.63(24)	1.63(34)
1.3	1.2	1.04(9)	1.03(12)

Table 4.4: The 3rd and 4th column provide the exponent $w(h)$ in the asymptotic estimate (4.26) for $h = 100, 500$. The numbers in brackets state the errors in trailing digits of the exponents. These values are compared with the prediction $2-\alpha$, Eq. (4.25) in 2nd column.

Correlation $\langle r(t)r(t+\ell\, t^q)\rangle_\beta$ with $\ell > 0$ and $0 < q < 2$ constant

In Sec. 3.4.3, it has been noted for the SM that this correlation function depends on q. We consider separately the two case: $0 < q < 1$ and $1 < q < 2$.

• **Case** 1 : For $0 < q < 1$ and $0 < \alpha < 2$, we have:

$$\langle x(m+\ell\, m^q)x(m)\rangle_\alpha \sim \frac{4}{2-\alpha} m^{2-\alpha}, \quad \text{as } m \to \infty. \tag{4.27}$$

This will be compared with the expected power-law behaviour of the corresponding LLg$^+$correlation:

$$\langle r(t)r(t+\ell\, t^q)\rangle_\beta \sim d(\ell, q) t^{w(\ell,q)}. \tag{4.28}$$

Figure 4.12 represents the correlation Eq. (4.28) for some β and q. The result shows a weak dependence (on the scale of the plot) on q for small values, say $q \leq 0.9$, and a quite good power-law behaviour, as in the SM case, Eq. (4.27). We report the data concerning this case in Tab. 4.5. The slopes of the lines in Fig. 4.12, *i.e.*, the estimated exponents $w(\ell, q)$, can be found in this table. For β fixed, $w(\ell, q)$ provides an approximation of the SM exponent $2-\alpha$ that seems to depend weakly on q (at least for small values of β). Again, we have a better agreement between the SM and

β	$2-\alpha$ Eq. (4.27)	$w(\ell,q)$ $q=0.1$	$w(\ell,q)$ $q=0.3$	$w(\ell,q)$ $q=0.7$	$w(\ell,q)$ $q=0.9$
0.1	1.99	1.991(2)	1.992(2)	1.990(1)	1.971(2)
0.3	1.93	1.931(7)	1.93(1)	1.92(2)	1.92(17)
0.5	1.83	1.80(3)	1.80(3)	1.80(2)	1.79(3)
0.6	1.77	1.76(14)	1.78(7)	1.77(7)	1.77(14)
0.8	1.64	1.64(33)	1.65(12)	1.63(34)	1.64(26)
1.3	1.2	1.02(12)	1.12(7)	1.02(12)	

Table 4.5: The columns 3−6 provide the exponent $w(\ell,q)$ of the asymptotic estimate (4.28) for $q=0.1,\ 0.3,\ 0.7$, $\ell=1$ with varying β. The numbers in brackets $(\cdot)$ provide the error in the trailing digits of the exponents. These values are compared with the SM exponent $2-\alpha$, Eq. (4.27) in 2$^{\rm nd}$ column.

the LLg$^+$at small and moderate values of β. Indeed, the latter case is problematic as can be seen in Figs. 4.12(e-f) where, besides the weak dependence on small q, two different linear behaviours (in log-log plot) can be appreciated. These behaviours may represent two different pre-asymptotic and asymptotic regimes. Similarly we can see that as the parameter β and the exponent q increase, we gradually loose the good agreement with the SM correlation function. These less convincing results are appearing due to the fact that poor statistics in our numerical simulations.

• **Case 2 :** For $1<q<2$ the $\langle x(m+\ell\, m^q)x(m)\rangle_\alpha$ correlation with $1<q<2$ also depends on the choice of α:

$$\langle x(m+\ell\, m^q)x(m)\rangle_\alpha \sim \begin{cases} \frac{2\,\ell^{1-\alpha}}{1-\alpha}\, m^{1+q\,(1-\alpha)}\,, & \text{for} \quad 0<\alpha<1\,, \\ \frac{2\,\alpha}{(2-\alpha)\,(\alpha-1)}\, m^{2-\alpha}\,, & \text{for} \quad 1<\alpha<2\,. \end{cases} \tag{4.29}$$

They are compared with the corresponding LLg$^+$ correlation function Eq. (4.28).

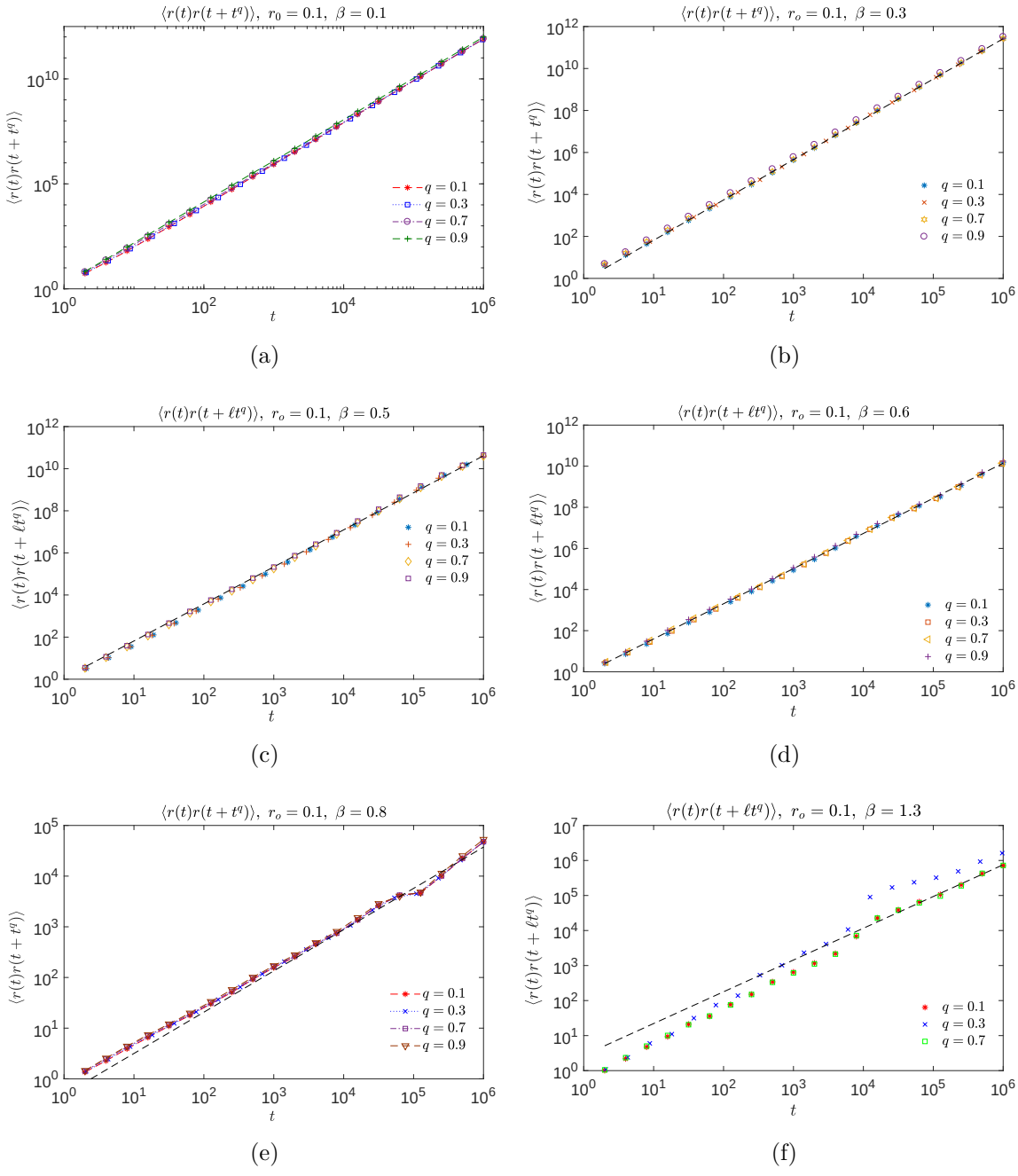

Figure 4.12: Log-log plot of the correlation $\langle r(t)r(t+\ell\, t^q)\rangle_\beta$ as a function of time t with $\ell = 1$, of some values of q, for given β. The dashed line in the plots represent the best fit in the asymptotic regime.

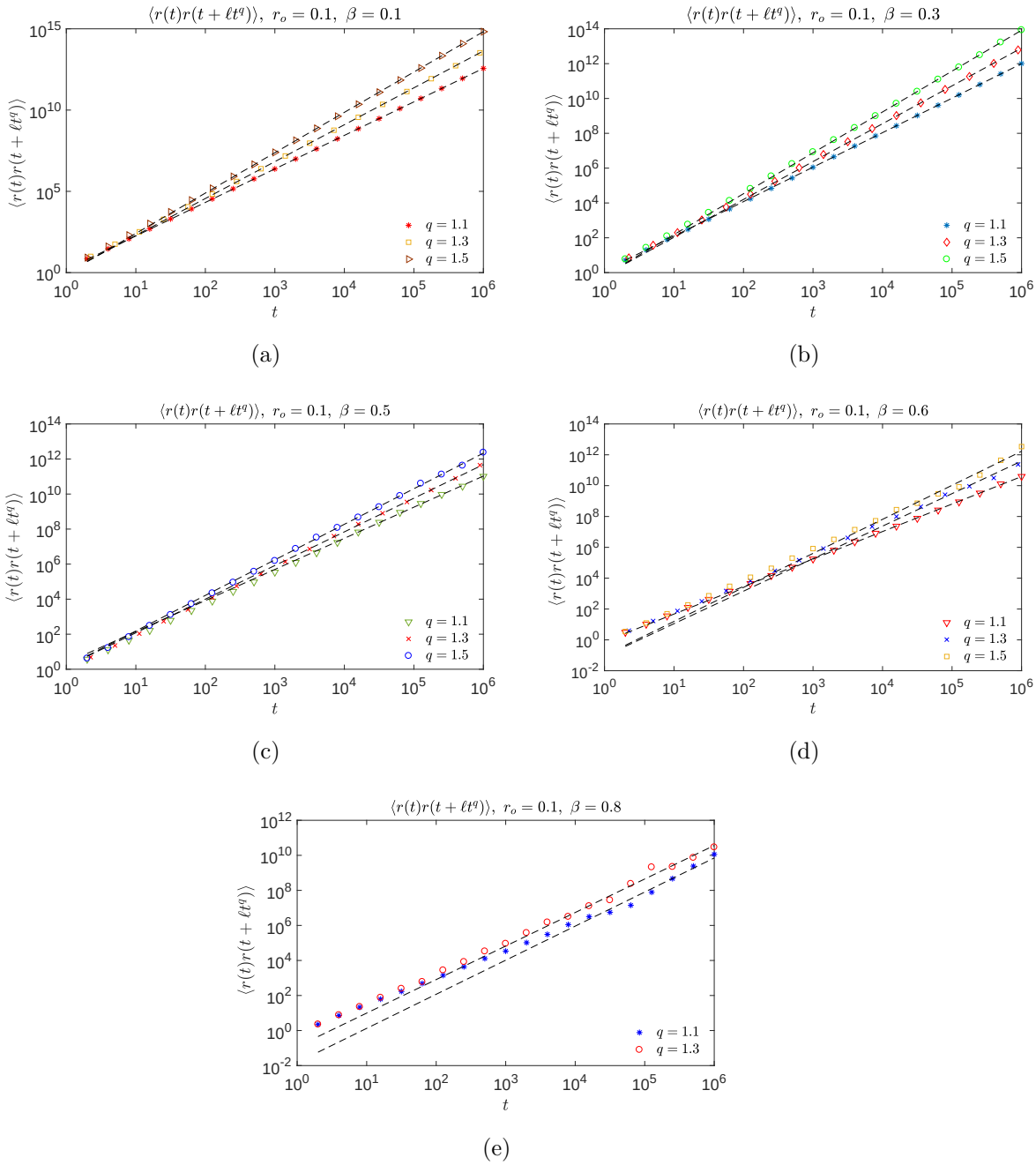

Figure 4.13: Log-log plot for correlation function $\langle r(t)r(t+\ell t^q)\rangle_\beta$ as a function of time t for given β, $\ell = 1$ with some fixed q's. The dashed lines represent different pre-asymptotic and asymptotic behaviours.

Figure 4.13 represents the correlation Eq. (4.28) for $\beta = 0.1, 0.3, 0.5, 0.6, 0.8$, with $\ell = 1$ and fixed $q = 1.1, 1.3, 1.5$. The dashed lines in Figs. 4.13, are least square fit to the data. The angular coefficients of the asymptotic (dashed) lines in the figures,

β	ζ $q = 1.1$ Eq. (4.29)	$w(\ell, q)$ $q = 1.1$	ζ $q = 1.3$ Eq. (4.29)	$w(\ell, q)$ $q = 1.3$	ζ $q = 1.5$ Eq. (4.29)	$w(\ell, q)$ $q = 1.5$
0.1	2.09	2.059(2)	2.29	2.271(7)	2.49	2.49(1)
0.3	2.02	1.99(1)	2.21	2.16(1)	2.40	2.36(3)
0.5	1.92	1.85(1)	2.08	1.95(1)	2.25	2.06(1)
0.6	1.85	1.82(5)	2.01	1.99(3)	2.16	2.2(2)
0.8	1.71	1.7(1)	1.84	1.8(1)	1.97	1.9(3)

Table 4.6: The columns 3, 5 and 7 provide the exponent $w(\ell, q)$ of the asymptotic estimate Eq. (4.28) for $q = 1.1, 1.3, 1.5$, $\ell = 1$ with varying β. The numbers in brackets $(\cdot)$ provide the error in the trailing digits of the exponents. These values are compared with the SM exponent $\zeta = 1 + q(1 - \alpha)$, Eq. (4.29), in 2^{nd}, 4^{th} and 6^{th} columns respectively.

i.e., the estimated exponents $w(\ell, q)$, can be found in Tab. 4.6. Again we have pretty nice agreement between the SM and the LLg$^+$ at least for moderate values of β. Although we have reported our results up to $\beta = 0.8$ (that means $\alpha = 0.3556$, according to the functional relationship shown in Eq. (4.14)). In Figs. 4.13(a-c) we observed power law behaviour, also for short times. While the forthcoming cases the agreement for larger β's is problematic, as can be seen in Figs. 4.13(d-e). Here we also see two different linear regimes on log-log scale. These two behaviours distinguish pre-asymptotic and asymptotic regimes.

4.5 Summary

In this chapter we established the equivalence of the position auto-correlation function of the SM and the LLg. We started by revisiting the notion of moments of displacement for the one dimensional LLg both analytically and numerically and then extended it to correlation functions. It holds based on the relation, Eq. (4.14)

between the parameter α and β of the SM and the LLg, respectively. Since there are no analytical expression for the position auto-correlation functions of the LLg. We explored in how far those of the SM provide a faithful description. In chapter 3 we explicitly calculated the position auto-correlation function of the SM in different scaling forms by considering the functional relationship between two times, whereas in the LLg the same time relation have been considered for numerical computation of position auto-correlation functions.

We hence established statistical equivalence of the moments of displacement as well as the position auto-correlation functions up to low scatterers density (*cf.* Eq. (4.1)). At larger density the equivalence seems to be gradually lost. This could have been possible due to poor statistics.

Chapter 5

Universality class in anomalous diffusion

"Nothing happens until something moves"

— Albert Einstein

In this chapter, we present a generic dynamics, which we develop in search of a universality class, called Fly-and-Die dynamics. The dynamics is analytically tractable, and upon tuning a single parameter, it gives rise to different types of anomalous diffusion. Trajectories of the system are never periodic, first they fly ballistically from an initial position. Then, when they reach a certain pre-determined position they never move again (they die). The moments and the time-auto-correlation function are computed explicitly. They have the same asymptotic scaling as those of the SM. Moreover this dynamics can be mapped to other anomalous transport process by matching the exponent of the mean-square displacement and the prefactor according to the power-law tails. Subsequently the dynamics provides the dependence of all other moments and of the same correlation functions. We also compute the velocity auto-correlation function of the FnD, which can be used to distinguish different dynamics in the class.

5.1 The Fly-and-Die dynamics

We label trajectories by their initial position, x_0. Until time $t_c(x_0)$, the trajectory moves along the positive x axis with unit velocity. At time $t_c(x_0)$ it stops and remains at position $x_0 + t_c(x_0)$ for all later times. Accordingly, we call this a FnD dynamics. Its position at time t is given by

$$x(x_0,t) = \begin{cases} x_0 + t\,, & \text{for} \quad t \le t_c(x_0)\,, \\ x_0 + t_c(x_0)\,, & \text{for} \quad t \ge t_c(x_0). \end{cases} \tag{5.1a}$$

Super-diffusive motion is expected to emerge when the distribution of the times for the flights, $t_c(x_0)$, has a power-law tail. To be concrete, we consider here the case

$$t_c(x_0) = \left(\frac{b}{x_0}\right)^{1/\xi}\,, \tag{5.1b}$$

with initial conditions x_0 uniformly distributed in the interval $[0,1]$ and control parameter ξ. In the following we explore the moments for the displacement, the position-position and the velocity-velocity auto-correlation function of this ensemble of trajectories.

5.1.1 Moments of displacement

The probability $P(>t)$ to perform a flight longer than t amounts to the fraction of initial conditions x_0 with $t_c(x_0) > t$. It is given by

$$P(>t) = x_0(t) = \frac{b}{t^\xi}\,. \tag{5.2}$$

Consequently, for $p \neq \xi$ the p^{th} moment of the displacement takes the form

$$\begin{aligned} \langle |\Delta x(t)|^p \rangle &= \langle |x(x_0,t) - x_0|^p \rangle\,, \\ &= \int_0^1 \mathrm{d}x_0\, |x(x_0,t) - x_0|^p\,, \\ &= \int_0^{P(>t)} \mathrm{d}x_0\, t^p + \int_{P(>t)}^1 \mathrm{d}x_0\, \left(t_c(x_0)\right)^p\,, \\ &= b\, t^{p-\xi} + \frac{\xi\, b^{p/\xi}}{\xi - p}\, \left(1 - b^{1-p/\xi}\, t^{p-\xi}\right)\,, \\ &= \frac{p\, b}{p-\xi}\, t^{p-\xi} + \frac{\xi}{\xi - p}\, b^{p/\xi}\,, \qquad \text{for } p \neq \xi\,, \end{aligned} \tag{5.3a}$$

and an analogous calculation yields

$$\begin{aligned}\langle|\Delta x(t)|^p\rangle &= \int_0^{P(>t)} \mathrm{d}x_0\, t^p + \int_{P(>t)}^1 \mathrm{d}x_0\, x_0^{-1}\,, \\ &= b\, t^{p-\xi} - b\,\xi\, \ln P(>t)\,, \\ &= b + b\, \ln \frac{t^\xi}{b} \qquad \text{for } p = \xi\,. \end{aligned} \tag{5.3b}$$

In the limit of long times, $t \gg b^{1/\xi}$, we hence find the scaling

$$\langle|\Delta x(t)|^p\rangle \sim \begin{cases} \frac{\xi}{\xi - p}\, b^{p/\xi}\,, & \text{for} \quad p < \xi\,, \\ b\, \ln \frac{t^\xi}{b}\,, & \text{for} \quad p = \xi\,, \\ \frac{p\, b}{p-\xi}\, t^{p-\xi}\,, & \text{for} \quad p > \xi\,. \end{cases} \tag{5.4}$$

In particular the mean-square displacement, $\langle|\Delta x|^2\rangle$, approaches a constant value for $\xi > 2$. It grows logarithmically for $\xi = 2$, and according to a power-law with an exponent $\gamma = 2 - \xi$ for $0 < \xi < 2$. In the part $0 < \xi < 1$ of the latter regime the dynamics is super-diffusive with exponent $\gamma = 2 - \xi > 1$. For $\xi = 1$ we find normal diffusion, and for $1 < \xi < 2$ the FnD dynamics exhibits sub-diffusion. The FnD dynamics, Eq. (5.1), can therefore give rise to behaviour reflecting all scenarios for the anomalous diffusion. In the following we focus on the regime of super-diffusive behaviour, $0 < \xi < 1$. In this range we have (*cf.* Eq. (5.3a))

$$\langle|\Delta x(t)|^2\rangle = \frac{2b}{\gamma}\, \left(t^\gamma - \frac{2-\gamma}{2}\, b^{\gamma/(2-\gamma)} \right)\,. \tag{5.5}$$

We will come back to this dependence when discussing the asymptotics of the position auto-correlation function.

5.1.2 Position auto-correlation function

The position auto-correlation function for the FnD dynamics is defined as

$$\begin{aligned}\phi(t_1, t_2) &= \langle \Delta x(t_1)\, \Delta x(t_2)\rangle\,, \\ &= \langle (x(x_0, t_1) - x_0)\, (x(x_0, t_2) - x_0)\rangle\,, \\ &= \int_0^1 \mathrm{d}x_0\, (x(x_0, t_1) - x_0)\, (x(x_0, t_2) - x_0)\,. \end{aligned} \tag{5.6}$$

In order to evaluate the integral we follow the convention that t_2 is always larger or equal to t_1. Accordingly we split the integration range into three intervals

$0 < x_0 < P(> t_2)$ The trajectory is still flying at time t_2 such that $\Delta x(t_1) = t_1$ and $\Delta x(t_2) = t_2$.

$P(> t_2) < x_0 < P(> t_1)$ The trajectory is still flying at time t_1 but it has died by the time t_2. Consequently, $\Delta x(t_1) = t_1$ and $\Delta x(t_2) = t_c(x_0)$.

$P(> t_1) < x_0 < 1$ The trajectory died before t_1. Consequently, $\Delta x(t_1) = \Delta x(t_2) = t_c(x_0)$.

Splitting the integral and performing a calculation analogous to the derivation of Eq. (5.3), one finds [1]

$$\phi(t_1,t_2) = \begin{cases} \frac{b\,t_1\,t_2^{\gamma-1}}{\gamma-1} - \frac{(2-\gamma)\,b\,t_1^{\gamma}}{\gamma\,(\gamma-1)} - \frac{(2-\gamma)\,b^{2/(2-\gamma)}}{\gamma}\,, & \gamma \neq 1\,, \\ b\,t_1\,\ln\frac{t_2}{t_1} + 2b\,t_1 - b^2\,, & \gamma = 1\,. \end{cases} \tag{5.7}$$

For $t_1 = t_2$ this reduces to the mean-square displacement, Eq. (5.5).

In the literature one commonly normalizes the correlation function (5.7) by the variance calculated at either of the two times, or by the geometric mean of the variance, $[\langle|\Delta x(t_1)|^2\rangle\,\langle|\Delta x(t_2)|^2\rangle]^{1/2}$. The normalized variance is a function of t_2/t_1 in that case and it approaches one for $t_2/t_1 \to 1$, because $\phi(t_1,t_2)$ may tend to $\langle|\Delta x(t_1)|^2\rangle$ plus terms that become negligible in that limit.

For the representation of the asymptotics on double logarithmic scale this is not convenient. We rather normalize therefore by the time difference $h = t_2 - t_1$. For $\gamma \neq 1$ this provides

$$\begin{aligned} \frac{(\gamma/b)\,\phi(t_1,t_2)}{h^\gamma} &\simeq \frac{\gamma}{\gamma-1}\,\frac{t_1}{h}\,\left(\frac{t_1}{h}+1\right)^{\gamma-1} - \frac{2-\gamma}{\gamma-1}\,\left(\frac{t_1}{h}\right)^{\gamma}\,, \\ &\simeq \frac{\gamma}{\gamma-1}\,\left(\frac{t_1}{h}\right)^{\gamma}\left[\left(1+\frac{h}{t_1}\right)^{\gamma-1} - \frac{2-\gamma}{\gamma}\right], \end{aligned} \tag{5.8a}$$

[1] In appendix. B.1 we give the full derivation.

which gives rise to the asymptotic scaling

$$\frac{(\gamma/b)\ \phi(t_1,t_2)}{h^\gamma} \sim \begin{cases} 2\ \left(\frac{t_1}{h}\right)^\gamma\,, & \text{for} \quad t_1 \gg h\,, \\ \frac{\gamma}{\gamma-1}\ \frac{t_1}{h}\,, & \text{for} \quad t_1 \ll h\,, \gamma \neq 1\,, \\ \frac{t_1}{h}\ \ln\frac{h}{t_1}\,, & \text{for} \quad t_1 \ll h\,, \gamma = 1\,. \end{cases} \tag{5.8b}$$

Therefore Eq. (5.8), establishes a scaling form: when normalizing by h^γ, the correlation function $\phi(t_1,t_2)$ is a function of a single argument t_1/h.

We hence predict a data collapse when plotting the left hand side of Eq. (5.8) as function of t_1/h. The asymptotics for large t_1/h amounts to the mean-square displacement, where $h = 0$. In this regime we see a scaling with the exponents, γ, characterizing the anomalous growth of the mean-square displacement. The asymptotics for small t_1/h amounts to situations where t_1 and t_2 are very far separated in time (*i.e.*, $t_2 \gg t_1$). When both times are large one commonly observes that the correlation function decays with h like $1/h$, in accordance with the prediction of Eq. (5.8b).

5.1.3 3-point position auto-correlation function

The 3-point position auto-correlation function for the FnD dynamics is defined as

$$\begin{aligned} \phi(t_1,\,t_2,\,t_3) &= \langle \Delta x(t_1)\ \Delta x(t_2)\ \Delta x(t_3)\rangle \\ &= \langle (x(x_0,t_1)-x_0)\ (x(x_0,t_2)-x_0)\ (x(x_0,t_3)-x_0)\rangle \\ &= \int_0^1 \mathrm{d}x_0\ (x(x_0,t_1)-x_0)\ (x(x_0,t_2)-x_0)\ (x(x_0,t_3)-x_0)\,, \end{aligned} \tag{5.9}$$

where it is assumed that $t_1 < t_2 < t_3$. Accordingly, we split the integration range into four intervals

$0 < x_0 < P(>t_3)$ **:** The trajectories are still flying at time t_3 such that $\Delta x(t_1) = t_1,\ \Delta x(t_2) = t_2,\ \Delta x(t_3) = t_3$.

$P(>t_3) < x_0 < P(>t_2)$ **:** The trajectories are still flying until time t_2 but it has died by the time t_3. Consequently, $\Delta x(t_1) = t_1,\ \Delta x(t_2) = t_2,$ and $\Delta x(t_3) = t_c(x_0)$.

$P(> t_2) < x_0 < P(> t_1)$ **:** The trajectories are still flying until time t_1 but it has died by the time t_2. One have, $\Delta x(t_1) = t_1$, $\Delta x(t_2) = \Delta x(t_3) = t_c(x_0)$.

$P(> t_1) < x_0 < 1$ **:** The trajectories died before t_1. Consequently, $\Delta x(t_1) = \Delta x(t_2) = \Delta x(t_3) = t_c(x_0)$.

Splitting the integral, and working out the respective integrals[2] for $\gamma \neq 1$,

$$\phi(t_1,\, t_2,\, t_3) = \frac{b}{\gamma-1}\, t_1\, t_2\, t_3^{\gamma-1} - \frac{b\,(2-\gamma)}{\gamma(\gamma-1)}\, t_1\, t_2^{\gamma} - \frac{b\,(2-\gamma)}{\gamma(\gamma+1)}\, t_1^{\gamma+1} - \frac{b^{3/(2-\gamma)}\,(2-\gamma)}{\gamma+1}\,. \tag{5.10}$$

Assume the following relationship between three different times, we get

1. $t_2 = t_1 + h_1$, as $t_1 \to \infty$, and $h_1 > 0$ finite.

2. $t_3 = t_2 + h_2$, as $t_2 = t_1 + h_1$, where $t_1 \to \infty$, and $h_2 > 0$ finite.

Provided that $h_1 = h_2$, and $t_1 \to \infty$, one can write expression for $\gamma \neq 1$ as

$$\frac{(\gamma/b)\,\phi(t_1,t_2,t_3)}{h^{\gamma+1}}$$
$$\simeq \frac{\gamma}{\gamma-1}\left(\frac{t_1}{h}\right)^{\gamma+1}\left[\left(1+\frac{h}{t_1}\right)\left(1+\frac{2\,h}{t_1}\right)^{\gamma-1} - \frac{2-\gamma}{\gamma}\left(1+\frac{h}{t_1}\right)^{\gamma} - \frac{(2-\gamma)(\gamma-1)}{\gamma(\gamma+1)}\right], \tag{5.11a}$$

which has the following asymptotic scaling

$$\frac{(\gamma/b)\,\phi(t_1,t_2,t_3)}{h^{\gamma+1}} \sim \begin{cases} \frac{3\,\gamma}{\gamma+1}\left(\frac{t_1}{h}\right)^{\gamma+1}, & \text{for} \quad t_1 \gg h, \\ \frac{t_1}{h}\,, & \text{for} \quad t_1 \ll h. \end{cases} \tag{5.11b}$$

We predict a data collapse also for the 3-point correlation function when plotting the l.h.s of Eq. (5.11b) as a function of t_1/h. For $t_1/h > 0$, the correlation function $\phi(t_1,t_2,t_3)$ asymptotically scales as a $\gamma+1$ power law, as the third moment does with t_1.

The case when t_1, t_2 are fixed and $t_3 \to \infty$, one find the asymptotic scaling as

$$\frac{(\gamma/b)\,\phi(t_1,t_2,t_3)}{h_2^{\gamma+1}} \sim \frac{\gamma}{\gamma-1}\left(1+\frac{h_1}{t_1}\right)\left(\frac{t_1}{h_2}\right)^2, \qquad t_2 > t_1,\; h_2 \gg t_1, \tag{5.11c}$$

where $h_2 = t_3 - t_2$. This reduces to the $(\gamma/b)\,\phi(t_1,t_2,t_3)/h^{\gamma+1} \sim \frac{\gamma}{\gamma-1}\,(t_1/h)^2$, if $t_1 = t_2$ are fixed and $h = t_3 - t_1$.

[2]See appendix. B.2 for the detailed derivation.

Remark 5.1.1. *For $\xi > 0$, $\gamma = 2 - \xi$ and $t_1 = t_2 = t_3$, Eq.* (5.10) *reduces to the third moment of displacement, Eq.* (5.4) *with $p = 3$.*

5.1.4 n-point position auto-correlation function

The n-point position auto-correlation function for the FnD dynamics is defined as

$$\begin{aligned}\phi(t_1, t_2, \cdots t_n) &= \langle \Delta x(t_1)\, \Delta x(t_2) \cdots \Delta x(t_n) \rangle\,, \\ &= \langle (x(x_0, t_1) - x_0)\ (x(x_0, t_2) - x_0) \cdots\ (x(x_0, t_n) - x_0) \rangle\,, \\ &= \int_0^1 \mathrm{d}x_0\ (x(x_0, t_1) - x_0)\ (x(x_0, t_2) - x_0) \cdots\ (x(x_0, t_n) - x_0)\ ,\end{aligned}$$

where it is assumed that $t_1 \leq t_2 \leq \cdots \leq t_n$. Accordingly, we split the integration range into n intervals

$0 < x_0 < P(> t_n)$ The trajectories are still flying at time t_n such that $\Delta x(t_1) = t_1,\ \Delta x(t_2) = t_2, \cdots, \Delta x(t_{n-1}) = t_{n-1},\ \Delta x(t_n) = t_n$.

$P(> t_n) < x_0 < P(> t_{n-1})$ The trajectories are still flying until time t_{n-1} but it has died by the time t_n. Consequently, $\Delta x(t_1) = t_1,\ \Delta x(t_2) = t_2,\ \cdots, \Delta x(t_{n-1}) = t_{n-1}$ and $\Delta x(t_n) = t_c(x_0)$.
$\vdots$

$P(> t_1) < x_0 < 1$ The trajectories died before t_1. Consequently, $\Delta x(t_1) = \Delta x(t_2) = \cdots = \Delta x(t_n) = t_c(x_0)$.

Splitting the integral and performing a calculation, one finds

$$\begin{aligned}\phi(t_1, t_2, \cdots t_n) = &\int_0^{P(>t_n)} \mathrm{d}x_0\ (x(x_0, t_1) - x_0)\ (x(x_0, t_2) - x_0) \cdots\ (x(x_0, t_n) - x_0) \\ &+ \int_{P(>t_n)}^{P(>t_{n-1})} \mathrm{d}x_0\ (x(x_0, t_1) - x_0)\ (x(x_0, t_2) - x_0) \cdots\ (x(x_0, t_n) - x_0) \\ &\vdots \\ &+ \int_{P(>t_1)}^{1} \mathrm{d}x_0\ (x(x_0, t_1) - x_0)\ (x(x_0, t_2) - x_0) \cdots\ (x(x_0, t_n) - x_0)\ .\end{aligned} \tag{5.12a}$$

thus, recalling Eq. (5.1b), we have

$$\begin{aligned}
&\phi(t_1, t_2, \cdots t_n) \\
&= (t_1\, t_2 \cdots t_n) \int_0^{b/t_n^\xi} \mathrm{d}x_0 \;+\; (t_1\, t_2 \cdots t_{n-1}) \int_{b/t_n^\xi}^{b/t_{n-1}^\xi} \mathrm{d}x_0 \left(\frac{b}{x_0}\right)^{1/\xi} \;+\; (t_1\, t_2 \cdots t_{n-2}) \times \\
&\quad \int_{b/t_{n-1}^\xi}^{b/t_{n-2}^\xi} \mathrm{d}x_0 \left(\frac{b}{x_0}\right)^{2/\xi} \;+\; \cdots \;+\; t_1 \int_{b/t_2^\xi}^{b/t_1^\xi} \mathrm{d}x_0 \left(\frac{b}{x_0}\right)^{(n-1)/\xi} \;+\; \int_{b/t_1^\xi}^{1} \mathrm{d}x_0 \left(\frac{b}{x_0}\right)^{n/\xi} .
\end{aligned} \tag{5.12b}$$

This provides us with a general expression on the n-point position auto-correlation function

$$\phi(t_1, t_2, \cdots t_n) = \sum_{j=0}^{n} \left(\left(\prod_{k=1}^{n-j} t_k \right) \int_{b/t_{n-j+1}^\xi}^{b/t_{n-j}^\xi} \mathrm{d}x_0 \left(\frac{b}{x_0}\right)^{j/\xi} \right) , \tag{5.13}$$

where formally $t_{n+1} = \infty$ and $t_0 = b^{1/\xi}$.

Provided that $\gamma = 2 - \xi$, $n = 2$ and some integral manipulation, the previous expression turns to Eq. (5.7).

Lemma 5.1.2. *The n-point position auto-correlation function provide the following scaling expression for the times $t_1 \le t_2 \le t_2 \le \cdots < t_n$, with $h = t_j - t_{j-1}$= const. for $j \in \{2, 3, \cdots, n\}$,*

$$\frac{(\gamma/b)\; \phi(t_1, t_2, \cdots t_n)}{h^{n-(2-\gamma)}} \sim \begin{cases} \frac{n\,\gamma}{n-(2-\gamma)} \left(\frac{t_1}{h}\right)^{n-(2-\gamma)}, & \textit{for} \quad t_1 \gg h, \\ \frac{t_1}{h}, & \textit{for} \quad t_1 \ll h, \end{cases}$$

where $\gamma = 2 - \xi$.

Proof. See appendix B.3. □

5.1.5 Velocity auto-correlation function

The trajectories fly with the velocity $v = 1$, till they stop, $v = 0$. Therefore only those trajectories contribute to the VACF with $t_1 \le t_2$, that are still flying at time

t_2. Thus denoting the VACF by $\phi_v(t_1, t_2)$, we obtain

$$\begin{aligned}\phi_v(t_1,t_2) &= \int_0^1 \mathrm{d}x_0\, \Delta v(x_0,t_1)\, \Delta v(x_0,t_2)\,, \\ &= \int_0^1 \mathrm{d}x_0\ (v(x_0,t_1)-v_0)\ (v(x_0,t_2)-v_0)\ , \\ &= \int_0^{P(>t_2)} \mathrm{d}x_0\ (v(x_0,t_1)-v_0)\ (v(x_0,t_2)-v_0)\ . \end{aligned} \tag{5.14}$$

Using Eq. (5.2) and assuming $\xi = 2-\gamma$, we have

$$\phi_v(t_1,t_2) = \int_0^{b/t_2^{2-\gamma}} \mathrm{d}x_0. \tag{5.15}$$

Hence the VACF scales asymptotically as

$$\phi_v(t_1,t_2) \sim b\, t_1^{\gamma-2}, \qquad 0<\gamma<2, \tag{5.16}$$

where $h = t_2 - t_1$, $h > 0$ and $t_1 \to \infty$.

This behaviour is not shared by 2-times VACF of SM *cf.* Eq. (3.67). Hence it can be used to distinguish the FnD from the SM.

5.2 Testing the scaling of 2-point position correlations

In this section, we test the scaling form of the position auto-correlation function (*cf.* Eq. (5.8)) of the FnD dynamics with the SM and the LLg position correlations.

We start by recalling the moments of displacement of SM (*cf.* Eq. (3.20)). They exhibit the same scaling as the FnD dynamics in Eq. (5.4) if $b \equiv 2$ and $\alpha \equiv \xi = 2-\gamma$, except for $p < \alpha$, which requires a more detailed analysis [53]. In Sec. 3.4 we provided expression with different scaling forms. For the position auto-correlation function of the SM: we derived a single scaling expression of auto-correlation function. Recalling Eq. (3.30b) and rearrange terms, introducing $n - m = h$, in analogy to the notion adopted in Eq. (5.8), we find

$$\frac{(\gamma/2)\,\phi(m,n)}{h^\gamma} \simeq \frac{\gamma}{\gamma-1}\ \left(\frac{m}{h}\right)^\gamma\ \left[\left(1+\frac{h}{m}\right)^{\gamma-1} - \frac{2-\gamma}{\gamma}\right]. \tag{5.17}$$

This expression agrees with Eq. (5.8) when one identifies $b \equiv 2$. Therefore the FnD dynamics faithfully captures the parameter dependence of the moments of the displacement and the position auto-correlation function of the SM. Both processes belong to the same class of transport processes.

5.2.1 Data analysis

Now we compare the prediction Eqs. (5.8) and (5.17) of the SM and FnD dynamics with numerical data of the LLg position correlation functions. In Chp. 4 we established a large set of numerical data of LLg correlations where we varied t_2 at fixed t_1, t_1 and t_2 for a fixed time difference $h = t_2 - t_1$, and t_1 while fixing t_2 to a values $t_1 + t_1^q$ for different fixed values of q. In these different settings we observed that the position auto-correlation function of the SM followed the dependence Eq. (3.30) when one measures r in units of r_0, time in units of r_0/v, and adopting the mapping of parameters provided by requesting $\gamma = 2 - \alpha$ and Eq. (4.13).

We also performed simulations with another characteristic scale length $r_0 = 1$. Formally, this change can be accounted for by measuring all length scales in multiples of r_0 and times in multiples of r_0/v. This give rise to an additional factor $r_0^{\gamma-2}/v^\gamma$ on the l.h.s of Eqs. (5.8) and (5.17).

In Fig. 5.1 we show the data of Sec. 4.3 in the scaling form suggested by Eq. (5.8). The prediction provides an excellent data collapse of all data, irrespective of the choice of the characteristic length scale r_0 and the particular choice for the relation of t_1 and t_2. Moreover, there also is excellent agreement with the theoretical prediction of the FnD dynamics Eqs. (5.8), that is shown by the dashed (black) lines. We have augmented them here by data where we also vary r_0 and we also checked that this correlation function does not change when all trajectories start to the right from an ideally reflecting impurity (In Chp. 4 we denote this as the LLg$^+$dynamics). In the inset of panels we show the relative deviation of the numerical data and the theoretical prediction. For $t_1 < h$ the numerical data tend to systematically fall below the theoretical prediction. The effect is small, only about 5% for $\beta = 0.1$, but it grows for increasing β — reaching a factor of 5 for $\beta = 0.6$. Even in the latter

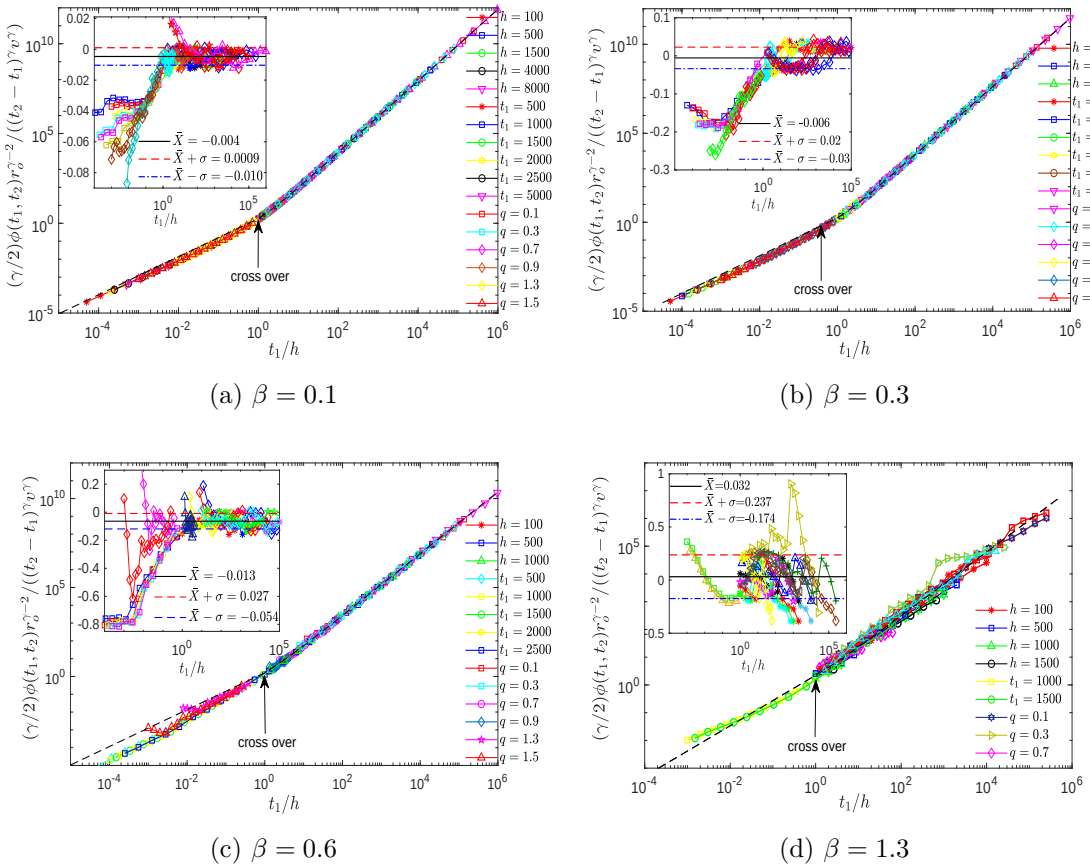

(a) $\beta = 0.1$ (b) $\beta = 0.3$

(c) $\beta = 0.6$ (d) $\beta = 1.3$

Figure 5.1: The position auto-correlation functions $\phi(t_1, t_2)$ of the LLg for some β's. We obtain a data collapse for a vast data set of combinations of t_1 and t_2 by plotting the left-hand side of Eqs. (5.8) as function of t_1/h. The different symbols denote data for $r_0 = 0.1$ and $r_0 = 1$ where we varied t_2 at fixed time difference $h = t_2 - t_1$, time t_1 and where we varied t_1 while setting $t_2 = t_1 + t_1^q$ (*cf.* legend). The dashed lines show the parameter dependence Eq. (5.8) predicted by the FnD dynamics. The inset shows the relative deviation of the numerical data and the theoretical prediction (*i.e.*, the difference divided by the predicted value). We observe, that the data collapse gradually gets worse as β is getting larger presumably due to poor statistics of numerical data (*cf.* Fig. 5.1d).

case we consider the agreement to be excellent, however, because even for $t_1 < h$ our data cover 5 orders of magnitude on both axes and a factor of five is not a large error on those scales. Moreover, the agreement for $t_1 > h$ is sufficiently perfect at least for small β. In this case the relative deviation of the data from the prediction are (*cf.* insets of Fig. 5.1):

$$\bar{X} \pm \sigma = \begin{cases} -0.004 \pm 0.006, & \text{for} \quad \beta = 0.1, \\ -0.006 \pm 0.026, & \text{for} \quad \beta = 0.3, \\ -0.01 \pm 0.04, & \text{for} \quad \beta = 0.6, \\ 0.032 \pm 0.21, & \text{for} \quad \beta = 1.3. \end{cases}$$

The data shown in Fig. 5.1 suggest that the exponent of the power-law is perfectly matched. The relative deviation characterizes in how far the FnD dynamics also captures the prefactor of the dynamics. However, Fig. 5.1d, suggests that we need much more statistics in numerical simulation for larger β. Although the FnD theoretical prediction agrees with numerical data even for larger β, the results are not uniform as they should be.

In Fig. 5.2 we show the numerical estimates for different data sets of the correlations functions and for the mean-square displacement. These estimates are acquired by averaging the logarithm of the ratio of the numerical data of the LLg and theoretical predictions, (inset in Fig. 5.1) for positive t_1/h. Different symbols refer to different data sets that are indicated in the legends. This data shows that the mean-square displacement and the position auto-correlation function match perfectly — also for different characteristic scale lengths $r_0 = 0.1$ and 1. When β approaches 1 the scatter in the data increases substantially because substantially more data are needed to provide an accurate estimate of the expectation values defining the correlation functions and the displacement. However, in all cases there is excellent agreement between the prediction of the FnD dynamics and our numerical findings on the LLg.

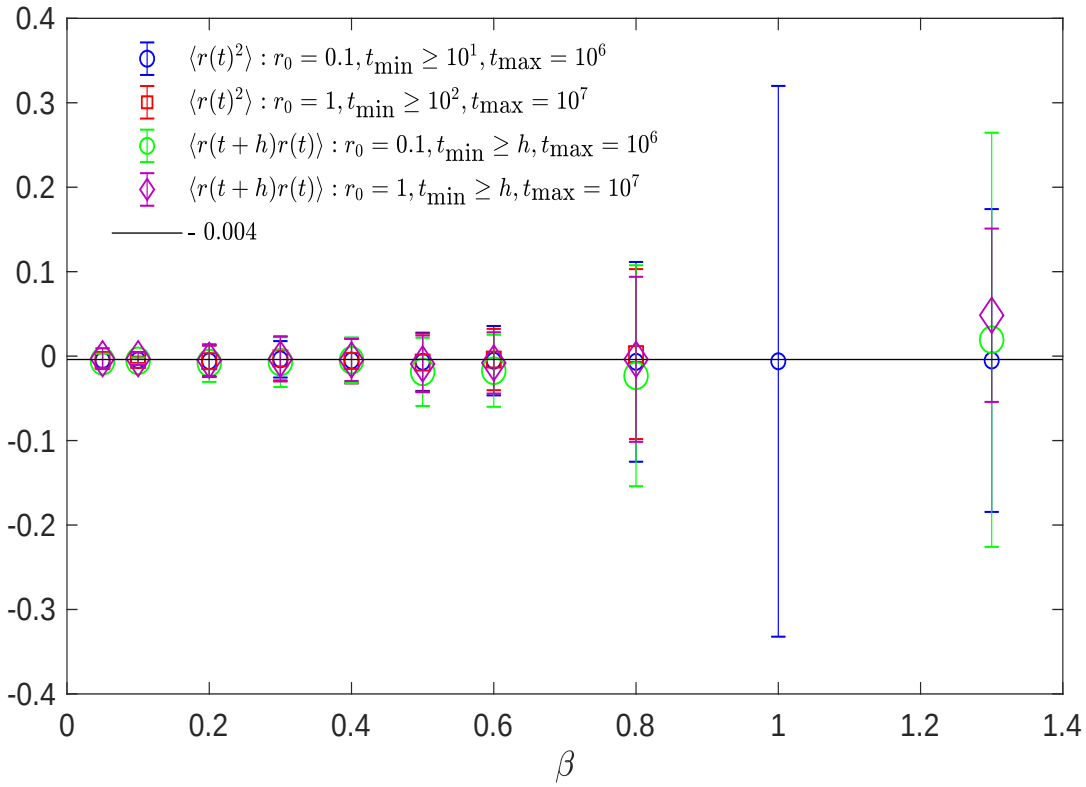

Figure 5.2: For different sets of data, that are indicated in the legend, we show an average (points) and the standard deviation (error bars) of the logarithm of the ratio of the LLg data and the theoretical prediction of the SM, as shown in the insets of Fig. 5.1. Data for the mean-square displacement and the position auto-correlation function for different choices of the relation t_1 and t_2 lie on the same line.

5.3 Testing the scaling of 3-point position correlations

In this section we explore the equivalence of the 3-point position auto-correlation function of the FnD, SM and the LLg. Since in section 5.2, the 2-point position auto-correlation function provides the faithful description of these systems, we try here to extend this equivalence to 3-point correlations. We start by recalling the scaling form of 3-point correlation of FnD dynamics represented in Eq. (5.11) and

see how far it captures the 3-point position correlation[3] scaling of the SM. In this regard, we recall Eq. (A.19), perform simple computation and take $\alpha = 2 - \gamma$, that allow us to write 3-point position correlation $\phi(o, n, m)$ scaling of the SM in the following form

$$\phi(o, n, m) \sim \frac{2}{\gamma - 1} m\, n\, o^{\gamma-1} - \frac{2(2-\gamma)}{\gamma(\gamma-1)} m\, n^{\gamma} - \frac{2(2-\gamma)}{\gamma(\gamma+1)} m^{\gamma}, \quad m \leq n \leq o. \tag{5.18}$$

For $m = n = o$, this reduces to third moment of displacement, Eq. (3.20) with $p = 3$. Reconsider Eq. (5.18), rearrange some terms and introduce

1. $n = m + h_1$, as $m \to \infty$, and $h_1 > 0$ finite.

2. $o = n + h_2$, as $n = m + h_1$, where $m \to \infty$, and $h_2 > 0$ finite ,

provided that $h_1 = h_2$, one can write the scaling form of 3-point position auto-correlation as:

$$\frac{(\gamma/2)\,\phi(m, n, o)}{h^{\gamma+1}}$$
$$\sim \frac{\gamma}{\gamma - 1} \left(\frac{m}{h}\right)^{\gamma+1} \left[\left(1 + \frac{h}{m}\right)\left(1 + \frac{2\,h}{m}\right)^{\gamma-1} - \frac{2-\gamma}{\gamma}\left(1 + \frac{h}{m}\right)^{\gamma} - \frac{(2-\gamma)(\gamma-1)}{\gamma(\gamma+1)}\right]. \tag{5.19}$$

This expression agrees with Eq. (5.11) when $b \equiv 2$. Therefore the FnD dynamics faithfully describes also the third moment of the displacement and the 3-point position auto-correlation function of the SM. These transport processes belong to a universality class when trajectories with very long initial ballistic flights dominate the long-time scaling of displacement and position auto-correlation function.

5.3.1 Data analysis

In this section we compare the prediction of the FnD dynamics and the SM with numerical data of the LLg. We amply data for different relationships between the three times. The different settings between times are: (a) varying t_1, t_2 and t_3 for a fixed time difference $h = t_2 - t_1 = t_3 - t_2$; (b) varying t_1 setting $t_2 = t_1 + t_1^q$

[3]The scaling form of the 3-point position auto-correlation function is provided in appendix A.4.

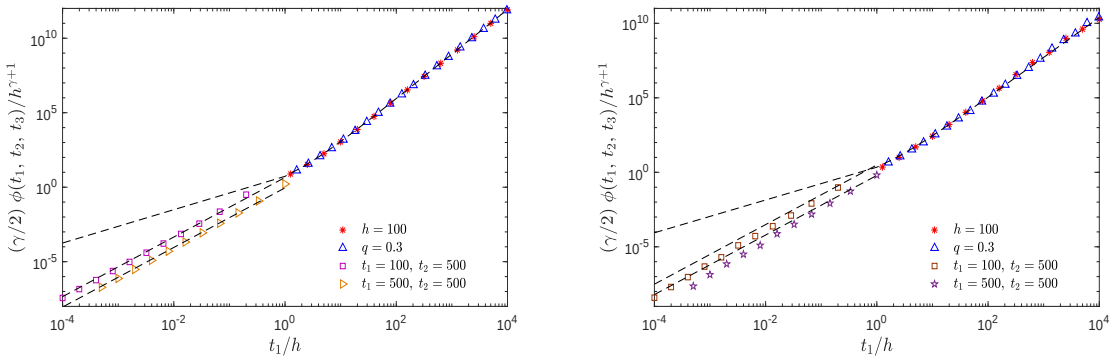

(a) $\beta = 0.1$ (b) $\beta = 0.6$

Figure 5.3: The 3-point position auto-correlation function $\phi(t_1, t_2, t_3)$ of the LLg are plotted for $\beta = 0.1$ (left panel) and $\beta = 0.6$ (right panel) as a function of t_1/h. We obtain a nice data collapse for different LLg data and a significant agreement with the theoretical prediction of the FnD dynamics represented by dashed line (*cf.* r.h.s Eq. (5.11b) for $t_1 > h$ and Eq. (5.11c) for $h > t_1$). For $t_1 > h$ we choose different relationship between times by setting $t_1 \to \infty$ and fixed composition of times *i.e.*, $h = t_2 - t_1 = t_3 - t_2 = 100$; the relation $t_2 = t_1 + t_1^{0.3}$, $t_3 = t_1 + 2\,t_1^{0.3}$ and two choices for t_1, t_2 fixed either $t_2 > t_1$ or $t_1 = t_2$.

and $t_3 = t_1 + 2t_1^q$ for some fixed value of $q < 1$; (c) fixing $t_1 \leq t_2 =$ fixed and varying t_3. In all these functional relationship between the times we find that the position auto-correlation function of the SM followed the dependence Eq. (A.19), when one measure r in units of r_0, time in units of r_0/v, and adopting the mapping of parameters α and β provided by the requesting $\gamma + 1 = 3 - \alpha$. For $t_1 > h$ it scales like third moment of displacement Eq. (3.20) for $p = 3$.

This is demonstrated in Figure 5.3, for the data collapse for one parameter dependent 3-point position auto-correlation function with different functional relationship between three times. For $t_1 > h$, we observe an excellent match between the LLg data and quantitative prediction of the FnD dynamics in Eq. (5.11). For $t_1 > h$ this correlation scales as the third moment of displacement of the FnD dynamics Eq. (5.4) with $p = 3$ and requesting $\xi = 2 - \gamma$. For $t_1 < h$, there is a different scaling and the agreement becomes gradually worse as β increases. The three times

t_1, t_2 and t_3 are far separated for the asymptotic scaling of small t_1/h. We conclude that to the very least for small β, —3-point correlation function of the FnD dynamics can capture the main features of correlation function for non-trivial anomalous transport processes.

5.4 Summary

We introduced the FnD dynamics with the aim to establish a minimalistic model for anomalous diffusion. It reproduces the asymptotic scaling of the SM for variable characterizing the displacement. Moreover the FnD and the SM capture some ingredients of a more realistic model, the LLg. In particular we presented a one parameter dependent expression for position auto-correlation function of the FnD and the SM that has excellent agreement with the numerically computed position auto-correlation functions of the LLg. For super-diffusive transport the moments of displacement and the position auto-correlation functions of the FnD, SM and the LLg are dominated by ballistic trajectories. It is conjecture that the moments and the auto-correlation function apply for a wide class of such systems. Even for entirely different microscopic dynamics the models agree as far as characteristics of the displacement are concerned. On the other hand, the moments and correlations of the velocities may differ.

Chapter 6

Conclusions and future perspectives

In this chapter, we conclude this thesis by presenting the

- conclusions of the research work on transport properties and a conjecture on universality class obtained in this thesis

- an outline of some future aspects of work.

Before going to conclusions let us briefly summarize our main results.

Chapters 1 and 2 gave the vital foundation to this thesis. They provided the recent developments in literature and reviewed the general framework of the diffusion processes. Although this can not capture the whole story, the references provided in the bibliography can be a pivotal point for further illustration.

The core part of the thesis is divided into two parts. In Chapter 3 we explicitly computed the SM position auto-correlation functions and demonstrated their statistical equivalence with LLg correlations in chapter 4. In Chapter 5 we propose a universality class of anomalous transport in the super-diffusive regime.

6.1 Conclusion

The conclusions are drawn for similarities and dis-similarities for the transport properties of dynamical systems. During the discussion we unfold some issues arising in microscopic dynamics.

Equivalence of position auto-correlation function in the SM and the LLg The investigation of the relation between the SM and the LLg started in [53] with the demonstration of the equivalence of the scalings of the time-dependent moments of the displacement. Because it is well known that moments do not sufficiently characterise transport processes [58], while the position auto-correlations could, we have extended that study here to position auto-correlation functions. We analytically computed the position auto-correlation function of the SM, and we derived the asymptotic behaviour of this function in several cases corresponding to different relations between the two times. Then, we numerically estimated the position auto-correlation function of the LLg, in order to estimate its asymptotic behaviour. Unlike the case of moments [10] there are no analytical results available for the time dependent auto-correlation function of the LLg. In general time correlations in anomalous transport of even moderately complex models constitute by and large an open problem.

Our numerical results indicate that there is an equivalence of the asymptotic scalings of the position auto-correlation functions of the SM and the LLg. As established in [53] for the equivalence of moments, the agreement is based on the matching of the transport exponent, γ. Hence, the parameters α and β obey the relation Eq. (4.14). No further parameters are adjusted to also achieve the matching of the auto-correlation function.[1] As the diffusion parameter of the LLg increases, the agreement between the numerical data and the proposed expressions for the asymp-

[1] Actually, we did not take the parameters suggested by the relation (4.14) for the equivalence of the moments, in order to find the data collapse for the correlations. On the contrary, we looked for the parameters that provide the best data collapse for the correlations, and we found that their values are indeed with good accuracy those given by Eq. (4.14).

totic scaling of the auto-correlation function becomes less convincing. Presently, it is not clear whether the correspondence only holds for small values of diffusion parameter, or whether the emerging discrepancies are due to the increasing difficulty of obtaining good statistics with growing β.

We emphasise that the agreement of the moments and the time-dependent auto-correlation for the displacement hold in spite of the fact that the SM and the LLg exhibit entirely different dynamics. Intuition on the properties of the SM and of the LLg can be obtained by observing the relative motion of two points. Consequently, any function of any finite number of points, evaluated along a trajectory of the SM, turns periodic in a finite time. This situation is totally different from that of the LLg. Its nature renders the distance between any two particles stochastic, and this holds for any function of a finite number of points.

We conclude that even the position auto-correlations do not suffice, in general, to distinguish different dynamics at the level of transport properties. This might be seen as a negative result, but it was used here to indirectly investigate some of the elusive properties of the LLg. This approach may look puzzling at first glance. However, it is quite natural within the framework of statistical mechanics, and of transport processes in particular. Indeed, the details of the microscopic dynamics of large systems usually do not strongly affect the behaviour of physically relevant macroscopic quantities. The latter can thus agree even for systems with vastly different microscopic dynamics. This observation lies at the heart of the success of highly idealized models in describing complex phenomena; even simple models may indeed capture the essential ingredients determining the behaviour of a selected and limited number of observables. Theoretical models for critical phenomena and universality constitute examples of this fact [14, 22, 33, 57]. The present work raises the question whether the transport exponents and the corresponding two-points auto-correlation functions might be a kind of counterpart of critical exponents, suitable for the characterisation of transport phenomena: they afford an analogously coarse but analogously useful description of the systems at hand.

Universal class in anomalous transport

The moments of the displacement and the position auto-correlation functions of many systems that show super-diffusive transport are commonly dominated by ballistic trajectories. In this dissertation, we argue that the moments and the displacement have a universal shape. It only depends on the exponent η characterizing the mean-square displacement and the prefactor of that asymptotic power law. We introduced the FnD dynamics as the simplest representative in this class of systems. For this dynamics it is straightforward to analytically calculate the functional dependencies, and we verified that they faithfully agree with findings for the SM and the LLg. Based on the analytical solution of the FnD dynamics we established a scaling relation that allows to represent the correlation function in a scaling form where it only depends on the ratio of times. The excellent agreement between the numerical data of LLg and the prediction obtained by the FnD dynamics (symbols and dashed lines in Fig. 5.1) establishes a new way to analyze correlations in anomalous transport and it suggests that the FnD dynamics indeed can take the role of a protopypical system that provides novel insight into universal features of system showing anomalous transport.

It is conjectured that some deterministic dynamics, such as Lorentz gas with infinite horizon [16, 44] and polygonal channel with closed horizon, with asymptotic transport are also dominated by the ballistic trajectories. Numerical investigation of these billiard system confirm the original assumption on the SM and the polygonal channels. Such billiard lie in the same class as the SM, FnD and LLg dynamics.

6.2 Future perspective

In future work, we will explore more properties of the SM, FnD and the LLg dynamics to examine the strong equivalence in the deterministic of the SM and the FnD systems with the stochastic LLg dynamics. To gain more insight, it may be helpful to fully characterise the statistical equivalence of multiple and n-points position auto-correlation functions and to also investigate entirely different microscopic

dynamics.

A space-independent Slicer dynamics is under construction that features a time-reversible, exactly solvable dynamics featuring all possible transport phenomena. So far we observed only ballistic transport. However this work can not be complete until we also find anomalous transport.

Appendix A

Details of calculations for the Slicer Map correlation functions

A.1 Derivation for the position correlation function of the SM

In this appendix we compute the asymptotics of the sums defined in Eqs. (3.18a) and (3.32). We have

$$\begin{aligned}\Delta_k(\alpha) = \ell_k^+(\alpha) - \ell_{k-1}^+(\alpha) &= \frac{1}{(k-1+2^{1/\alpha})^\alpha} - \frac{1}{(k+2^{1/\alpha})^\alpha}\,, \\ &= \frac{1}{k^\alpha}\left(\left(1+\frac{2^{1/\alpha}-1}{k}\right)^{-\alpha} - \left(1+\frac{2^{1/\alpha}}{k}\right)^{-\alpha}\right)\,,\end{aligned}$$

and by Taylor expansion

$$\Delta_k(\alpha) = \frac{\alpha}{k^{\alpha+1}}\left(1-\tilde{c}(\alpha)\frac{1}{k}+O\left(\frac{1}{k^2}\right)\right)\,, \tag{A.1a}$$

where

$$\tilde{c}(\alpha) = (1+\alpha)\,\left(2^{\frac{1}{\alpha}}-\frac{1}{2}\right) > 0, \qquad \text{with} \quad \alpha > 0\,. \tag{A.1b}$$

Then, the sum in Eq. (3.18a) can be written as:

$$\sum_{k=1}^{n-1} k^2\,\Delta_k(\alpha) = \sum_{k=1}^{n-1}\frac{\alpha}{k^{\alpha-1}}\,\left(1-f(k)\right)\,, \tag{A.2a}$$

where

$$f(k) := \tilde{c}(\alpha)\,\frac{1}{k} + O\left(\frac{1}{k^2}\right)\,. \tag{A.2b}$$

The previous equation implies the existence of an integer n_0 such that:

$$\frac{1}{2}\,\tilde{c}(\alpha)\,k^{-1} < f(k) < \frac{3}{2}\,\tilde{c}(\alpha)\,k^{-1}\,, \qquad \text{for} \quad k > n_0\,. \tag{A.3}$$

Then, for $m > n_0$ we have:

$$\sum_{k=1}^{n-1} k^2 \Delta_k(\alpha) = \sum_{k=1}^{n-1} \frac{\alpha}{k^{\alpha-1}} - \sum_{k=1}^{n_0} \frac{\alpha\, f(k)}{k^{\alpha-1}} - \sum_{k=n_0}^{n-1} \frac{\alpha\, f(k)}{k^{\alpha-1}}\,, \tag{A.4a}$$

where

$$\frac{1}{2}\,\tilde{c}(\alpha) \sum_{k=n_0}^{n-1} \frac{1}{k^{\alpha}} \le \sum_{k=n_0}^{n-1} \frac{f(k)}{k^{\alpha-1}} \le \frac{3}{2}\,\tilde{c}(\alpha) \sum_{k=n_0}^{n-1} \frac{1}{k^{\alpha}}\,. \tag{A.4b}$$

Therefore, the last sum in Eq. (A.4a) is of the order of $\sum_{k=n_0}^{n-1} k^{-\alpha}$, for $m \to \infty$. We evaluate the scaling of the two other terms of Eq. (A.4a) based on the Euler-Maclaurin sum formula:

Lemma A.1.1. (Euler-Maclaurin sum formula) *For a smooth function $g(x)$, the full asymptotic behaviour of*

$$G(n) = \sum_{k=0}^{n} g(k)\,, \tag{A.5}$$

is given by

$$G(n) \sim \frac{1}{2}g(n) + \int_0^n g(t)\;\mathrm{d}t + C + \sum_{j=1}^{\infty} (-1)^{j+1} \frac{B_{j+1}}{(j+1)!} g^{(j)}(n)\,, \qquad \textit{as} \quad n \to \infty\,. \tag{A.6}$$

Here C is a constant depending on g, and B_j are the Bernoulli numbers, thus

$$C = \lim_{m\to\infty} \left(\sum_{j=1}^{m} \frac{(-1)^j B_{j+1}}{(j+1)!} f^{(j)}(0) + \frac{1}{2} f(0) + \frac{(-1)^m}{(m+1)!} \int_0^{\infty} B_{m+1}(t - [t]) f^{(m+1)}(t)\,\mathrm{d}t \right), \tag{A.7}$$

where $[t]$ is the largest integer less than t.

Specifically, for $g(k) = k^p$ and $p \neq -1$ one has

$$\sum_{k=0}^{m} k^p \sim \frac{m^{p+1}}{p+1} + \frac{1}{2} m^p + C + \sum_{j=1}^{\infty} (-1)^{j+1} \frac{B_{j+1}}{(j+1)!} \prod_{\ell=0}^{j-1} (p-\ell)\, m^{p-j}\,, \qquad \textit{as} \quad m \to \infty\,, \tag{A.8a}$$

while $p = -1$ entails:

$$\sum_{k=1}^{m} k^{-1} \sim \ln m + C + \frac{1}{2\,m} - \frac{B_2}{2\,m^2} - \frac{B_4}{4\,m^4} - \cdots\,, \qquad \textit{as} \quad m \to \infty\,. \tag{A.8b}$$

Proof. See for instance [6]. □

For $\alpha > 2$ Eq. (A.8a) entails that the sum Eq. (A.2a) converges to a finite value, as reported in Eq. (3.18a).

For $\alpha = 2$ Eq. (A.8b) provides

$$\sum_{k=1}^{n-1} k^2 \, \Delta_k(\alpha) \sim 2\alpha \, \ln n \,, \qquad \text{for} \quad \alpha = 2 \,, \tag{A.9a}$$

i.e.,the logarithmic scaling reported in Eq. (3.18a).

For $0 < \alpha < 2$ we have that the two sums depending on m in Eq. (A.4a) diverge:

$$\sum_{k=1}^{m} \frac{\alpha}{k^{\alpha-1}} \sim \frac{\alpha}{2-\alpha} m^{2-\alpha} \,, \qquad \sum_{k=m_0}^{m} \frac{\alpha f(k)}{k^{\alpha-1}} = \mathcal{O}(m^{1-\alpha}) \,, \qquad \text{as} \quad m \to \infty \,,$$

where the second sum is estimated using Eq. (A.4b). From Eq. (A.4a), we then obtain

$$\sum_{k=1}^{n-1} k^2 \Delta_k(\alpha) \sim \frac{\alpha}{2-\alpha} \, n^{2-\alpha} \,, \qquad \text{for} \quad 0 < \alpha < 2 \,. \tag{A.9b}$$

This concludes the derivation of Eq. (3.18a).

Equation (3.32) can be obtained by the same line of argumentation. Using Eq. (A.1a), the sum in Eq. (3.32) yields:

$$\sum_{k=1}^{n} k \, \Delta_k(\alpha) = \frac{\alpha}{1+\alpha} \, \sum_{k=1}^{n} \frac{1+\alpha}{k^{\alpha}} \, (1 - f(k)) \,. \tag{A.10}$$

This is essentially the same expression as Eq. (A.2a). Consequently, according to Eq. (A.8a) the sum takes a finite value for $\alpha > 1$. Moreover, introducing the substitutions into Eq. (A.9b) yields

$$\sum_{k=1}^{n} k \, \Delta_k(\alpha) \sim \frac{\alpha}{1+\alpha} \, \frac{1+\alpha}{1-\alpha} \, n^{1-\alpha} = \frac{\alpha}{1-\alpha} \, n^{1-\alpha} \,, \qquad \text{for} \quad 0 < \alpha < 1 \,, \tag{A.11}$$

which is the the non-trivial scaling reported in Eq. (3.32). Analogously, the logarithmic scaling in Eq. (3.32) is obtained from Eq. (A.9a), where the right-hand-side must be evaluated for $\alpha = 1$ due to the substitution. This concludes the derivation of Eq. (3.32).

A.2 Proof of lemma 3.5.3

We start the proof with the integral representation for the Harmonic numbers

$$H_x = \int_0^1 \frac{1-t^x}{1-t}\,. \tag{A.12}$$

Let

$$S = \sum_{k=1}^{n/2} \frac{1}{(2k+1)(2k+2)} = \sum_{k=1}^{n/2} \left(\frac{1}{2k+1} - \frac{1}{2k+2}\right)\,.$$

and note that

$$\int_0^1 \mathrm{d}x\, x^{2k} = \frac{1}{2k+1}\,, \qquad \text{and} \qquad \int_0^1 \mathrm{d}x\, x^{2k+1} = \frac{1}{2k+2}\,.$$

The sum S can be written as

$$S = \sum_{k=1}^{n/2} \int_0^1 \mathrm{d}x\, \left(x^{2k} - x^{2k+1}\right) = \int_0^1 \mathrm{d}x\, (1-x) \sum_{k=1}^{n/2} x^{2k}\,.$$

As the finite sum appearing here is geometric, it can be summed as following

$$\sum_{k=1}^{n/2} x^{2k} = \frac{x^2(1-x^n)}{1-x^2}\,.$$

Thus one has

$$S = \int_0^1 \mathrm{d}x\, \frac{x^2(1-x^n)}{1+x} = \int_0^1 \mathrm{d}x\, \left[\frac{x^2}{1+x} - \frac{x^{n+2}}{1+x}\right] = I_1 - I_2\,.$$

The first integral I_1 is trivial, one has

$$I_1 = \int_0^1 \mathrm{d}x\, \frac{x^2}{1+x} = \int_0^1 \mathrm{d}x\, \left(x - 1 + \frac{1}{1+x}\right) = \left[\frac{x^2}{2} - x + \ln(1+x)\right]_0^1 = -\frac{1}{2} + \ln(2)\,.$$

To evaluate integral I_2,

$$I_2 = \int_0^1 \mathrm{d}x\, \frac{x^{n+2}}{1+x} \cdot \frac{1-x}{1-x} = \int_0^1 \mathrm{d}x\, \frac{(1-x)x^{n+2}}{1-x^2}\,.$$

We introduce $x \mapsto \sqrt{x}$

$$\begin{aligned}
I_2 &= \frac{1}{2}\int_0^1 \mathrm{d}x\, \frac{x^{(n+1)/2} - x^{n/2+1}}{1-x}\,, \\
&= \frac{1}{2}\int_0^1 \mathrm{d}x\, \frac{(1-x^{n/2+1}) - (1-x^{(n+1)/2})}{1-x}\,, \\
&= \frac{1}{2}\int_0^1 \mathrm{d}x\, \frac{1-x^{n/2+1}}{1-x} - \frac{1}{2}\int_0^1 \mathrm{d}x\, \frac{1-x^{(n+1)/2}}{1-x}\,, \\
&= \frac{1}{2}\left(H_{\frac{n}{2}+1} - H_{\frac{n+1}{2}}\right),
\end{aligned}$$

where Eq. (A.12) is used in the previous expression.

Thus

$$\sum_{k=1}^{n/2} \frac{1}{(2k+1)(2k+2)} = \frac{1}{2}\left(H_{\frac{n+1}{2}} - H_{\frac{n}{2}+1} - 1 + \ln(4)\right) . \tag{A.13}$$

which proves Lemma 3.5.3.

A.3 Proof of proposition 3.5.1

Proof. We start with even n. We have

$$\begin{aligned} &2(-1)^{n+1}\sum_{k=1}^{n}(-1)^k\Delta_k(\alpha) \\ &\qquad = 2\left(\Delta_1(\alpha) - \Delta_2(\alpha) + \Delta_3(\alpha) - \Delta_4(\alpha) + \Delta_5(\alpha)\cdots - \Delta_n(\alpha)\right). \end{aligned} \tag{A.14}$$

Recalling $\Delta_k(\alpha) = \ell_k^+(\alpha) - \ell_{k-1}^+(\alpha)$ we have:

$$\begin{aligned} &2(-1)^{n+1}\sum_{k=1}^{n}(-1)^k\Delta_k(\alpha) \\ &= 2\left(-\ell_0^+(\alpha) + 2\left(\ell_1^+(\alpha) - \ell_2^+(\alpha) + \ell_3^+(\alpha) - \ell_4^+(\alpha) + \cdots + \ell_{n-1}^+(\alpha) - \ell_n^+(\alpha)\right) + \ell_n^+(\alpha)\right), \\ &= -1 - 4\left(\Delta_2(\alpha) + \Delta_4(\alpha) + \Delta_6(\alpha) + \cdots + \Delta_n(\alpha)\right) + 2\,\ell_n^+(\alpha), \\ &= -1 - 4\sum_{k=1}^{n/2}\Delta_{2k}(\alpha) + 2\,\ell_n^+(\alpha), \end{aligned} \tag{A.15}$$

where $\ell_0^+(\alpha) = 1/2$ and

$$\begin{aligned} \Delta_{2k}(\alpha) := \ell_{2k}^+(\alpha) - \ell_{2k-1}^+(\alpha) &= \left(2k - 1 + 2^{1/\alpha}\right)^{-\alpha} - \left(2k + 2^{1/\alpha}\right)^{-\alpha} , \\ &= \frac{\alpha}{(2k)^{\alpha+1}}\left(1 - \frac{\widetilde{c}(\alpha)}{2k} + \mathcal{O}\left(k^{-2}\right)\right), \end{aligned} \tag{A.16}$$

with $\tilde{c}(\alpha)$ presented in Eq. (A.1b).

An analogous derivation for *odd* n, completes the proof of proposition 3.5.1. □

A.4 3-point position auto-correlation function of the SM

We introduce the 3-point position auto-correlation function (*cf.* Sec. 3.4) as

$$\phi(o,n,m) := \langle \pi_{\mathbb{Z}}(S^o(\hat{\mathrm{x}}))\ \pi_{\mathbb{Z}}(S^n(\hat{\mathrm{x}}))\ \pi_{\mathbb{Z}}(S^m(\hat{\mathrm{x}}))\rangle := \langle \Delta\hat{\mathrm{x}}_o\, \Delta\hat{\mathrm{x}}_n\, \Delta\hat{\mathrm{x}}_m\rangle \tag{A.17a}$$

$$= 2\int_{1/2}^{1} \min\{\widetilde{m}_{\alpha,m}(x), m\}\ \min\{\widetilde{m}_{\alpha,n}(x), n\}\ \min\{\widetilde{m}_{\alpha,o}(x), o\}\ \mathrm{d}x\,, \qquad m \le n \le o\,. \tag{A.17b}$$

The integration interval $\mathrm{I} := (1/2, 1]$ can be subdivided in four parts, $\mathrm{I} = E_m^< \cup E_{m,n} \cup E_{n,o} \cup E_o^>$, defined by

$$\begin{cases} E_m^< = \{x \in \mathrm{I} \,:\, \widetilde{m}_{\alpha,m}(x) \le m\}\,, \\ E_{m,n} = \{x \in \mathrm{I} \,:\, m < \widetilde{m}_{\alpha,n}(x) \le n\}\,, \\ E_{n,o} = \{x \in \mathrm{I} \,:\, n < \widetilde{m}_{\alpha,o}(x) \le o\}\,, \\ E_o^> = \{x \in \mathrm{I} \,:\, o < \widetilde{m}_{\alpha,o}(x)\}\,. \end{cases} \tag{A.18a}$$

In each sub-interval the integrand in Eq. (A.17b) corresponds to

$$\Rightarrow \begin{cases} \min\{\widetilde{m}_{\alpha,m}(x), m\}\ \min\{\widetilde{m}_{\alpha,n}(x), n\}\ \min\{\widetilde{m}_{\alpha,o}(x), o\} = \widetilde{m}_{\alpha,m}(x)\, \widetilde{m}_{\alpha,n}(x)\, \widetilde{m}_{\alpha,o}(x)\,, \\ \min\{\widetilde{m}_{\alpha,m}(x), m\}\ \min\{\widetilde{m}_{\alpha,n}(x), n\}\ \min\{\widetilde{m}_{\alpha,o}(x), o\} = m\ \widetilde{m}_{\alpha,n}(x)\ \widetilde{m}_{\alpha,o}(x)\,, \\ \min\{\widetilde{m}_{\alpha,m}(x), m\}\ \min\{\widetilde{m}_{\alpha,n}(x), n\}\ \min\{\widetilde{m}_{\alpha,o}(x), o\} = m\, n\ \widetilde{m}_{\alpha,o}(x)\,, \\ \min\{\widetilde{m}_{\alpha,m}(x), m\}\ \min\{\widetilde{m}_{\alpha,n}(x), n\}\ \min\{\widetilde{m}_{\alpha,o}(x), o\} = m\, n\, o\,. \end{cases} \tag{A.18b}$$

Rewriting the resulting integrals in terms of sums over the intervals where $\overline{m}_\alpha(x)$ takes the constant value k (*cf.* Eq. (3.17)), one has:

$$\begin{aligned}
\phi(o,n,m) \; &= 2 \int\limits_{E_m^<} \widetilde{m}_{\alpha,o}(x)\, \widetilde{m}_{\alpha,n}(x)\, \widetilde{m}_{\alpha,m}(x)\; \mathrm{d}x + 2\,m \int\limits_{E_{m,n}} \widetilde{m}_{\alpha,o}(x)\, \widetilde{m}_{\alpha,n}(x)\; \mathrm{d}x \\
&\quad + 2\,m\,n \int\limits_{E_{n,o}} \widetilde{m}_{\alpha,o}(x)\; \mathrm{d}x + 2\,m\,n\,o \int\limits_{E_n^>} \mathrm{d}x\,, \\
&\sim 2 \sum_{k=1}^{m} k^3\, \Delta_k(\alpha) + 2\,m \sum_{k=m+1}^{n} k^2\, \Delta_k(\alpha) + 2\,m\,n \sum_{k=n+1}^{o} k\, \Delta_k(\alpha) \\
&\quad + 2\,m\,n\,o \sum_{k=o+1}^{\infty} \Delta_k(\alpha)\,, \qquad\qquad m \le n \le o\,. \qquad \text{(A.19)}
\end{aligned}$$

Appendix B

Supporting derivations of the correlation functions

This appendix presents the explicit derivation of position auto-correlation functions of the FnD dynamics defined in Eqs. (5.7), (5.8), (5.10) and (5.11), and the proof of lemma 5.1.2.

B.1 Derivation of the universal scaling for the FnD dynamics

According to the flight of the trajectory, the integral in Eq. (5.6) splits into three intervals:

$$\begin{aligned}\phi(t_1,t_2) &= \int_0^{P(>t_2)} \mathrm{d}x_o \,(x(x_o,t_1)-x_o)\;(x(x_o,t_2)-x_o) \\ &+ \int_{P(>t_2)}^{P(>t_1)} \mathrm{d}x_o \,(x(x_o,t_1)-x_o)\;(x(x_o,t_2)-x_o) \\ &+ \int_{P(>t_1)}^{1} \mathrm{d}x_o \,(x(x_o,t_1)-x_o)\;(x(x_o,t_2)-x_o)\,. \qquad \text{(B.1)}\end{aligned}$$

From Eq. (5.2), one finds

$$\begin{aligned}\phi(t_1,t_2) &= \int_0^{b/t_2^{\xi}} \mathrm{d}x_o\, t_1\, t_2 + \int_{b/t_2^{\xi}}^{b/t_1^{\xi}} \mathrm{d}x_o\, t_1 \left(\frac{b}{x_o}\right)^{1/\xi} + \int_{b/t_1^{\xi}}^{1} \mathrm{d}x_o \left(\frac{b}{x_o}\right)^{2/\xi} \\ &= b\; t_1 t_2^{1-\xi} + \frac{b^{1/\xi}\xi}{\xi-1}\left(\frac{b^{(\xi-1)/\xi}}{t_1^{\xi-1}} - \frac{b^{(\xi-1)/\xi}}{t_2^{\xi-1}}\right) t_1 + \frac{b^{2/\xi}\xi}{\xi-2}\left(1 - \frac{b^{(\xi-2)/\xi}}{t_1^{\xi-2}}\right).\end{aligned}$$

Since $\xi = 2-\gamma$, the correlation function takes the form

$$\phi(t_1,t_2) = b\; t_1\, t_2^{\gamma-1} + \frac{b\,(2-\gamma)}{1-\gamma}\, t_1^{\gamma} - \frac{b\,(2-\gamma)}{1-\gamma} t_1 t_2^{\gamma-1} + \frac{b\,(2-\gamma)}{\gamma}\, t_1^{\gamma} - \frac{(2-\gamma)\, b^{2/(2-\gamma)}}{\gamma}.$$

This allow us to write the correlation function as

$$\phi(t_1,t_2) = \frac{b}{\gamma-1}\, t_1\, t_2^{\gamma-1} - \frac{b\,(2-\gamma)}{\gamma(\gamma-1)}\, t_1^{\gamma} - \frac{(2-\gamma)\, b^{2/(2-\gamma)}}{\gamma}, \qquad \gamma \neq 1\,. \tag{B.2}$$

By introducing the difference $h = t_2 - t_1$, we rewrite Eq. (B.2) for $\gamma \neq 1$:

$$\begin{aligned}\phi(t_1,t_2) &= \frac{b}{\gamma}\left(\frac{\gamma}{\gamma-1} t_1 (t_1+h)^{\gamma-1} - \frac{2-\gamma}{\gamma-1}\, t_1^{\gamma} - (2-\gamma)\, b^{\gamma/(2-\gamma)}\right), \\ &= h^{\gamma}\frac{b}{\gamma}\left(\frac{\gamma}{\gamma-1}\frac{t_1}{h}\left(\frac{t_1}{h}+1\right)^{\gamma-1} - \frac{2-\gamma}{\gamma-1}\left(\frac{t_1}{h}\right)^{\gamma} - \frac{(2-\gamma)\, b^{\gamma/(2-\gamma)}}{h^{\gamma}}\right),\end{aligned}$$

and normalize by the γ-power of the time difference h

$$\frac{(\gamma/b)\phi(t_1,t_2)}{h^{\gamma}} \simeq \frac{\gamma}{\gamma-1}\left(\frac{t_1}{h}\right)^{\gamma}\left(\left(1+\frac{h}{t_1}\right)^{\gamma-1} - \frac{2-\gamma}{\gamma}\right), \qquad \gamma \neq 1\,. \tag{B.3}$$

This expression for the correlations of the FnD dynamics allows us to collapse all numerical simulation data of the LLg on the same curve.

B.2 Scaling form of the 3-point position correlation for the FnD dynamics

To derive the 3-point position auto-correlation function. We recall Eq. (5.9) and split the integral into four domains

$$\begin{aligned}\phi(t_1,t_2,t_3) &= \int_0^{P(>t_3)} \mathrm{d}x_0\ (x(x_0,t_1)-x_0)\ (x(x_0,t_2)-x_0)\ (x(x_0,t_3)-x_0)\\ &+\int_{P(>t_3)}^{P(>t_2)} \mathrm{d}x_0\ (x(x_0,t_1)-x_0)\ (x(x_0,t_2)-x_0)\ (x(x_0,t_3)-x_0)\\ &+\int_{P(>t_2)}^{P(>t_1)} \mathrm{d}x_0\ (x(x_0,t_1)-x_0)\ (x(x_0,t_2)-x_0)\ (x(x_0,t_3)-x_0)\\ &+\int_{P(>t_1)}^{1} \mathrm{d}x_0\ (x(x_0,t_1)-x_0)\ (x(x_0,t_2)-x_0)\ (x(x_0,t_3)-x_0)\,. \end{aligned} \tag{B.4}$$

Introducing Eq. (5.2), yields

$$\phi(t_1,\,t_2,\,t_3) = \\ t_1\,t_2\,t_3 \int_0^{b/t_3^\xi} \mathrm{d}x_0 + t_1\,t_2 \int_{b/t_3^\xi}^{b/t_2^\xi} \mathrm{d}x_0 \left(\frac{b}{x_0}\right)^{1/\xi} + t_1 \int_{b/t_2^\xi}^{b/t_1^\xi} \mathrm{d}x_0 \left(\frac{b}{x_0}\right)^{2/\xi} + \int_{b/t_1^\xi}^{1} \mathrm{d}x_0 \left(\frac{b}{x_0}\right)^{3/\xi}.$$

Therefore

$$\phi(t_1,\,t_2,\,t_3) = \frac{b}{1-\xi}\,t_1\,t_2\,t_3^{1-\xi} + \frac{b\,\xi}{(1-\xi)(\xi-2)}\,t_1\,t_2^{2-\xi} + \frac{b\,\xi}{(2-\xi)(\xi-3)}\,t_1^{3-\xi} + \frac{b^{3/\xi}\,\xi}{\xi-3}\,.$$

Since $\gamma = 2-\xi$, thus we find for $\gamma \neq 1$

$$\phi(t_1,\,t_2,\,t_3) = \frac{b}{\gamma-1}\,t_1\,t_2\,t_3^{\gamma-1} - \frac{b\,(2-\gamma)}{\gamma(\gamma-1)}\,t_1\,t_2^{\gamma} - \frac{b\,(2-\gamma)}{\gamma(\gamma+1)}\,t_1^{\gamma+1} - \frac{b^{3/(2-\gamma)}\,(2-\gamma)}{\gamma+1}\,. \tag{B.5}$$

Introducing the (time) difference $h = t_3 - t_2 = t_2 - t_1$, and normalize by $h^{\gamma+1}$, this reduces to

$$\frac{(\gamma/b)\,\phi(t_1,t_2,t_3)}{h^{\gamma+1}} \simeq \\ \frac{\gamma}{\gamma-1}\left(\frac{t_1}{h}\right)^{\gamma+1}\left[\left(1+\frac{h}{t_1}\right)\left(1+\frac{2\,h}{t_1}\right)^{\gamma-1} - \frac{2-\gamma}{\gamma}\left(1+\frac{h}{t_1}\right)^{\gamma} - \frac{(2-\gamma)(\gamma-1)}{\gamma(\gamma+1)}\right]. \tag{B.6}$$

Surprisingly this expression for the 3-point position correlation of the FnD dynamics also allows us to collapse all numerical simulation data of the LLg on the same curve.

B.3 Proof of lemma 5.1.2

We start by recalling Eq. (5.12b). Integration amounts to

$$\phi(t_1,t_2,\cdots,t_n) \;=\; \frac{b}{1-\xi}\left(t_1t_2\cdots t_n^{1-\xi}\right)+\frac{b\,\xi}{(1-\xi)(\xi-2)}\left(t_1t_2\cdots t_{n-1}^{2-\xi}\right)\;+\;\cdots$$
$$+\;\frac{b\,\xi}{(n-\xi-1)(\xi-n)}\,t_1^{n-\xi}\;+\;\frac{b^{n/\xi}\,\xi}{\xi-n},\qquad\qquad \xi\neq 1. \quad \text{(B.7)}$$

In what follows we assume $\xi = 2-\gamma$ and normalize by the $n-(2-\gamma)$ power of the time difference $h = t_j - t_{j-1}$= const. for $j \in \{2,3,\cdots,n\}$. Thus we find

$$\frac{(\gamma/b)\,\phi(t_1,t_2,\cdots,t_n)}{h^{n-(2-\gamma)}}$$
$$\simeq \frac{\gamma}{\gamma-1}\left(\frac{t_1}{h}\right)^{n-(2-\gamma)}\left[\left(\left(1+\frac{h}{t_1}\right)\cdots\left(1+\frac{(n-1)\,h}{t_1}\right)^{\gamma-1}\right)\;-\;\frac{2-\gamma}{\gamma}\left(\left(1+\frac{h}{t_1}\right)\cdots\right.\right.$$
$$\left.\left.\times\left(1+\frac{(n-2)\,h}{t_1}\right)^{\gamma}\right)\;-\;\cdots\;-\;\frac{(2-\gamma)\,(\gamma-1)}{(n+\gamma-3)\,(n+\gamma-2)}\right]. \quad \text{(B.8)}$$

Asymptotic scaling for $t_1 \gg h$, leads to

$$\frac{(\gamma/b)\,\phi(t_1,t_2,\cdots,t_n)}{h^{n-(2-\gamma)}} \simeq \frac{\gamma}{\gamma-1}\left(\frac{t_1}{h}\right)^{n-(2-\gamma)}\left[1-\sum_{k=2}^{n}\frac{(2-\gamma)\,(\gamma-1)}{(k+\gamma-3)(k+\gamma-2)}\right]. \quad \text{(B.9)}$$

The sum in Eq. (B.9) has telescopic structure. This allows us to rewrite it as

$$\sum_{k=2}^{n}\frac{1}{(k+\gamma-3)\,(k+\gamma-2)}=\sum_{k=2}^{n}\left(\frac{1}{(k+\gamma-3)}-\frac{1}{(k+\gamma-2)}\right)=\frac{n-1}{(\gamma-1)\,(n+\gamma-2)}. \quad \text{(B.10)}$$

Substituting Eq. (B.10) in to (B.9), we find the scaling for the $n-$point correlation function

$$\frac{(\gamma/b)\,\phi(t_1,t_2,\cdots,t_n)}{h^{n-(2-\gamma)}} \sim \frac{n\,\gamma}{n-(2-\gamma)}\left(\frac{t_1}{h}\right)^{n-(2-\gamma)}, \qquad t_1 \gg h. \quad \text{(B.11)}$$

Analogous asymptotic scaling for $t_1 \ll h$, completes the proof of lemma 5.1.2.

Bibliography

[1] E. Aghion, D. A. Kessler, and E. Barkai. Large fluctuations for spatial diffusion of cold atoms. *Phys. Rev. Lett.*, **118** (26):260601, 2017.

[2] R. Artuso and G. Cristadoro. *Anomalous Transport*. Eds. R. Klages, G. Radons, I.M. Sokolov Wiley-VCH, Berlin, 2008.

[3] E. Barkai and V. Fleurov. Stochastic one-dimensional Lorentz gas on a lattice. *J. Stat. Phys.*, **96** (1-2):325–359, 1999.

[4] E. Barkai, V. Fleurov, and J. Klafter. One-dimensional stochastic Lévy-Lorentz gas. *Phys. Rev. E*, **61** (2):1164–1169, 2000.

[5] C. W. J. Beenakker, C. W. Groth, and A. R. Akhmerov. Nonalgebraic length dependence of transmission through a chain of barriers with a Lévy spacing distribution. *Phys. Rev. B*, **79** (2):024204, 2009.

[6] C. M. Bender and S. A. Orszag. *Advanced mathematical methods for scientist and engineers: Asymptotic methods and perturbation theory*. Springer, 1979.

[7] A. Bianchi, G. Cristadoro, M.and Lenci, and M. Ligabò. Random walks in a one-dimensional Lévy random environment. arxiv:1411.0586v2, 2016.

[8] I. N. Bronshtein, K. A. Semendyayev, G. Musiol, and H. Mühlig. *Handbook of Mathematics*. Springer-Verlag Berlin Heidelberg, 2007.

[9] R. Burioni, L. Caniparoli, S. Lepri, and A. Vezzani. Lévy-type diffusion on one-dimensional directed cantor graphs. *Phys. Rev. E*, **81** (1):011127, 2010.

[10] R. Burioni, L. Caniparoli, and A. Vezzani. Lévy walks and scaling in quenched disordered media. *Phys. Rev. E*, **81** (6):060101, 2010.

[11] R. Burioni and D. Cassi. Random walks on graphs: ideas, techniques and results. *J. Phys. A: Math. Gen.*, **38** (8):R45–R78, 2005.

[12] F. Cecconi, D. del Castillo-Negrete, M. Falcioni, and A. Vulpiani. The origin of diffusion: The case of non chaotic systems. *Physica D*, **180** (3-4):129–139, 2003.

[13] A. V. Chechkin, R. Metzler, V. Y. Gonchar, J. Klafter, and L. V. Tanatarov. First passage and arrival time densities for Lévy flights and the failure of the method of images. *arXiv:cond-mat/0309449v1*.

[14] S. Chibbaro, L. Rondoni, and A. Vulpiani. *Reductionism, Emergence and Levels of Reality. The Importance of Being Borderline*. Springer Verlag, Heidelberg, 2014.

[15] S. Denisov, J. Klafter, and M. Urbakh. Dynamical heat channels. *Phys. Rev. Lett.*, **91** (19):194301, 2003.

[16] C. P. Dettmann. Diffusion in the Lorentz gas. *Commun. Theor. Phys*, **62** (4):521–540, 2014.

[17] C. P. Dettmann and E. G. D. Cohen. Microscopic chaos and diffusion. *J. Stat. Phys*, **101** (3-4):775–817, 2000.

[18] J. R. Dorfman. *An introduction to chaos in non-equilibrium statistical mechanics*. Cambridege University Press, Cambridge, 1999.

[19] L. Ermann, G. G. Carlo, and M. Saraceno. Transport phenomena in the asymmetric quantum multibaker map. *Phys. Rev. E*, **77** (1):011126, 2008.

[20] W. Feller. *An Introduction to Probability Theory and Its Applications Vol. 2, 2nd Edition*. Wiley, USA, 1991.

[21] D. Froemberg, M. Schmiedeberg, E. Barkai, , and V. Zaburdaev. Asymptotic densities of ballistic Lévy walks. *Phys. Rev. E*, **91** (2):022131, 2015.

[22] G. Gallavotti. *Statistical Mechanics*. Springer Verlag, Berlin, 1999.

[23] P. Gaspard. *Chaos, scattering and statistical mechanics*. Cambridge University Press, 2005.

[24] T. Geisel, J. Nierwetberg, and A. Zacherl. Accelerated diffusion in Josephson junctions and related chaotic systems. *Phys. Rev. Lett.*, **54** (7):616–619, 1985.

[25] C. Giberti, L. Rondoni, M. Tayyab, and J. Vollmer. Equivalence of correlations in the slicer map and the Lévy-Lorentz gas. *https://arxiv.org/abs/1709.04980*, 2017.

[26] E. Gutkin. Billiard dynamics: An updated survey with the emphasis on open problems. *Chaos*, **22** (2):026116, 2012.

[27] J. W. Haus and K. W. Kehr. Diffusion in regular and disordered lattices. *Phys. Rep.*, **150** (5-6):263–406, 1987.

[28] A. Igarashi, L. Rondoni, A. Botrugno, and M. Pizzi. Nonlinear diffusion and transient osmosis. *Commun. Theor. Phys*, **56** (2):352–366, 2011.

[29] F. Dyson J. Havil. *Gamma: Exploring Euler's Constant*. Princeton University Press, 2010.

[30] O. G. Jepps, S. K. Bathia, and D. J. Searles. Wall mediated transport in confined spaces: exact theory for low density. *Phys. Rev. Lett.*, **91** (12):126102, 2003.

[31] O. G. Jepps, C. Bianca, , and L. Rondoni. Onset of diffusive behavior in confined transport systems. *Chaos*, **18** (1):013127, 2008.

[32] O. G. Jepps and L. Rondoni. Thermodynamics and complexity of simple transport phenomena. *J. Phys. A: Math. Gen.*, **39** (6):1311–1338, 2006.

[33] L. P. Kadanoff. *Statistical physics: statics, dynamics and renormalization.* World Scientific, Singapore, 2000.

[34] J. Klafter, A. Blumen, G. Zumofen, and M. F. Shlesinger. Lévy-walk approach to anomalous diffusion. *Physica A*, **168** (1):637–645, 1990.

[35] J. Klafter and R. Silbey. Derivation of the continuous-time random-walk equation. *Phys. Rev. Lett.*, **44** (2):55–58, 1980.

[36] R. Klages. *Deterministic diffusion in one-dimensional chaotic dynamical systems.* Wissenschaft & Technik-Verlag, Berlin, 1996.

[37] R. Klages. *Microscopic chaos, fractals and transport in nonequilibrium statistical mechanics*, volume 24 of Advanced Series in Nonlinear Dynamics. World Scientific, Singapore, 2007.

[38] R. Klages. *Applied dynamical systems; From deterministic chaos to deterministic diffusion.* Lecture notes v 1.3; Queen Mary, University of London, 2010.

[39] R. Klages, G. Radons, and I. M. Sokolov (Eds.). *Anomalous Transport: Foundations and Applications.* Wiley-VCH, Weinheim, 2008.

[40] B. Li, J. Wang, L. Wang, and G. Zhang. Anomalous heat conduction and anomalous diffusion in nonlinear lattices, single walled nanotubes, and billiard gas channels. *Chaos*, **15** (1):015121, 2005.

[41] L. Mátyás, T. Tél, and J. Vollmer. Multibaker map for thermodynamic cross effects in dynamical systems. *Phys. Rev. E*, **62** (1):349–365, 2000.

[42] G. F. Mazenko. *Nonequilibrium statistical mechanics.* WILEY-VCH Verlag GmbH & Co. KGaA, 2008.

[43] E. W. Montroll and G. H. Weiss. Random walks on lattices. II. *J. Math Phys.*, **6** (2):167, 1965.

[44] B. Moran, W. G. Hoover, and S. Bestiale. Diffusion in a periodic Lorentz gas. *J. Stat. Phys*, **48** (3-4):709–726, 1987.

[45] E. Ott. *Chaos in dynamical systems*. Cambridge University Press, Cambridge, 1992.

[46] H. Poincaré. *New Methods of Celestial Mechanics: Integral invariants and asymptotic properties of certain solutions, D. Goroff (Ed.)*. AIP Press, 1992.

[47] H. Poincaré. *The Three-Body Problem and the Equations of Dynamics, translated by B. D. Popp*. Springer International Publishing, 2017.

[48] Y. Pomeau and P. Manneville. Intermittent transition to turbulence in dissipative dynamical systems. *Commun. Math. Phys.*, **74** (2):189–197, 1980.

[49] L. Reichl. *A modern course in statistical physics, 2nd edition*. John Wiley, New York, 1998.

[50] F. Reif. *Fundamentals of statistical and thermal physics*. McGraw-Hill, Auckland, 1965.

[51] D. Ruelle. Differentiation of SRB states. *Comm. Math. Phys.*, **187** (1):227–241, 1997.

[52] D. Ruelle. General linear response formula in statistical mechanics, and the fluctuation dissipation theorem far from equilibrium. *Phys. Lett. A*, **245** (3-4):220–224, 1998.

[53] L. Salari, L. Rondoni, C. Gibert, and R. Klages. A simple non-chaotic map generating subdiffusive, diffusive, and superdiffusive dynamics. *Chaos*, **25** (7):073113, 2015.

[54] D. Sands. Topological conditions for positive Lyapunov exponent in unimodal maps. *PhD Thesis, University of Cambridge, St Johns College*, 1993.

[55] M. F. Shlesinger and J. Klafter. *Lévy walks versus Lévy flights. In On Growth and Form: Fractal and Non-Fractal Patterns in Physics, Eds. H. E. Stanley and N. Ostrowsky, 279 - 283*. Martinus Nijhoff Publishers, Dordrecht, 1986.

[56] M. F. Shlesinger, G. M. Zaslavski, and J. Klafter. Strange kinetics. *Nature*, **363** (6424):31–37, 1993.

[57] B. Simon. *The statistical mechanics of lattice gases*. Princeton University Press, 1993.

[58] I. M. Sokolov. Models of anomalous diffusion in crowded environments. *Soft Matter*, **8** (35):9043–9052, 2012.

[59] S. Tasaki and P. Gaspard. Thermodynamic behavior of an area-preserving multibaker map with energy. *Theor. Chem, Acc.*, **102** (1-6):385–396, 1999.

[60] J. Vollmer. Chaos, spatial extension, transport, and non-equilibrium thermodynamics. *Phys. Rep*, **372** (2):131–267, 2002.

[61] G. H. Weiss and R. J. Rubin. *Random Walks: Theory and Selected Applications, Eds. I. Prigogine and Stuart A. Rice*. Chapter in Adv. Chem. Phys., 1983.

[62] D. K. Wójcik and J. R. Dorfman. Diffusive-ballistic crossover in 1d quantum walks. *Phys. Rev. Lett.*, **90** (23):230602, 2003.

[63] G. M. Zaslavsky. Chaos, fractional kinetics, and anomalous transport. *Physics Reports*, **371** (6):461–580, 2002.

[64] G. Zumofen and J. Klafter. Scale-invariant motion in intermittent chaotic systems. *Phys. Rev. E*, **47** (2):851–863, 1993.